

Lateral Path-Following Control for Automated Vehicle Platoons

W. Jansen

Master of Science Thesis



Lateral Path-Following Control for Automated Vehicle Platoons

MASTER OF SCIENCE THESIS

For the degree of Master of Science in Mechanical Engineering at Delft
University of Technology

W. Jansen

June 30, 2016

Faculty of Mechanical, Maritime and Materials Engineering (3mE) · Delft University of
Technology

TNO innovation
for life

The work in this thesis was supported by TNO Automotive. Their cooperation is hereby gratefully acknowledged.

 **TU Delft** Delft
University of
Technology

Copyright © Delft Center for Systems and Control (DCSC)
All rights reserved.

DCSC

DELFT UNIVERSITY OF TECHNOLOGY
DEPARTMENT OF
DELFT CENTER FOR SYSTEMS AND CONTROL (DCSC)

The undersigned hereby certify that they have read and recommend to the Faculty of
Mechanical, Maritime and Materials Engineering (3mE) for acceptance a thesis
entitled

LATERAL PATH-FOLLOWING CONTROL FOR AUTOMATED VEHICLE PLATOONS

by

W. JANSEN

in partial fulfillment of the requirements for the degree of
MASTER OF SCIENCE MECHANICAL ENGINEERING

Dated: June 30, 2016

Supervisor(s):

Prof.dr.ir. N. v.d. Wouw

Dr.ir. E. Semsar-Kazerooni

Reader(s):

Prof.dr.ir. B. De Schutter

Dr.ir. R. Happee

Abstract

Nowadays, traffic congestion on highways is still an increasing problem, in the Netherlands and worldwide. Hence, there is an increasing societal demand for innovative solutions for this problem. Preferably, these solutions also contribute to the reduction of fuel consumption (and hence emissions) and higher traffic safety. This has raised the interest in the development of automated highway (platooning) systems. If vehicles would drive together in a platoon with small inter-vehicle time gaps of well below one second, the road capacity of existing roads can be increased significantly. Moreover, due to the lower aerodynamic drag, especially for truck platoons, the emissions and fuel consumption can be reduced. Driving safely at small inter-vehicle time gaps, however, requires vehicle automation in both longitudinal and lateral direction, due to the relatively large reaction time of a human driver. Most research activities regarding automated vehicle platoons focus on the longitudinal control of a vehicle, and less research has been performed on the aspect of lateral automation. Hence, one of the main motivations for this work is to focus on the development of a lateral controller for cooperative vehicle platoons.

A vehicle-following control strategy is proposed, in which the design strategy is based on vehicle path-following rather than on direct vehicle-following. The former approach shows better tracking performance based on numerous research studies. For the controller design, a linear vehicle model is used and the error dynamics of a vehicle with respect to a reference path, generated by a preceding vehicle, are derived. A static output feedback control law is designed in combination with two different feedforward controller that are compared to each other. The first feedforward controller is based on the control input of the preceding vehicle, which is obtained through wireless inter-vehicle communication and the second feedforward controller is based on the curvature of the reference path.

As a result of the vehicle-following control strategy, the lateral dynamics of the individual vehicles are coupled through the cooperative control law. Therefore, string stability in the lateral direction should be taken into account in the controller design, as well. In literature, lateral string stability has been achieved for direct vehicle-following control methods, but this concept is not well developed in the scope of lateral control methods for vehicle path-following for platooning. In this work, a method has been developed to analyze the platoon dynamics in the frequency-domain, where the lateral control of each individual vehicle is based on

the proposed vehicle path-following control method. Marginal lateral string-stable behavior is obtained for the designed lateral controller including a feedforward controller based on wireless inter-vehicle communication. This is evidenced both in frequency-domain and in time-domain simulation.

Finally, the control algorithm has been implemented and tested on an experimental vehicle. Different lateral maneuvers, such as driving a sinusoidal path, are performed both at low and high speed. The experimental data validates the theoretical results and shows that the lateral dynamics of automated vehicle platoons can successfully be controlled using the proposed path-following control method.

List of Symbols

Acronyms

ACC	Adaptive Cruise Control
CACC	Cooperative Adaptive Cruise Control
CAN	Controller Area Network
CoG	Center of Gravity
GPS	Global Positioning System
HMI	Human-Machine Interface
ITS	Intelligent Transport System
ITS-G5	Set of protocols and parameters specified in the ETSI Standard ES 202 663
PAS	Park Assist System
V2V	Vehicle-to-Vehicle

Greek Symbols

α	slip angle
β	body slip angle
Δ	interval
δ	steering angle
Γ	complementary sensitivity function
γ	actuator delay
κ	curvature of a path
ω	frequency; natural frequency steering system
ϕ	sensing delay
ψ	heading angle
τ	cutoff frequency low-pass filter
θ	angular of the reference path with respect to a global reference frame
ζ	damping ratio for steer dynamics

Miscellaneous

η	matrix containing vehicle motion parameters
ξ	matrix containing relative position measurements
lim	limit
\mathbb{R}	set of real $n \times m$ matrices
\mathcal{H}	angular rate of change of the vehicle's direction of motion
\mathcal{K}	transfer function
\mathcal{P}	open-loop vehicle plant
$\mathcal{L}(\cdot)$	Laplace transform
$\min x$	minimum of x
$\underline{\xi}$	relative position measurement

Roman symbols

A	system matrix
a	distance from center of gravity to front axis
B	input matrix
b	distance from center of gravity to rear axis

C	output matrix; cornering stiffness; polynomial coefficient
d	inter-vehicle distance
e	error
F	force
G	vehicle transfer function
H	low-pass filter
I	moment of inertia; identity matrix
j	imaginary number
K	static feedback gain vector
k	feedback gain
l	length
m	vehicle mass
n	number of points
O	origin
p	constant depending on vehicle parameters
q	state vector
R	rotation matrix
S	reference frame
s	Laplace variable; position on the reference path
T	transformation matrix
t	time
v	vehicle velocity
x	global x position
y	global y position
Z	error states vector
z	system output

Subscripts

c	cutoff frequency
cl	closed-loop
d	delay time
e	error
f	front
fb	feedback
ff	feedforward
g	global reference
i,j	indices
i-1	preceding vehicle
la	look-ahead point
m	measurement
n	natural frequency
r	rear
ref	reference
s	position variable of the position on the reference path
x,y,z	x,y,z direction

Table of Contents

Acknowledgements	ix
1 Introduction	1
1-1 Background	2
1-1-1 Error definitions	2
1-1-2 Vehicle platoon definition	4
1-1-3 Lateral control based on vehicle-following	4
1-1-4 Lateral string stability	7
1-1-5 Summary	8
1-2 Problem statement	9
1-3 Research approach	9
1-4 Outline	10
2 Lateral vehicle dynamics modelling	11
2-1 Equations of motion for a single track vehicle	11
2-1-1 Global vehicle motion	15
2-1-2 Steering dynamics	15
2-2 Error dynamics	16
2-2-1 Derivation of the error dynamics for $\dot{\psi}_{e,i}$	18
2-2-2 Derivation of the error dynamics for $\dot{y}_{e,i}$	18
3 Lateral control design	23
3-1 Control objective	23
3-1-1 Requirements on controller design	23
3-2 Output feedback control	24
3-2-1 The role of heading information in the feedback law	26

3-2-2	Transient response characteristics	29
3-2-3	Influence of gain k_1	30
3-2-4	Internal dynamics	31
3-3	Feedforward control input	31
3-3-1	Feedforward based on the curvature of the reference path	31
3-3-2	Feedforward controller based on steer input of preceding vehicle	34
3-4	Evaluation of the control requirements	37
3-4-1	Summary	39
4	Lateral string stability	41
4-1	Platoon dynamics	42
4-2	String stability analysis	46
4-2-1	Case 1: Static output feedback control without feedforward	46
4-2-2	Case 2: Static output feedback and feedforward	47
4-2-3	Case 3: Static output feedback and filtered feedforward	48
4-2-4	Case 4: Static output feedback with filtered feedforward and filtered path	49
4-3	Time-domain simulations	50
4-3-1	Model description	51
4-4	Discussion	56
5	Experiments	59
5-1	Practical implementation	59
5-1-1	Path generation	59
5-1-2	Effect of sensing delay on path generation	62
5-1-3	Calculation of the control errors	64
5-1-4	Design of feedforward controller	65
5-2	Experimental setup	68
5-2-1	Test description	68
5-3	Experiment results	69
5-4	Discussion	74
6	Conclusions and recommendations	77
6-1	Conclusions	77
6-2	Recommendations	79
A	Closed-loop poles	81
B	Calculation of the control errors	85
C	Implementaion of feedforward control based on wireless communication	87

List of Figures

1-1	Overview of the most common error definitions for lateral vehicle-following control	3
1-2	Illustration of a vehicle platoon	4
2-1	Illustration of the vehicle's center of gravity moving in space	12
2-2	Schematic representation of a single track vehicle model	14
2-3	Schematic representation of the error dynamics	17
3-1	Illustration of a 'sinusoidal' lane-change maneuver	24
3-2	Stability conditions for the control gains k_1 and k_2	26
3-3	Closed-loop pole locations for $k_1 = 0.05$ and varying k_2	27
3-4	Response of $y_{e,i}$ and ψ_i of a single track model with steer input $\delta_{ref,i}$	28
3-5	Transient response characteristics of the closed-loop system	29
3-6	Closed-loop pole locations for $v_{x,i} = 20$ m/s	30
3-7	Bode plot of the inverse vehicle transfer function $G_1^{-1}(s)$ and $H_2(s)G_1^{-1}(s)$	33
3-8	The effect of a lateral disturbance on the timing of the feedforward input	35
3-9	Illustration of relating the steer input of a preceding vehicle to its path	36
3-10	Feedback gains k_1 and k_2 versus the longitudinal vehicle speed $v_{x,i}$	37
3-11	Conditions for the gains k_1 and k_2 to obtain a critically damped response	38
3-12	Bode plot of the closed-loop system $G_{cl}(s)$ for multiple longitudinal speeds	39
4-1	block scheme of the lateral control structure for one vehicle in a platoon	44
4-2	Schematic representation of the block $\mathcal{K}(s)$	44
4-3	Block scheme of the simplified lateral control structure for one vehicle in a platoon	45
4-4	Illustration of the coupled lateral dynamics of multiple vehicles in a platoon	45
4-5	Complementary sensitivity function $ \Gamma_{i,1}(j\omega) $ for multiple control gains	47

4-6	Complementary sensitivity function $\Gamma_{i,2}(s)$	48
4-7	Complementary sensitivity function $\Gamma_{i,3}(s)$	49
4-8	Complementary sensitivity function $\Gamma_{i,4}(s)$	50
4-9	Illustration of the simulation model of a vehicle platoon	51
4-10	Example of the initial condition for the simulation model	52
4-11	Simulation of a lane-change maneuver with only static feedback control	53
4-12	Simulation of a lane-change maneuver with feedback and feedforward control	53
4-13	Simulation of a lane-change maneuver with feedback and filtered feedforward control	54
4-14	Simulation of a lane-change maneuver for a filtered feedforward input and reference path $\dot{\theta}_{s,i}$	54
4-15	Simulation of a left hand corner for a filtered reference path $\dot{\theta}_{s,i}$	55
4-16	Effect of filtering $\dot{\theta}_{s,i}$ on the reference path in x_i and y_i coordinates	56
5-1	Illustration of relative position measurements that move within the vehicle's frame	60
5-2	Illustration of the process of adding a new point and removing an old point from the history buffer	62
5-3	Illustration of the influence of sensing delay on the path generation of a preceding vehicle	63
5-4	Bode plot of the inverse vehicle transfer function $G_1^{-1}(s)$ together with $H_2(s)G_1^{-1}(s)$ and $H_1(s) \left G_1^{-1}(0) \right $	66
5-5	Complementary sensitivity function $\Gamma_{i,5}(s)$	68
5-6	Illustration of the test setup	69
5-7	Illustration of the REW test track in Lelystad, The Netherlands	69
5-8	Experimental data	71
5-9	Frequency content of the reference curvature and $\Gamma_{i,5}(j\omega)$ for different cutoff frequencies	72
5-10	Reproduction of experimental results in simulation model	73
A-1	Closed-loop pole locations for $v_{x,i} = 10$ m/s	82
A-2	Closed-loop pole locations for $v_{x,i} = 30$ m/s	83
A-3	Closed-loop pole locations for $v_{x,i} = 40$ m/s	84
C-1	Relating the steer input of a preceding vehicle to its path in practice	88

Acknowledgements

This master thesis is the end result of eight years of studying Mechanical Engineering in Delft. During these years I gained incredible experiences and made a lot of new friends. I am also very glad that I had the opportunity to do other activities during my study time, such as building a high performance race car and become the number 1 in the Formula Student competition with the 'DUT Racing Team' and my internship at Tesla Motors in California. I would like to thank all the people around me that helped me to achieve of what I am today. First of all, I would like to thank my supervising professor from the TU Delft, Nathan van de Wouw for helping and supporting me throughout the whole graduation process. I would also like to thank my supervisors from TNO, Elham Semsar-Kazerooni and Jeroen Ploeg, for their help and enthusiasm during the project, but also for all the interesting discussions we had and the careful reading of my final thesis and all the progress reports.

Also, I would like to thank my parents for always supporting me through my entire education and for all the opportunities they gave me. I am very grateful for their encouragements and for giving me the freedom to do what I want to do. Furthermore, I would like to thank all my friends and fellow students for having a great time throughout my study time and finally, I would like to thank my girlfriend, Marit for her love and support, and for giving me the energy to finish this graduation project.

Delft, University of Technology
June 30, 2016

W. Jansen

Chapter 1

Introduction

The capacity of existing road networks is limited, which causes traffic jams. At the same time, there is an increasing societal demand to reduce fuel consumption and emissions without compromising traffic safety. These issues have resulted in an increasing interest in the development of cooperative driving.

One way to increase road capacity is to decrease the inter-vehicle distance while maintaining the same velocity level. As this would seriously compromise traffic safety, given the relatively large reaction time of humans, vehicle automation is required. This gave rise to the idea of forming an automated vehicle platoon. A platoon of vehicles can be considered as an interconnection of dynamical systems through an underlying communication and sensing network. An example of a vehicle platooning controller is Cooperative Adaptive Cruise Control (CACC) [1]. CACC makes use of Vehicle-to-Vehicle (V2V) communication in addition to conventional Adaptive Cruise Control (ACC) sensors. This functionality allows vehicles to drive at small time gaps of well below one second, while still maintaining a high level of safety. If small inter-vehicle time gaps can be realized, traffic throughput can be increased which reduces traffic congestion. On top of that, a small inter-vehicle distance reduces the aerodynamic drag of each individual vehicle, especially for heavy-duty vehicles. As a consequence, fuel efficiency is increased and emissions are reduced [2], [3].

Until now, most research regarding automated vehicle platoons has mainly focused on longitudinal vehicle control [4], [1]. The next step is to also further develop the lateral control, such that vehicles can drive fully autonomously in a platoon. Autonomous steering not only adds to the comfort of the driver, it is also necessary when driving at small time gaps of well below one second. Namely, the small inter-vehicle distance significantly limits the ability to see upcoming corners. In [5], the average driver reaction time was found to be approximately one second. If the time gap between two vehicles is significantly reduced below one second, a human driver cannot properly track the lateral motion of its preceding vehicle anymore. Hence, also lateral automation is required to drive safely at small time gaps of well below one second.

Another problem that is related to the short inter-vehicle distance is that lane markings are not reliably detected by on-board cameras [6]. Hence, the only reference that remains

for lateral control is the preceding vehicle, which brings the lateral control problem into a vehicle-following control problem. The main difference between vehicle-following and lane following, from a control point-of-view, is that in the vehicle-following approach, the lateral dynamics of individual vehicles are coupled which means that a lateral disturbance might propagate through the platoon of vehicles. Therefore, it is important to also consider the string stability of a vehicle platoon in the lateral direction.

The focus of this thesis will be on the design and implementation of a lateral vehicle-following controller for automated vehicle platoons. This work will not only focus on the lateral of one single vehicle, but also considers the lateral dynamics of the whole vehicle platoon.

1-1 Background

Recent developments in autonomous driving have raised an interest in lateral control of autonomous vehicles. Therefore, lateral control of vehicles is a topic which is well covered in literature. The majority of the research that has been performed regarding lateral control, focuses on the lateral control of one single vehicle, see [7], [8], and only a few examples can be found where vehicle platoons are addressed, [9] and [6]. Although some control strategies are suitable to control the lateral dynamics of one single vehicle, not all of them are suitable to control the lateral dynamics of a vehicle platoon. For example, cutting the corner of a preceding vehicle is not a big problem for one single vehicle, but might become a serious problem for longer vehicle platoons. This chapter gives an overview of how the vehicle-following control problem is formulated in literature and reflects the different approaches with respect to the lateral control of vehicle platoons. Different aspects regarding the lateral control problem are discussed. First, a vehicle platoon is defined in Section 1-1-2. Then, in Section 1-1-3, different lateral control approaches to vehicle-following found in literature are discussed. This includes design of both feedback and feedforward controllers. Section 1-1-4 focusses on the lateral string stability of vehicle platoons and, finally, a brief summary is given in Section 1-1-5.

1-1-1 Error definitions

In order to compare different control approaches that appeared in literature, Figure 1-1 is used. This figure represents a generalized vehicle-following scenario and will be used throughout the remainder of this chapter.

First, all variables in Figure 1-1 will be introduced to provide a better understanding of the figure. The figure shows two vehicles: The ego-vehicle, which is referred to as vehicle i , and its preceding vehicle denoted by $i - 1$. First, three reference frames are introduced, a global frame $\underline{\bar{e}}^g$, a frame attached to the ego-vehicle $\underline{\bar{e}}^i$ and a frame attached to the preceding vehicle $\underline{\bar{e}}^{i-1}$. The global right-hand frame is defined by a set of three orthonormal vectors $\underline{\bar{e}}^g := [\bar{e}_x^g, \bar{e}_y^g, \bar{e}_z^g]^T$. The frames $\underline{\bar{e}}^i$ and $\underline{\bar{e}}^{i-1}$ consist, similar to frame $\underline{\bar{e}}^g$, of a set of three orthonormal vectors: $\underline{\bar{e}}^i := [\bar{e}_x^i, \bar{e}_y^i, \bar{e}_z^i]^T$ and $\underline{\bar{e}}^{i-1} := [\bar{e}_x^{i-1}, \bar{e}_y^{i-1}, \bar{e}_z^{i-1}]^T$, where \bar{e}_x^i and \bar{e}_x^{i-1} are oriented in the forward direction along the longitudinal vehicle axis. Furthermore, the origins of frame $\underline{\bar{e}}^i$ and $\underline{\bar{e}}^{i-1}$ are fixed to the Centers of Gravity (CoG) of vehicle i and $i - 1$, respectively. Finally, \bar{e}_z^g is parallel to both \bar{e}_z^i and \bar{e}_z^{i-1} , which are pointing in the vertical direction of vehicles i and $i - 1$, respectively.

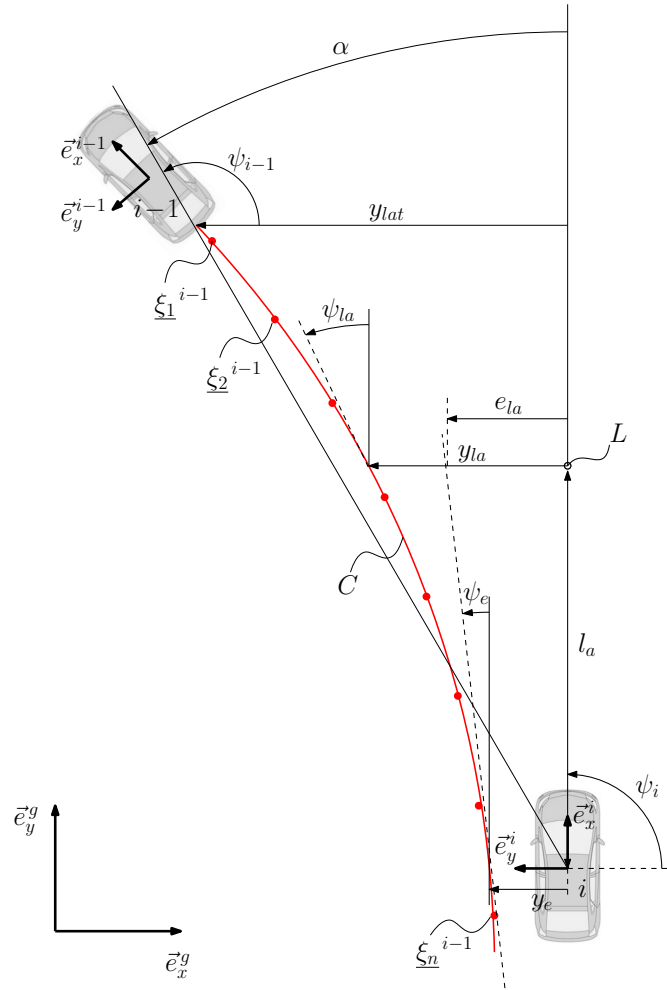


Figure 1-1: Overview of the most common error definitions for lateral vehicle-following control obtained from in literature.

The angle ψ_i is the angle between \vec{e}_x^g and \vec{e}_x^i and ψ_{i-1} is the angle between \vec{e}_x^g and \vec{e}_x^{i-1} . The path of vehicle $i-1$, C (in red), is represented by the matrix $\underline{\xi}^{i-1}$ that consists of rear bumper measurements $[\xi_1^{i-1}, \xi_2^{i-1}, \dots, \xi_n^{i-1}]^T$ at different discrete time instances, indexed $1, 2, \dots, n$ obtained through e.g. camera and radar measurements. Each individual relative position measurement ξ_j^{i-1} contains an x and y coordinate with respect to the frame \vec{e}^i , so $\xi_j^{i-1} := [x_j^{i-1}, y_j^{i-1}]$. The angle α is the bearing angle of vehicle $i-1$ with respect to vehicle i and y_{lat} is the lateral offset of vehicle i with respect to vehicle $i-1$. The point L is referred to as the ‘virtual control point’ or the ‘look-ahead point’ and is located on the longitudinal axis of vehicle i at a look-ahead distance l_a from the origin of frame \vec{e}^i . Figure 1-1 shows that the lateral offset and heading error with respect to the path C can be measured at the look-ahead point L and at the CoG of vehicle i . The lateral offset and heading error measured at the look-ahead point L are represented by y_{la} and ψ_{la} , respectively, and the lateral offset and heading error measured at the CoG are represented by y_e and ψ_e , respectively. Hence, y_e is the distance from the CoG of vehicle i to the path of vehicle $i-1$ and ψ_e is the angle between \vec{e}_x^i and the tangent of the path of vehicle $i-1$. Finally, e_{la} is the lateral offset of the

look-ahead point with respect to the tangent of the path of vehicle $i - 1$.

1-1-2 Vehicle platoon definition

First of all, let us define what is a vehicle platoon. A vehicle platoon can be interpreted as a dynamic system that consists of multiple sub-systems (the individual vehicles), which are ‘virtually’ connected to each other [10], [4]. Forward-looking sensors, which are used in conventional ACC systems, are used to measure the relative position of a preceding vehicle and wireless communication allows vehicles to exchange real time state information. In this way, feedforward information can be obtained, for example in the form of the commanded steer input of the preceding vehicle. An illustration of a vehicle platoon is depicted in Figure 1-2. Each vehicle in the string is assigned with an index increasing in upstream platoon direction. The inter-vehicle distance between two vehicles i and $i - 1$ is assigned with d_i and each vehicle has a velocity of v_i .

If all the vehicles in the platoon are identical in terms of their dynamics, as suggested in Figure 1-2, the platoon is said to be homogeneous.

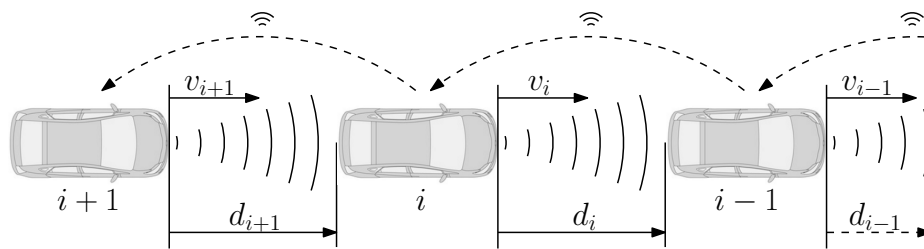


Figure 1-2: Illustration of a vehicle platoon.

1-1-3 Lateral control based on vehicle-following

In this section, different lateral control methods that are found in literature are discussed. Most lateral control approaches rely on road infrastructure (e.g., lane markings) for the control reference. However, as mentioned in the introduction, lane markings cannot reliably be detected by a camera when vehicles drive at small time gaps because the view is significantly occluded by a preceding vehicle [6]. Therefore, this thesis work specifically focuses on vehicle-following, which means that a preceding vehicle is used as a reference for lateral control.

In literature, two main different approaches can be distinguished for vehicle-following. These will be referred to as ‘Direct vehicle-following’ and ‘Vehicle path-following’. Both approaches are now further illustrated and compared.

Direct vehicle-following

The concept of direct vehicle-following is based on the idea that the following vehicle directly steers towards its preceding vehicle based on its current relative position. The principle of direct vehicle-following is also currently applied by TNO Automotive [11], [12]. Other publications that formulate the vehicle-following control problem in a similar way are [13]

and [6], where the work of the latter specifically focuses on vehicle platoons.

Although direct vehicle-following is relatively easy to implement, the main downside of this approach is that the controller only uses the current relative position. Therefore, the following vehicle does not necessarily follow the same path as its preceding vehicle. The result is that vehicles cut corners because each vehicle steers directly towards its predecessor [14]. This especially becomes a problem for longer vehicle platoons, because there is no guarantee that vehicles stay inside the lane (or not). Moreover, in contrast to vehicle path-following, the options to compensate for sensing delays for direct vehicle-following, are limited as is discussed in Section 1-1-3.

Vehicle path-following

With vehicle path-following on the other hand, the path driven by the preceding vehicle is used as a reference for the lateral controller. This approach is more complex because the path of the preceding vehicle needs to be obtained first, but it has some interesting advantages over direct vehicle-following.

The authors in [15] show a way to determine the path of the preceding vehicle that is only based on forward-looking sensors. Therefore, multiple relative position measurements are stored over time together with the motion parameters of the vehicle, (i.e., vehicle speed and yaw rate). The relative position measurements construct the path of the preceding vehicle as shown by the points $\xi_1^{i-1}, \xi_2^{i-1}, \dots, \xi_n^{i-1}$ in Figure 1-1, and the vehicle motion parameters are used to correct old relative position measurements for the vehicle motion over time, see [16]. Once the path of the preceding vehicle is correctly obtained, vehicle path-following is similar to lane following which is thoroughly covered in literature. From here on, both problems will be referred to as ‘path-following’.

Incorporating look-ahead distance

In majority of path-following control problem formulations, a virtual ‘look-ahead’ point is defined in front of the vehicle, (e.g., in [8] and [17]). This is illustrated in Figure 1-1 where L is the virtual look-ahead point defined at a look-ahead distance l_a in front of the center of gravity of the vehicle. The control error is determined based on the error of this look-ahead point with respect to the reference path.

The look-ahead point L provides information about where the vehicle will be in the near future, based on its current direction. This makes sense intuitively, because drivers also look forward to utilize future information in order to achieve a path-following task [7]. It is often reported in literature that increasing the look-ahead distance provides more damping and improves stability, because it creates more phase margin [7], [18], [19]. Often, the look-ahead distance is speed dependent because it is shown that the phase margin decreases for higher speeds [20], [21].

Multiple error definitions of the look-ahead point with respect to the reference path exist. The authors in [16], for example, not only consider the lateral offset of the look-ahead point with respect to the reference path, but also a heading error. This lateral offset and heading error are represented by y_{la} and ψ_{la} in Figure 1-1. A similar approach was used in both [22] and [23]. The addition of the heading error boils down to adding a derivative control action

that provides damping in a similar way as the damping effect of increasing the look-ahead distance.

Even though incorporating a look-ahead distance provides more damping to the system and also makes sense intuitively, a well-known disadvantage is that vehicles cut corners because the CoG is not forced to track the reference path. Although this does not seem a serious problem for one single vehicle that follows the lane markings, it becomes a serious problem for a string of vehicles, because the lateral error made by one vehicle grows along the platoon of vehicles.

In order to prevent cutting corners, an alternative error definition is proposed in [24] and [7]. The idea is to measure both the lateral offset and heading error with respect to the CoG of the vehicle instead of the look-ahead point L . These error signals are represented in Figure 1-1 by y_e and ψ_e , respectively. These error signals can be used to determine the look-ahead error e_{la} with respect to the tangent of the reference path as is illustrated in Figure 1-1. The look-ahead error e_{la} is given by

$$e_{la} = y_e + l_a \sin(\psi_e). \quad (1-1)$$

With this error definition, vehicles do not cut corners anymore because now the CoG is actually forced to track the reference path.

Sensing delay

Another important aspect that affects the lateral control performance is sensing delay. For example, the camera and radar installed on the vehicles that are used for experimental validation at TNO, have a delay of about 0.2 seconds. For a direct vehicle-following approach, such a delay would have a significant impact on the stability and the performance due to the direct effect of the sensing delay on the feedback signal. As a result of sensing delay, the phase margin of the system decreases and the closed-loop system can become unstable [18]. The effect of the camera delay on the phase margin can be decreased to some extent by further increasing the look-ahead distance.

In case of vehicle path-following on the other hand, sensing delay does not directly affect the feedback signal, but it does affect the generation of the reference path. The relative position measurements that are used to construct the reference path are now delayed which induces an error in the path construction. Potentially, if the sensing delay time is known, the error that is made by constructing the reference path could be reduced by compensating through the relative position measurements for the vehicle motion during the sensing delay time.

Feedforward input

In addition to feedback control, often also feedforward control is applied to improve the tracking performance. Different designs of feedforward steer inputs are found in literature. Most of them are based on the curvature of the reference path and significantly increase the tracking performance. In [19] for example, a vehicle path-following model is used to obtain the

required steady-state steering angle which is characterized by the reference curvature and vehicle speed. Although this feedforward input significantly increases the tracking performance, small errors are made for transient curvatures.

An alternative feedforward control input is presented in [11] and [6]. These efforts specifically focus on the lateral control of vehicle platoons using a direct vehicle-following approach. The implemented feedforward input is based on the commanded steer input of the preceding vehicle. However, due to the time gap between two vehicles, applying this feedforward input yields conflicting control objectives between the feedforward and feedback controllers [11]. This seems to be another significant disadvantage of the direct vehicle-following control strategy.

Therefore, path-following control methods seem to have better options regarding feedforward steer inputs than direct vehicle-following control methods, which is an important advantage.

1-1-4 Lateral string stability

When vehicles follow the lane markings on the road, the lateral dynamics of vehicles are not coupled because each vehicle has a fixed reference. Due to the absence of coupling in terms of lateral dynamics, the lateral error from one vehicle does not propagate to the next. However, when each vehicle uses its predecessor as a reference, the lateral motion of one vehicle directly affects the behavior of the next vehicle through the cooperative control law. Hence, a lateral error made by one vehicle can grow along the platoon of vehicles.

The disturbance propagation over the string of vehicles is referred to by the notion of string stability. A distinction can be made between longitudinal and lateral string stability. Longitudinal string stability is a well-known property of a vehicle platoon [25], [26]. Platoon stability in the lateral direction, on the other hand, is not addressed very often in literature.

The general idea of string stability is that the effect of disturbances that influence the response of one of the vehicles should not be amplified in upstream platoon direction. In literature, various definitions of string stability of a vehicle platoon are available. In [9], longitudinal and lateral dynamics are considered both and the control gains related to the longitudinal dynamics are a function of the index of the vehicle in the platoon. In this work, string stability of a platoon is assessed by considering the maximum singular values of the transfer function relating the lateral and rotational position of two consecutive vehicles.

The authors of [6] achieved \mathcal{L}_2 string stability in the lateral direction. Similar as in the previous discussed work, a direct vehicle-following control approach is adopted since the lateral control error is based on the current relative position between two consecutive vehicles. The propagation of a lateral error ϵ of one vehicle to its following vehicle is described by the transfer function $H(j\omega)$. If this transfer function has a magnitude less than 1, lateral string stability is ensured, i.e.,

$$\|H(j\omega)\|_\infty = \left\| \frac{\epsilon_i(j\omega)}{\epsilon_{i-1}(j\omega)} \right\|_\infty \leq 1 \Rightarrow \left| \frac{\epsilon_i(j\omega)}{\epsilon_{i-1}(j\omega)} \right| \leq 1 \forall \omega. \quad (1-2)$$

An almost identical approach is described in [27] and [11]. In both research works, also a direct vehicle-following control principle is adopted and lateral string stability is assessed in

a similar way.

It stands out that in all the research projects discussed so far, the lateral control of each individual vehicle is based on a direct vehicle-following control principle. Although the described methods successfully achieve lateral string stability, the adopted direct vehicle-following control approach yields vehicles to cut corners. This is explicitly shown in experimental results in [27]. The corner cutting behavior is undesired and therefore another lateral control method is required which prevents vehicles to cut corners while still ensuring laterally string-stable behavior.

1-1-5 Summary

In this section, the main observations from literature regarding lateral control are summarized. First, it was observed that the traffic congestion problem can be improved by driving at small inter-vehicle distances. Short inter-vehicle distances, at the same time, improve fuel efficiency due to the lower aerodynamic drag and therefore reduces emissions. Cooperative adaptive cruise control can be used to realize a platoon of vehicles that can drive safely at time gaps of well below one second. However, for driving at these small time gaps, autonomous steering is also required due to the limited reaction time of a human driver. Also, due to the small inter-vehicle distance, lane markings are not reliably detected and hence a vehicle-following control approach should be used instead of lane keeping.

Based on literature studies, two main different approaches to vehicle-following can be distinguished which are categorized as direct vehicle-following and vehicle path-following. It was observed that the vehicle path-following approach is more complex to execute, because first the path of a preceding vehicle has to be constructed. However, path-following has some important advantages over direct vehicle-following:

1. In contrast to direct vehicle-following, with vehicle path-following, a vehicle has the objective to actually follow the path generated by its predecessor. This is important, because otherwise there is no guarantee whether a vehicle stays inside the lane of the lead vehicle.
2. Secondly, the relative heading angle of the preceding vehicle is not measurable. Consequently, in case of direct vehicle-following, no proper heading information is available. If the path of the preceding vehicle is constructed on the other hand, the heading angle with respect to the path can be determined and this information significantly improves the damping and therefore the tracking performance of the controller.
3. Another advantage of vehicle path-following is that it is easy to add an additional feedforward input to improve the tracking performance. A good feedforward input significantly reduces the tracking error and is therefore important to consider when comparing different control methods. In case of direct vehicle-following, it is hard to determine a feedforward input that has no conflicting control objective with the feedback control input. This is another advantage of vehicle path-following over direct vehicle-following.

When vehicles drive in a platoon and use their preceding vehicle as a control reference instead of the lane markings on the road, their lateral dynamics are coupled. The performance of

a platoon can then be assessed by evaluating the stability of the string of vehicles. Most research regarding lateral string stability is based on the principle of direct vehicle-following. Although lateral string stability can be achieved, the result of the direct vehicle-following control approach is that vehicles cut corners. This is undesired behavior and therefore another control method is required which prevents vehicles to cut corners while still ensuring laterally string-stable behavior.

Based on literature results, we decide to pursue a path-following control approach in order to prevent vehicles to cut corners. What still is an open question is how lateral string stability can be achieved for a vehicle platoon if the lateral control is based on vehicle path-following instead of direct vehicle-following. For direct vehicle-following the lateral control error is based on the relative position with respect to its predecessor; therefore, the states of two consecutive vehicles are directly related to each other. For vehicle path-following, on the other hand, first the path needs to be constructed and the control input of the following vehicle depends on its relative position with respect to the path of its preceding vehicle. Therefore, vehicle states cannot directly be related to each other and hence a new method is required to describe the platoon dynamics in case a path-following control method is adopted.

1-2 Problem statement

The aim of this master thesis is to design and implement a lateral controller on a vehicle driving in a platoon. The lateral control algorithm should be based on the path-following concept and also guarantee laterally string stable behavior. This is required to let vehicles drive safely at small inter-vehicle distances which increases the road capacity of existing roads, and also lowers the aerodynamic drag of the individual vehicles and hence their emissions and fuel consumption. However, when driving at small inter-vehicle distances, lane markings cannot reliably be detected and therefore a preceding vehicle has to be used as a reference for lateral control. In order to prevent vehicles to cut corners and to obtain better tracking performance, the path of a preceding vehicle has to be used as a control reference.

As a result of the vehicle-following control strategy, the lateral dynamics of the individual vehicles are coupled through the cooperative control law. This means that an error made by one vehicle, also affects the lateral motion of the next vehicle. Therefore, the lateral controller should not only guarantee stable vehicle-following behavior, but also provide laterally string-stable behavior for a string of vehicles. This means that the controller should have good tracking performance for low-frequency steer maneuvers and attenuate high-frequency disturbances in upstream platoon direction.

In literature, lateral string stability has been achieved for direct vehicle-following control methods. However, in order to also achieve laterally string-stable behavior for vehicle path-following, first a method has to be obtained to describe the platoon dynamics in case the lateral control of each individual vehicle is based on a vehicle path-following control method.

1-3 Research approach

This section describes the research steps that need to be taken in order to achieve the goal described in the previous section. First, the lateral vehicle dynamics have to be modeled in

order to describe the lateral motion of a vehicle. Apart from the planar vehicle dynamics, the Park Assist System (PAS) that is used to control the angle of the steering wheels, will be modeled as well. Since the controller design is mainly focused on highway driving scenarios, the tires are assumed to operate in the linear regime. Hence, the lateral dynamics can accurately be described by a single track model [28]. Furthermore, only low-frequency steering maneuvers are considered and it is assumed that the lateral controller runs in parallel to a longitudinal controller, the latter of which maintains a constant time gap with respect to the preceding vehicle.

Secondly, the error dynamics that describe the relative position and orientation of a vehicle with respect to a reference path have to be derived. Then, a control law needs to be designed that regulates the error states to zero. The control law should not only provide stable vehicle-following behavior, but also provide lateral string-stable behavior for a string of vehicles. It is desired that low-frequency steer maneuvers are well tracked, while high-frequency disturbances are attenuated in upstream platoon direction.

In order to follow the path of a preceding vehicle, first the path has to be constructed. Nowadays, many vehicles are equipped with forward-looking sensors such as a camera or radar for active safety features. In order to minimize the implementation cost and effort of realizing vehicle platoons, the goal is to obtain the path of a preceding vehicle, using only these cost-effective sensors.

For practical implementation of the lateral control algorithm, two Toyota Prius vehicles are available to serve as experimental vehicles. These vehicles are equipped with a camera, a radar and a wireless modem, operating according to the ITS-G5 standard [29], which allows inter-vehicle data exchange through wireless communication. Furthermore, the vehicles have a PAS that can be used to control the angle of the steering wheels.

This test platform can be used to implement and test the lateral control algorithm in order to validate the performance of the lateral controller.

1-4 Outline

The remainder of this thesis is organized as follows. First, in Chapter 2, the equations of motion for a single track vehicle are derived and used to derive the error dynamics which form the basis for the lateral controller design. In Chapter 3, the development of the lateral controller including a feedback and feedforward input is described. Hereafter, the closed-loop platoon dynamics are derived, which are used to evaluate the lateral string stability properties. Chapter 5, describes the practical implementation of the controller and the experimental setup and presents the experimental results. Finally, conclusions and recommendations are presented in Chapter 6.

Lateral vehicle dynamics modelling

In this chapter, the lateral dynamics for a vehicle are derived using a single track model. The lateral dynamics are then used to derive the error dynamics which have to be stabilized by a lateral controller later on.

First, in Section 2-1, the equations of motion for a single track vehicle model are derived. Besides the planar vehicle motion, also the dynamics of the steering system are considered. Then, in Section 2-2, the error dynamics are derived and presented as a Linear Time Invariant (LTI) system.

2-1 Equations of motion for a single track vehicle

The single track model is a simplified model that represents the lateral dynamics of a vehicle. This model is often denoted by the 'Bicycle model', because the front and rear axle are both represented by only one, instead of two wheels.

In order to derive the equations of motions for the single track model, first the position of the CoG with respect to a stationary reference frame is introduced. Figure 2-1 shows a single track vehicle in space with the stationary reference frame $S^g = \{O^g, \vec{e}_x^g, \vec{e}_y^g\}$ and a body-fixed frame $S^i = \{O^i, \vec{e}_x^i, \vec{e}_y^i\}$. The origin of the body-fixed frame O^i is located at the CoG of the vehicle and the vector \vec{e}_x^i is oriented in the forward direction along the longitudinal vehicle axis with an angle ψ with respect to \vec{e}_x^g . The position vector of the origin of the body-fixed frame O^i is given by

$$\vec{r}_{O^i/O^g} = [x \quad y] \vec{e}^g \quad (2-1)$$

where $\vec{e}^g = [\vec{e}_x^g \quad \vec{e}_y^g]^T$. The absolute velocity vector of O^i (i.e., with respect to O^g) is expressed in coordinates with respect to \vec{e}^i :

$$\begin{aligned} \dot{\vec{r}}_{O^i/O^g} &= [\dot{x} \quad \dot{y}] \vec{e}^g \\ &= [v_x \quad v_y] \vec{e}^i. \end{aligned} \quad (2-2)$$

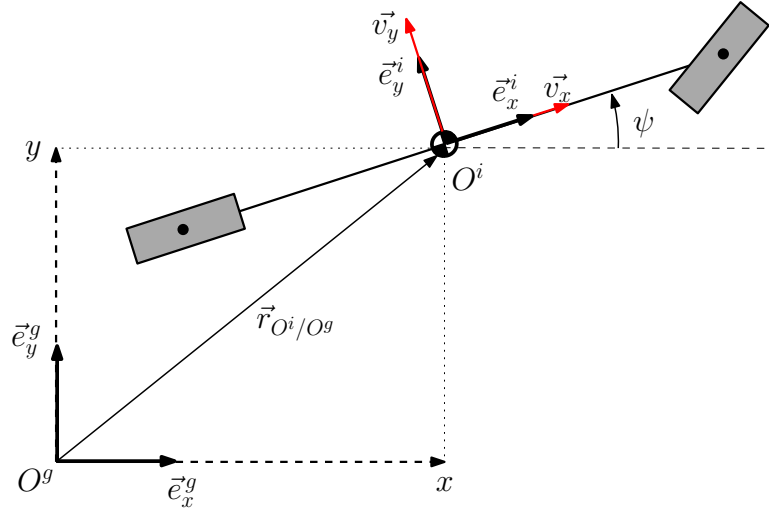


Figure 2-1: Illustration of the vehicle's center of gravity moving in space.

where $\underline{\vec{e}}^i = [\vec{e}_x^i \ \vec{e}_y^i]^T$. The velocity vector can be projected on the stationary reference frame using

$$\underline{\vec{e}}^i = R(\psi)^T \underline{\vec{e}}^g \quad (2-3)$$

where

$$R(\psi) = \begin{bmatrix} \cos(\psi) & -\sin(\psi) \\ \sin(\psi) & \cos(\psi) \end{bmatrix} \quad (2-4)$$

represents the rotation matrix around the vector $\vec{e}_z^g = \vec{e}_x^g \times \vec{e}_y^g$, and ψ is the yaw angle between \vec{e}_x^g and \vec{e}_x^i . The acceleration vector is then obtained by differentiating the velocity vector $\dot{\vec{r}}_{O^i/O^g}$ with respect to time, yielding

$$\ddot{\vec{r}}_{O^i/O^g} = [v_x \ v_y] \dot{\underline{\vec{e}}^i} + [\dot{v}_x \ \dot{v}_y] \underline{\vec{e}}^i. \quad (2-5)$$

Using (2-3), $\dot{\underline{\vec{e}}^i}$ is derived as follows:

$$\begin{aligned} \dot{\underline{\vec{e}}^i} &= \dot{R}(\psi)^T \underline{\vec{e}}^g + R(\psi)^T \dot{\underline{\vec{e}}^g} \\ &= \dot{\psi} \begin{bmatrix} -\sin(\psi) & \cos(\psi) \\ -\cos(\psi) & -\sin(\psi) \end{bmatrix} \underline{\vec{e}}^g \\ &= \dot{\psi} \begin{bmatrix} 0 & 1 \\ -1 & 0 \end{bmatrix} \begin{bmatrix} \cos(\psi) & \sin(\psi) \\ -\sin(\psi) & \cos(\psi) \end{bmatrix} \underline{\vec{e}}^g \\ &= \begin{bmatrix} 0 & \dot{\psi} \\ -\dot{\psi} & 0 \end{bmatrix} \underline{\vec{e}}^i. \end{aligned} \quad (2-6)$$

Substituting (2-6) in (2-5), the acceleration vector can be expressed as

$$\begin{aligned}\ddot{\vec{r}}_{O^i/O^g} &= [v_x \ v_y] \begin{bmatrix} 0 & \dot{\psi} \\ -\dot{\psi} & 0 \end{bmatrix} \underline{\vec{e}}^i + [\dot{v}_x \ \dot{v}_y] \underline{\vec{e}}^i \\ &= [\dot{v}_x - \dot{\psi}v_y \ \dot{v}_y + \dot{\psi}v_x] \underline{\vec{e}}^i\end{aligned}\quad (2-7)$$

where $\dot{\psi}$ is the yaw rate of the vehicle. Forces are generated by the tires as a result of slip with the road surface. The force acting on O^i is given by

$$\vec{F}_{O^i} = [F_x \ F_y] \underline{\vec{e}}^i, \quad (2-8)$$

where F_x is the longitudinal force in the $\underline{\vec{e}}_x^i$ direction and F_y the lateral force in the $\underline{\vec{e}}_y^i$ direction. Let m be the mass of the vehicle. The equations of motion of O^i are then given by

$$m\ddot{\vec{r}}_{O^i/O^g} = \vec{F}_{O^i}. \quad (2-9)$$

Hence, the lateral and longitudinal component are given by

$$m(\dot{v}_y + \dot{\psi}v_x) = F_y \quad (2-10)$$

and

$$m(\dot{v}_x - \dot{\psi}v_y) = F_x, \quad (2-11)$$

respectively.

Now, the single track model, as depicted in Figure 2-2, is introduced. As mentioned before, the vehicle's front and rear axle are each represented by only one wheel. The parameters of the single track model that are presented in Figure 2-2 are: Vehicle body slip angle β , front and rear tire slip angle, α_f and α_r , respectively, front and rear lateral tire forces F_{y_f} and F_{y_r} , the distance a between CoG and front axle, distance b between CoG and rear axle, steering angle δ , yaw rate $\dot{\psi}$, velocity vector of the front wheel \vec{v}_f , velocity vector of the rear wheel \vec{v}_r and the lateral and longitudinal velocity vectors of the CoG, v_y and v_x , respectively. Furthermore, the vehicle has a mass m and moment of inertia I_z , which is defined around the CoG and with respect to an axis spanned by $\underline{\vec{e}}_z^i = \underline{\vec{e}}_x^i \times \underline{\vec{e}}_y^i$. Additionally, small angle approximations are assumed for the angles $\alpha_f, \alpha_r, \beta$ and δ , such that $\sin(\cdot) \approx \cdot$, and $\cos(\cdot) \approx 1$.

Using the small angle approximation for the steer angle δ , the lateral force F_y is the sum of the front and rear lateral tire forces, i.e., $F_y = F_{y_f} + F_{y_r}$. Equivalently, the longitudinal force F_x is the sum of the front and rear longitudinal tire forces, i.e., $F_x = F_{x_f} + F_{x_r}$. Substituting these lateral tire forces into (2-10) and considering the sum of moments around O^i , the equations of motion for the frame S^i can be expressed as

$$\begin{aligned}m(\dot{v}_x - \dot{\psi}v_y) &= F_x \\ m(\dot{v}_y + \dot{\psi}v_x) &= F_{y_f} + F_{y_r} \\ I_z\ddot{\psi} &= aF_{y_f} - bF_{y_r}.\end{aligned}\quad (2-12)$$

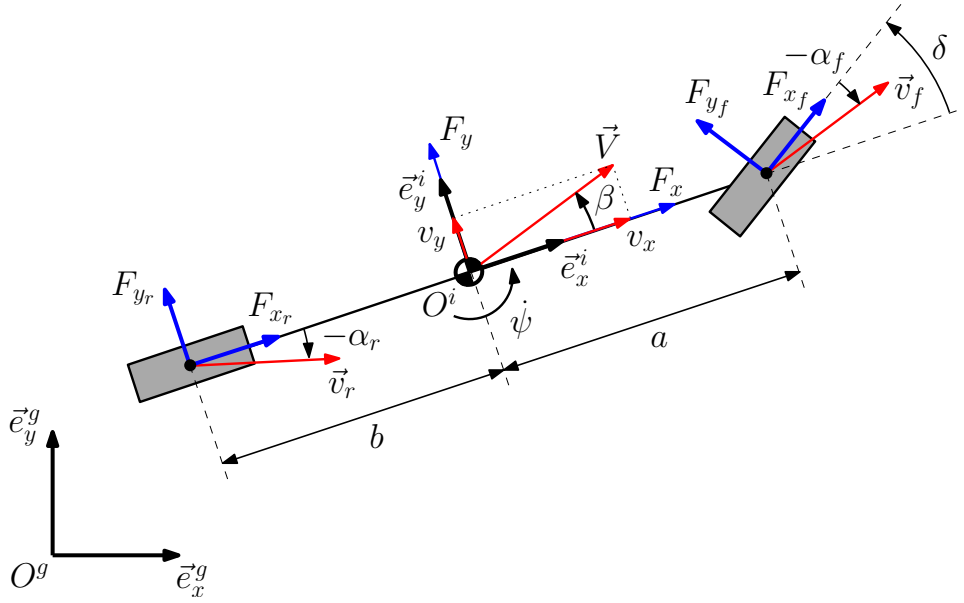


Figure 2-2: Schematic representation of a single track vehicle model.

Since normal highway driving is considered in this thesis, the tires are assumed to operate in the linear regime and therefore the lateral tire forces will be modeled using linear cornering characteristics. Hence, the lateral tire forces are defined as

$$\begin{aligned} F_{yf} &= -C_f \alpha_f \\ F_{yr} &= -C_r \alpha_r, \end{aligned} \quad (2-13)$$

where $C_f > 0$ and $C_r > 0$ are the cornering stiffness of the front and rear tire, respectively. The slip angle is the angle between the direction of the wheel and velocity vector of the wheel. The velocity vector of each wheel has a component in the \vec{e}_x^i and in the \vec{e}_y^i direction. For a single track model, the velocity component in the \vec{e}_x^i direction for both wheels equals the longitudinal velocity v_x of the CoG. This is because both wheels are located on the longitudinal vehicle axis. The lateral component of each wheel, however, consists of the sum of two components; the lateral velocity of the CoG v_y and the tangential velocity that is induced by the yaw rate $\dot{\psi}$. Assuming that the slip angles are small, the slip angles for the front and rear tires are given by

$$\begin{aligned} \alpha_f &= \frac{v_y + a\dot{\psi}}{v_x} - \delta \\ \alpha_r &= \frac{v_y - b\dot{\psi}}{v_x} \end{aligned} \quad (2-14)$$

according to [30]. By substituting the result of (2-13) and (2-14) in (2-12), the resulting dynamics of the single track model become

$$\begin{aligned}
\dot{v}_x &= \dot{\psi}v_y + \frac{F_x}{m} \\
\dot{v}_y &= -\frac{1}{v_x} \left(\frac{C_f + C_r}{m} \right) v_y + \left(\frac{1}{v_x} \left(\frac{-aC_f + bC_r}{m} \right) - v_x \right) \dot{\psi} + \left(\frac{C_f}{m} \right) \delta \\
\ddot{\psi} &= \frac{1}{v_x} \left(\frac{-aC_f + bC_r}{I_z} \right) v_y - \frac{1}{v_x} \left(\frac{a^2C_f + b^2C_r}{I_z} \right) \dot{\psi} + \left(\frac{aC_f}{I_z} \right) \delta.
\end{aligned} \tag{2-15}$$

2-1-1 Global vehicle motion

In this section, the kinematic expressions for the movement of the CoG in space will be derived. The position vector of the CoG in space was defined in (2-1). By differentiating (2-1) with respect to time, the velocity vector becomes

$$\dot{\vec{r}}_{O^i/O^g} = [\dot{x} \quad \dot{y}] \underline{\vec{e}}^g. \tag{2-16}$$

The velocity vector was also defined with respect to the body-fixed frame S^i in (2-2). By substituting (2-3) in (2-2), the velocity vector can be written as

$$\begin{aligned}
\dot{\vec{r}}_{O^i/O^g} &= [v_x \quad v_y] R(\psi)^T \underline{\vec{e}}^g \\
&= [v_x \quad v_y] \begin{bmatrix} \cos(\psi) & \sin(\psi) \\ -\sin(\psi) & \cos(\psi) \end{bmatrix} \underline{\vec{e}}^g \\
&= [v_x \cos(\psi) - v_y \sin \psi \quad v_x \sin(\psi) + v_y \cos(\psi)] \underline{\vec{e}}^g.
\end{aligned} \tag{2-17}$$

By comparing (2-16) and (2-17), the expression for the global velocity in x and y direction becomes

$$\begin{aligned}
\dot{x} &= v_x \cos(\psi) - v_y \sin(\psi) \\
\dot{y} &= v_x \sin(\psi) + v_y \cos(\psi).
\end{aligned} \tag{2-18}$$

2-1-2 Steering dynamics

In this section, the dynamics of the steering system are considered. The angle of the steering wheels is controlled by a ‘low-level controller’. The low-level controller is a closed-loop system that receives a commanded steer input from a high-level controller, and regulates the actual steering wheel angle to track the commanded steer input. The experimental vehicles, that are available at TNO for testing, are equipped with a Park Assist System (PAS) to control the angle of the steering wheels. The PAS has been identified as a second-order system with a delay γ by Fontys and TNO [31]. The dynamics of the steering system can be described by the following second-order system:

$$\ddot{\delta} = -2\zeta\omega_n\dot{\delta} + \omega_n^2(\delta_{ref} - \delta) \quad (2-19)$$

where ζ is the damping, ω_n the natural frequency, δ the actual steering wheel angle and δ_{ref} the commanded steering angle. The actuator delay $\gamma = 0.1$ s, was also identified in the PAS model. This delay is specifically related to the hardware of the available experimental vehicles which were originally not designed for controlling the steering wheels at high speed. Therefore, the actuator delay is not taken into account in the remainder of this thesis.

By combining the equations from (2-15), (2-18) and (2-19), the motion of a vehicle in space can be described by the following set of equations:

$$\begin{aligned} \dot{v}_x &= \dot{\psi}v_y + \frac{F_x}{m} \\ \dot{v}_y &= -\frac{1}{v_x} \left(\frac{C_f + C_r}{m} \right) v_y + \left(\frac{1}{v_x} \left(\frac{-aC_f + bC_r}{m} \right) - v_x \right) \dot{\psi} + \left(\frac{C_f}{m} \right) \delta \\ \ddot{\psi} &= \left(\frac{-aC_f + bC_r}{I_z v_x} \right) v_y - \left(\frac{a^2 C_f + b^2 C_r}{I_z v_x} \right) \dot{\psi} + \left(\frac{aC_f}{I_z} \right) \delta \\ \ddot{\delta} &= -2\zeta\omega_n\dot{\delta} + \omega_n^2(\delta_{ref} - \delta) \\ \dot{x} &= v_x \cos(\psi) - v_y \sin(\psi) \\ \dot{y} &= v_x \sin(\psi) + v_y \cos(\psi). \end{aligned} \quad (2-20)$$

From (2-20), it follows that the vehicle motion is described by a second-order differential equation of the steer system dynamics, and three second-order systems relating to the three degrees of motion (motion in the x,y-plane, and rotation about the vertical axis).

2-2 Error dynamics

In this section, the error dynamics of a vehicle i with respect to a reference path are derived using Figure 2-3. In this figure, the reference path is represented by the curve C . Furthermore, three reference frames are presented; a global stationary reference frame $S^g = \{O^g, \vec{e}_x^g, \vec{e}_y^g\}$, a body-fixed reference frame $S^i = \{O^i, \vec{e}_x^i, \vec{e}_y^i\}$ and a frame $S^s = \{O^s, \vec{e}_x^s, \vec{e}_y^s\}$, where the origin O^s is an orthogonal projection of O^i on the smooth curve C . Consequently, the unit vector \vec{e}_x^s is tangent to C by definition. The angle ψ_i is the angle between \vec{e}_x^g and \vec{e}_x^i , and θ_s is the angle between \vec{e}_x^g and \vec{e}_x^s . Furthermore, the vector \vec{V}_i is the velocity vector of the origin of the body-fixed frame S^i and is defined as

$$\vec{V}_i = [v_{x,i} \ v_{y,i}] \vec{e}^i. \quad (2-21)$$

Note that all variables that are related to the i^{th} vehicle in the platoon are now assigned by the index i . The velocity vector \vec{V}_i has an angle β_i with respect to the longitudinal vehicle axis \vec{e}_x^i , which is generally referred to as the body slip angle [28]. The body slip angle of a vehicle is given by

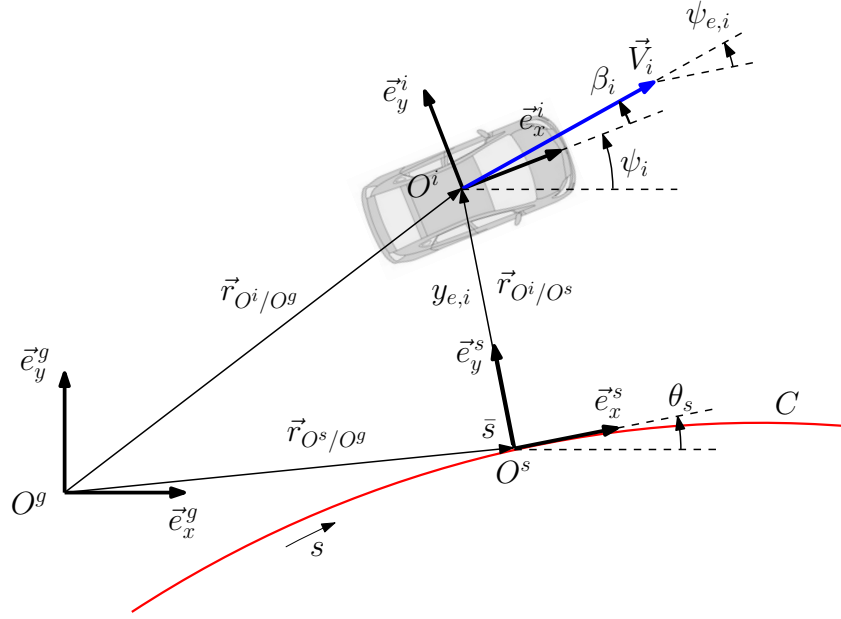


Figure 2-3: Schematic representation of the error dynamics of a vehicle with respect to a reference path.

$$\beta_i = \arctan\left(\frac{v_{y,i}}{v_{x,i}}\right), \quad (2-22)$$

which can be approximated by

$$\beta_i = \frac{v_{y,i}}{v_{x,i}} \quad (2-23)$$

for small body slip angles. The position on the path is parametrized by variable s and the position that is located at O^s is denoted by \bar{s} . The variable $y_{e,i}$ is the distance between O^i and O^s , and hence is the shortest distance between O^i and C , is given by

$$y_{e,i} = \vec{r}_{O^i/O^s} \cdot \vec{e}_y^s, \quad (2-24)$$

where \vec{r}_{O^i/O^s} is the position vector of the origin of the body-fixed frame with respect to the origin of frame S^s . In literature, the heading error $\psi_{e,i}$ of a vehicle with respect to a reference path is often defined as the angle between the longitudinal vehicle axis and the tangent of the reference path [24], [8]. This error definition, however, does not necessarily force the vehicle to move in the tangent direction of the reference path due to its body slip angle β_i . The objective is not necessarily to control the angle of the vehicle body with respect to the reference path to zero, but the angle between the vehicle velocity vector and the tangent of the reference path. Therefore, the body slip angle should be taken into account in the definition of the heading error, i.e.,

$$\psi_{e,i} = \psi_i + \beta_i - \theta_s, \quad (2-25)$$

which represents the angle between the velocity vector \vec{V}_i of the body-fixed frame and the tangent of curve C in point \bar{s} .

In order to describe the error dynamics, the time derivatives of the error states $y_{e,i}$ and $\psi_{e,i}$ must be derived. This is done in the next two sections

2-2-1 Derivation of the error dynamics for $\dot{\psi}_{e,i}$

First, the error dynamics for $\dot{\psi}_{e,i}$ will be derived. Using (2-23), the time derivative of $\psi_{e,i}$ can be expressed as

$$\begin{aligned}\dot{\psi}_{e,i} &= \dot{\psi}_i + \dot{\beta}_i - \dot{\theta}_s \\ &= \dot{\psi}_i + \frac{\dot{v}_{y,i}}{v_{x,i}} - \frac{v_{y,i}}{(v_{x,i})^2} \dot{v}_{x,i} - \dot{\theta}_s.\end{aligned}\quad (2-26)$$

For normal highway driving, the longitudinal velocity $v_{x,i}$ is relatively large while the lateral velocity $v_{y,i}$ is relatively small. Therefore, the term $\frac{v_{y,i}}{(v_{x,i})^2} \dot{v}_{x,i}$ will be small and can be neglected such that (2-26) reduces to

$$\dot{\psi}_{e,i} = \dot{\psi}_i + \frac{\dot{v}_{y,i}}{v_{x,i}} - \dot{\theta}_s. \quad (2-27)$$

If we substitute the expression for \dot{v}_y from (2-15) in (2-27), we finally obtain

$$\dot{\psi}_{e,i} = -p_1 v_{y,i} + p_2 \dot{\psi}_i + p_3 \dot{\delta}_i - \dot{\theta}_s \quad (2-28)$$

with constants

$$\begin{aligned}p_1 &= \frac{1}{v_x^2} \left(\frac{C_f + C_r}{m} \right), \\ p_2 &= \frac{1}{v_x^2} \left(\frac{-aC_f + bC_r}{m} \right), \\ p_3 &= \frac{1}{v_x} \left(\frac{C_f}{m} \right),\end{aligned}\quad (2-29)$$

and where $\dot{\theta}_s$ represents the angular rate of change of the curve C at point \bar{s} .

2-2-2 Derivation of the error dynamics for $\dot{y}_{e,i}$

Now, the error dynamics for $y_{e,i}$ will be derived. The velocity vector of the vehicle is given by

$$\dot{\vec{r}}_{O^i/O^g} = \dot{\vec{r}}_{O^s/O^g} + \dot{\vec{r}}_{O^i/O^s}. \quad (2-30)$$

Note that the frame S^s can only move in the \vec{e}_x^s direction because \vec{e}_x^s is defined to be always tangent to C . Consequently, the velocity in the \vec{e}_y^s direction is always zero and the velocity vector of frame S^s becomes

$$\dot{\vec{r}}_{O^s/O^g} = \dot{\bar{s}}\vec{e}_x^s. \quad (2-31)$$

From (2-24), it follows that $\vec{r}_{O^i/O^s} = y_e\vec{e}_y^s$. The time derivative of \vec{r}_{O^i/O^s} is given by

$$\dot{\vec{r}}_{O^i/O^s} = \dot{y}_{e,i}\vec{e}_y^s + y_{e,i}\dot{\vec{e}}_y^s. \quad (2-32)$$

By considering that $\underline{\vec{e}}^s = R(\theta_s)^T \underline{\vec{e}}^g$, its time derivative $\dot{\underline{\vec{e}}}^s$ can be derived in a similar way as in (2-6), i.e.

$$\dot{\underline{\vec{e}}}^s = \begin{bmatrix} 0 & \dot{\theta}_s \\ -\dot{\theta}_s & 0 \end{bmatrix} \underline{\vec{e}}^s. \quad (2-33)$$

From (2-33), it follows that

$$\dot{\vec{e}}_y^s = -\dot{\theta}_s\vec{e}_x^s \quad (2-34)$$

which can be substituted in (2-32) to obtain

$$\dot{\vec{r}}_{O^i/O^s} = \dot{y}_{e,i}\vec{e}_y^s - y_{e,i}\dot{\theta}_s\vec{e}_x^s. \quad (2-35)$$

By substituting both (2-31) and (2-35) into (2-30), the velocity vector of the body-fixed frame is obtained

$$\dot{\vec{r}}_{O^i/O^g} = \left[\dot{\bar{s}} - y_{e,i}\dot{\theta}_s \quad \dot{y}_{e,i} \right] \underline{\vec{e}}^s. \quad (2-36)$$

Also, from (2-2) it is known that

$$\dot{\vec{r}}_{O^i/O^g} = \begin{bmatrix} v_{x,i} & v_{y,i} \end{bmatrix} \underline{\vec{e}}^i \quad (2-37)$$

whose components, using $\underline{\vec{e}}^i = R(\psi_i - \theta_s)^T \underline{\vec{e}}^s$, can be expressed with respect to frame S^s (see Figure 2-3)

$$\dot{\vec{r}}_{O^i/O^g} = \begin{bmatrix} v_{x,i} \cos(\psi_i - \theta_s) - v_{y,i} \sin(\psi_i - \theta_s) & v_{x,i} \sin(\psi_i - \theta_s) + v_{y,i} \cos(\psi_i - \theta_s) \end{bmatrix} \underline{\vec{e}}^s, \quad (2-38)$$

where the angle $\psi_i - \theta_s$ represents the angle between the vehicle body and the reference path at \bar{s} . It is assumed that this angle is small, such that $\sin(\psi_i - \theta_s) \approx \psi_i - \theta_s$ and $\cos(\psi_i - \theta_s) \approx 1$. By comparing (2-36) and (2-38), and assuming that $\psi_i - \theta_s$ is small, it can be observed that

$$\dot{y}_{e,i} = v_{x,i}(\psi_i - \theta_s) + v_{y,i}. \quad (2-39)$$

Using (2-25), it follows that $\psi_i - \theta_s = \psi_{e,i} - \beta_i$ and hence, (2-39) is equivalent to

$$\dot{y}_{e,i} = v_{x,i}(\psi_{e,i} - \beta_i) + v_{y,i} \quad (2-40)$$

which, after substitution of (2-23) for β_i , becomes

$$\begin{aligned} \dot{y}_{e,i} &= v_{x,i}\left(\psi_{e,i} - \frac{v_{y,i}}{v_{x,i}}\right) + v_{y,i} \\ &= v_{x,i}\psi_{e,i}. \end{aligned} \quad (2-41)$$

Note that the heading error $\psi_{e,i}$ actually is the derivative of the lateral offset $y_{e,i}$, but only multiplied with a factor $v_{x,i}$. By combining the equations of (2-28) and (2-41), finally the error dynamics can be represented by the following set of equations

$$\begin{cases} \dot{y}_{e,i} = v_{x,i}\psi_{e,i} \\ \dot{\psi}_{e,i} = \left(-p_1v_{y,i} + p_2\dot{\psi}_i + p_3\delta_i\right) - \dot{\theta}_s \end{cases} \quad (2-42)$$

Also, it follows from (2-25), that $\psi_i = \psi_{e,i} - \frac{v_{y,i}}{v_{x,i}} + \theta_s$ which can be used to rewrite the expression for \dot{x} in (2-18) as

$$\dot{x}_i = v_{x,i} \cos\left(\psi_{e,i} - \frac{v_{y,i}}{v_{x,i}} + \theta_s\right) - v_{y,i} \sin\left(\psi_{e,i} - \frac{v_{y,i}}{v_{x,i}} + \theta_s\right). \quad (2-43)$$

Now, the following nonlinear state space system $\dot{q}'_i = f(q'_i, w_i) + g_1u_i + g_2w_i$ can be defined:

$$\begin{bmatrix} \dot{y}_{y,i} \\ \dot{\psi}_i \\ \dot{y}_{e,i} \\ \dot{\psi}_{e,i} \\ \dot{\delta}_i \\ \ddot{\delta}_i \\ \dot{x}_i \\ \dot{v}_{x,i} \end{bmatrix} = \begin{bmatrix} -\frac{C_f+C_r}{m} \frac{v_{y,i}}{v_{x,i}} + \frac{-aC_f+bC_r}{m} \frac{\dot{\psi}_i}{v_{x,i}} - v_{x,i}\dot{\psi}_i + \frac{C_f}{m} \delta_i \\ \frac{-aC_f+bC_r}{I_z} \frac{v_{y,i}}{v_{x,i}} - \frac{a^2C_f+b^2C_r}{I_z} \frac{\dot{\psi}_i}{v_{x,i}} + \frac{aC_f}{I_z} \delta_i \\ v_{x,i}\psi_{e,i} \\ -\frac{C_f+C_r}{m} \frac{v_{y,i}}{v_{x,i}^2} + \frac{-aC_f+bC_r}{m} \frac{\dot{\psi}_i}{v_{x,i}^2} + \frac{C_f}{m} \frac{\delta_i}{v_{x,i}} \\ \dot{\delta}_i \\ -\omega_n^2\delta_i - 2\zeta\omega_n\dot{\delta}_i \\ v_{x,i} \cos\left(\psi_{e,i} - \frac{v_{y,i}}{v_{x,i}} + \theta_s\right) - v_{y,i} \sin\left(\psi_{e,i} - \frac{v_{y,i}}{v_{x,i}} + \theta_s\right) \\ \dot{\psi}_i v_{y,i} \end{bmatrix} + \begin{bmatrix} 0 & 0 \\ 0 & 0 \\ 0 & 0 \\ 0 & 0 \\ \omega_n^2 & 0 \\ 0 & 0 \\ 0 & \frac{1}{m} \end{bmatrix} \begin{bmatrix} \delta_{ref} \\ F_x \end{bmatrix} + \begin{bmatrix} 0 & 0 \\ 0 & 0 \\ 0 & 0 \\ 0 & -1 \\ 0 & 0 \\ 0 & 0 \\ 0 & 0 \end{bmatrix} \begin{bmatrix} \theta_s \\ \dot{\theta}_s \end{bmatrix} \quad (2-44)$$

with state vector $q'_i = [v_{y,i} \ \dot{\psi}_i \ y_{e,i} \ \psi_{e,i} \ \delta_i \ \dot{\delta}_i \ x_i \ v_{x,i}]^T$, input $u_i = [\delta_{ref} \ F_x]^T$, disturbance term $w_i = [\theta_s \ \dot{\theta}_s]^T$ and $f(q'_i)$, $g_1(q'_i)$ and $g_2(q'_i)$ are defined accordingly. Note that the states

y_i and ψ_i , given in (2-20), are now replaced by the error states $y_{e,i}$ and $\psi_{e,i}$, respectively. The goal is to control only the lateral dynamics. Therefore, the global x_i -position is removed from the state space system because it is irrelevant for the lateral dynamics and the dynamics of the other states do not depend on x_i . Furthermore, the longitudinal velocity $v_{x,i}$ (and its time derivative $\dot{v}_{x,i}$) will be treated as time varying parameters from here on (fully controlled by a longitudinal controller). Consequently, $v_{x,i}$ is removed from the state vector q_i' as well, such that the system is reduced from 8th-order to 6th-order. Now, the system can be written in the form $\dot{q}_i = Aq_i + B_1u_i + B_2w_i$:

$$\begin{bmatrix} \dot{v}_{y,i} \\ \dot{\psi}_i \\ \dot{y}_{e,i} \\ \dot{\psi}_{e,i} \\ \ddot{\delta}_i \\ \ddot{\delta}_i \end{bmatrix} = \begin{bmatrix} -\frac{1}{v_{x,i}(t)} \left(\frac{C_f + C_r}{m} \right) & \frac{1}{v_{x,i}(t)} \left(\frac{-aC_f + bC_r}{m} \right) & -v_{x,i}(t) & 0 & 0 & \frac{C_f}{m} & 0 \\ \frac{1}{v_{x,i}(t)} \left(\frac{-aC_f + bC_r}{I_z} \right) & -\frac{1}{v_{x,i}(t)} \left(\frac{a^2C_f + b^2C_r}{I_z} \right) & 0 & 0 & 0 & \frac{aC_f}{I_z} & 0 \\ 0 & 0 & 0 & v_{x,i}(t) & 0 & 0 & 0 \\ -\frac{1}{v_{x,i}(t)} \left(\frac{C_f + C_r}{m} \right) & \frac{1}{v_{x,i}(t)} \left(\frac{-aC_f + bC_r}{m} \right) & 0 & 0 & \frac{1}{v_{x,i}(t)} \left(\frac{C_f}{m} \right) & 0 & 0 \\ 0 & 0 & 0 & 0 & 0 & 0 & 1 \\ 0 & 0 & 0 & 0 & 0 & -\omega_n^2 & -2\zeta\omega_n \end{bmatrix} \begin{bmatrix} v_{y,i} \\ \psi_i \\ y_{e,i} \\ \psi_{e,i} \\ \delta_i \\ \dot{\delta}_i \end{bmatrix} + \begin{bmatrix} 0 \\ 0 \\ 0 \\ 0 \\ 0 \\ \omega_n^2 \end{bmatrix} \delta_{ref,i} + \begin{bmatrix} 0 \\ 0 \\ 0 \\ -1 \\ 0 \\ 0 \end{bmatrix} \dot{\theta}_{s,i} \quad (2-45)$$

with the new state vector

$$q_i = [v_{y,i} \ \psi_i \ y_{e,i} \ \psi_{e,i} \ \delta_i \ \dot{\delta}_i]^T, \quad (2-46)$$

input $u_i = \delta_{ref,i}$, disturbance $w_i = \dot{\theta}_s$, and A, B_1 and B_2 are defined accordingly. In the literature, often the derivative error states $\dot{y}_{e,i}$ and $\dot{\psi}_{e,i}$ are used instead of vehicle states $v_{y,i}$ and $\dot{\psi}_i$. The reason why the vehicle states $v_{y,i}$ and $\dot{\psi}_i$ are used here is because this state representation yields only one disturbance term $\dot{\theta}_s$, whereas two disturbance terms $\dot{\theta}_s$ and $\ddot{\theta}_s$ appear when the derivative error states $\dot{y}_{e,i}$ and $\dot{\psi}_{e,i}$ are used instead. Later, when the platoon dynamics are analyzed in Chapter 4, it turns out to be more convenient, if the disturbance is described by only one variable instead of two. That is the reason for using the vehicle states $v_{y,i}$ and $\dot{\psi}_i$ instead of the derivative error states $\dot{y}_{e,i}$ and $\dot{\psi}_{e,i}$.

Looking at the equations in (2-45), it can be observed that the disturbance $\dot{\theta}_{s,i}$ only affects the error state $\psi_{e,i}$ and that $\psi_{e,i}$ only affects the other error state $y_{e,i}$. However, the other vehicle states $v_{y,i}, \psi_i, \delta_i$ and $\dot{\delta}_i$ are not effected at all by either $\psi_{e,i}$ or $y_{e,i}$. Hence the vehicle states $v_{y,i}, \dot{\psi}_i, \delta_i$ and $\dot{\delta}_i$ are not effected by the disturbance $\dot{\theta}_{s,i}$. This is an important insight which will come back later in this thesis.

Also, note that when the time-varying parameter $v_{x,i}$ is chosen to be constant (and hence $\dot{v}_{x,i} = 0$), the following constraint on the system is posed by the equations in (2-15)

$$\dot{\psi}_i v_{y,i} + \frac{F_x}{m} = 0. \quad (2-47)$$

Although this constraint is not of influence when driving in a straight line ($v_{y,i}, \dot{\psi}_i = 0$), when cornering it is assumed that $F_x = -m\dot{\psi}_i v_{y,i}$ such that the force equilibrium in (2-15) is satisfied.

Lateral control design

In order to follow a desired reference path, a steering controller has to be designed to fulfill the path-following control objective. The lateral controller design is based on the assumption that vehicle speed is constant, i.e. $\dot{v}_{x,i} = 0$. Furthermore, it is assumed that each vehicle in the platoon has identical dynamics, i.e., a homogeneous platoon is considered. In this chapter, first the control objective and requirements are formulated in Section 3-1. Then, a feedback control law and the stability criteria are introduced in Section 3-2. The influence of different control gains is discussed both in frequency and time-domain, and an important observation regarding the look-ahead distance is made. In Section 3-3, an additional feedforward input is presented to increase the tracking performance and, finally, in Section 3-4, it is evaluated whether the requirements that were posed in Section 3-1 are met.

3-1 Control objective

In the previous chapter, the error dynamics for the path-following control problem were derived. The control objective is to let the CoG of the vehicle track the desired reference path. In order to achieve this objective, the lateral offset $y_{e,i}$ and heading error $\psi_{e,i}$ must be regulated to zero, i.e.

- $\lim_{t \rightarrow \infty} y_{e,i}(t) = 0$
- $\lim_{t \rightarrow \infty} \psi_{e,i}(t) = 0$.

Moreover, the controller should ensure internal stability of the error dynamics.

3-1-1 Requirements on controller design

For the lateral control design, first a set of requirements is specified. Besides the stability and tracking requirement posed above, also the damping characteristics of the closed-loop system need to be considered. Since the system is of sixth order, it is not possible to specify one damping coefficient for the system. However, we are mainly interested in the response of

the error states $y_{e,i}$ and $\psi_{e,i}$, because these signals affect how the reference path evolves in upstream platoon direction. If there is overshoot in the response for these error signals, this overshoot will grow in upstream platoon direction, which is undesired. Hence, the controller should be designed such that the response for $y_{e,i}$ and $\psi_{e,i}$ is at least critically damped.

Secondly, the closed-loop system should have sufficient bandwidth to be able to follow the desired path. The bandwidth is defined as the frequency of the angular rate of change of the reference path $\dot{\theta}_s$ that the vehicle should be able to track. In order to obtain a minimum bandwidth requirement, a lane-change maneuver (as depicted in Figure 3-1) is considered as a 'worst case scenario' in terms of controller bandwidth. It is assumed that a lane-change maneuver can be described by a sinusoidal path. If the vehicle should be able to perform a lane-change within 3 seconds (as illustrated in Figure 3-1), the period of the sinusoidal path is 6 seconds which means that the controller should have a minimum bandwidth of $\frac{1}{6} = 0.167$ Hz. For the remainder of this thesis, this bandwidth will be used as a requirement for the controller design.

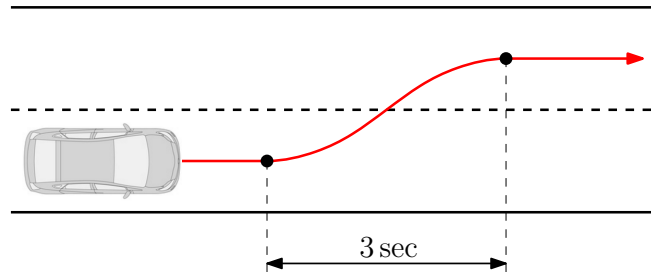


Figure 3-1: Illustration of a 'sinusoidal' lane-change maneuver.

Finally, in addition to the requirements for one single vehicle, also requirements for the response of a string of vehicles are posed. Namely, the controller should result in a laterally string-stable behavior for an infinite string of vehicles. This means that the controller should track low-frequency steering maneuvers of its preceding vehicle, but attenuate high-frequency disturbances such that these are damped out in upstream platoon direction.

All the controller requirements are briefly presented below:

- The controller should render the error dynamics internally asymptotically stable and the error states $y_{e,i}$ and $\psi_{e,i}$ should asymptotically converge to zero.
- The response of the error states $y_{e,i}$ and $\psi_{e,i}$ must be critically damped.
- The bandwidth of the closed-loop system should be at least 0.167 Hz.
- The controller has to yield laterally string-stable behavior.

3-2 Output feedback control

In order to fulfill the control objectives, stabilizing control is required. A static output feedback controller is designed that regulates both error states $y_{e,i}$ and $\psi_{e,i}$ to zero. Later, in

Section 3-4, it will be evaluated if this static output feedback controller meets all the requirements that were posed in the previous section. In order to control the error states $y_{e,i}$ and $\psi_{e,i}$ to zero, the following output feedback controller is adopted

$$\begin{aligned}\delta_{fb,i} &= -Kz_i \\ &= -[k_1 \ k_2]z_i,\end{aligned}\tag{3-1}$$

where the output z_i is defined as

$$z_i = C_1q_i,\tag{3-2}$$

with $C_1 = \begin{bmatrix} 0 & 0 & 1 & 0 & 0 & 0 \\ 0 & 0 & 0 & 1 & 0 & 0 \end{bmatrix}$. The control input $\delta_{fb,i}$ then becomes

$$\begin{aligned}\delta_{fb,i} &= -KC_1q_i \\ &= -(k_1y_{e,i} + k_2\psi_{e,i}).\end{aligned}\tag{3-3}$$

where the control gains k_1 and k_2 penalize the lateral offset $y_{e,i}$ and heading error $\psi_{e,i}$, respectively. If the output feedback control input $\delta_{fb,i} = -KC_1q_i$ is substituted in the state space system presented in (2-45), it can be shown that the expression for the closed-loop system matrix becomes $A_{cl,i} = A - B_1k_1C_1$. The stability of the closed-loop system under the control law in (3-3), is assessed by evaluating the eigenvalues of the closed-loop system matrix $A_{cl,i}$, which is given by

$$A_{cl,i} = \begin{bmatrix} -\frac{1}{v_{x,i}}\left(\frac{C_f+C_r}{m}\right) & \frac{1}{v_{x,i}}\left(\frac{-aC_f+bC_r}{m}\right) - v_{x,i} & 0 & 0 & \frac{C_f}{m} & 0 \\ \frac{1}{v_{x,i}}\left(\frac{-aC_f+bC_r}{I_z}\right) & -\frac{1}{v_{x,i}}\left(\frac{a^2C_f+b^2C_r}{I_z}\right) & 0 & 0 & \frac{aC_f}{I_z} & 0 \\ 0 & 0 & 0 & v_{x,i} & 0 & 0 \\ -\frac{1}{v_{x,i}^2}\left(\frac{C_f+C_r}{m}\right) & \frac{1}{v_{x,i}^2}\left(\frac{-aC_f+bC_r}{m}\right) & 0 & 0 & \frac{1}{v_{x,i}}\left(\frac{C_f}{m}\right) & 0 \\ 0 & 0 & 0 & 0 & 0 & 1 \\ 0 & 0 & -\omega_n^2k_1 & -\omega_n^2k_2 & -\omega_n^2 & -2\zeta\omega_n \end{bmatrix}.\tag{3-4}$$

The determinant of $(\lambda I - A_{cl})$ yields the characteristic equation of the system:

$$a_0 + a_1\lambda + a_2\lambda^2 + a_3\lambda^3 + a_4\lambda^4 + a_5\lambda^5 + \lambda^6 = 0.\tag{3-5}$$

The stability criteria for this system can be obtained using the Routh-Hurwitz criterion [32]. However, it turns out that the expressions that are required in the Routh-Hurwitz criterion are quite extensive. This makes it hard to determine stability conditions for the control gains k_1 and k_2 . Therefore, the stability criteria for k_1 and k_2 are obtained numerically. This is

done by iteratively evaluating the eigenvalues of (3-4) for a set of k_1 and k_2 gains. This analysis is done for different longitudinal vehicle speeds $v_{x,i}$, as can be observed in Figure 3-2. The region below the surface is the stable region of the closed-loop system. It can be observed that the stable region significantly reduces for higher vehicle speeds. For example, when $k_1 = 0.5$ and $k_2 = 2$, the system is stable for longitudinal vehicle speeds $v_{x,i} < 20$ m/s, but for higher vehicle speeds the system becomes unstable. Also, it can be observed that, for high speeds, the control gain k_2 needs to be significantly larger than k_1 in order to obtain stability. The reason for this is analyzed in more details in the next section.

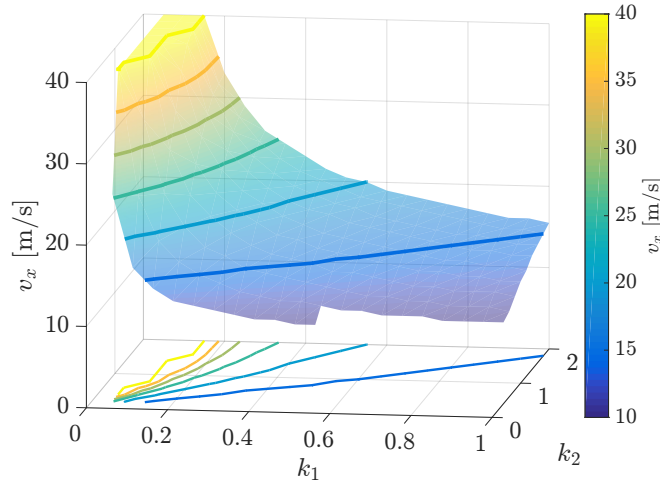


Figure 3-2: Stability conditions for the control gains k_1 and k_2 for different longitudinal vehicle speeds $v_{x,i}$ ranging from 10 - 40 m/s. The region below the surface induces stable behavior.

3-2-1 The role of heading information in the feedback law

In literature, the control error is often defined as the offset between a so-called 'look-ahead' point in front of the vehicle, and the reference path [19]. The concept is illustrated in Figure 1-1, where y_{la} is the position offset at the look-ahead point L . It is often reported that if the look-ahead distance is too small, the system is under-critically damped or might even become unstable [7], [33]. Increasing the look-ahead distance, has a similar effect as penalizing the heading error [24]. Therefore, let us investigate the influence of gain k_2 on the closed-loop response. The gain k_1 will be kept constant at 0.05 for now and will be varied later on to investigate the influence of k_1 on the closed-loop response.

Using the parameters of Table 3-1 and a longitudinal vehicle speed $v_{x,i} = 20$ m/s, the closed-loop poles of the system are obtained which are presented in Figure 3-4. The figure shows the closed-loop poles of the system for varying values of k_2 (between 0 and 2), and k_1 set equal to 0.05. The effect of the gain k_1 on the system response is discussed later in Section 3-2-3.

It can be observed that for small values of k_2 , two poles are in the right-half plane which indicates that the system is unstable. This corresponds to what is reported in literature, since increasing the gain k_2 is equivalent to increasing the look-ahead distance. In [7] and [24], however, it is shown that if the look-ahead distance is too large, the controller becomes too sensitive to vehicle yaw motion which induces yaw oscillations. The pole pair that is

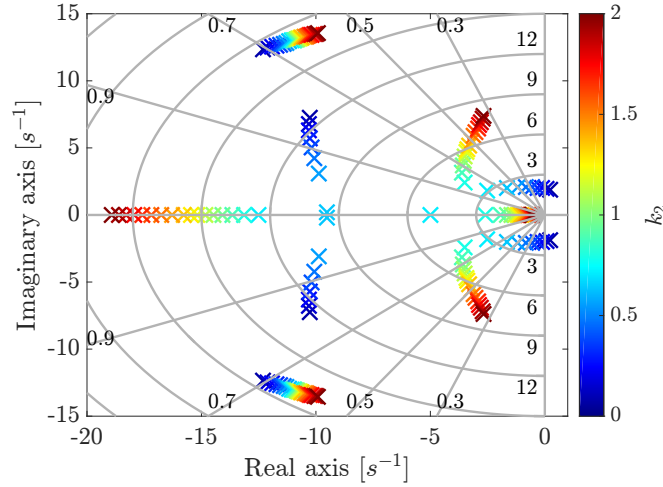


Figure 3-3: Closed-loop pole locations for $k_1 = 0.05$ and k_2 varying from 0 to 2, using vehicle parameters of Table 3-1 and longitudinal vehicle speed $v_{x,i} = 20$ m/s.

located closest to the origin is often referred to as the dominant pole pair. From Figure 3-3, it can be observed that the angle between the dominant pole pair and the real axis increases for larger values of k_2 . This indicates that the damping of these poles indeed decreases when the heading error is penalized more. If the control gains are designed carefully though, appropriate damping characteristics can be obtained.

A better explanation for the unstable poles for small values of k_2 , is obtained by further analyzing the dynamics of the single track model. Figure 3-4a shows the open-loop phase response of the response of vehicle rotation ψ_i and the lateral position error $y_{e,i}$ with respect to a straight reference path (assuming zero initial conditions, i.e. $y_{e,i}(0) = 0$) for a steer input $\delta_{ref,i}$. It can be observed that for low frequencies, the rotation ψ_i has a phase delay of 90 degrees and $y_{e,i}$ a delay of 180 degrees with respect to the steer input $\delta_{ref,i}$. At higher frequencies the phase delay drops by another 180 degrees (to 360 degrees) due to two extra poles which are related to the steering dynamics.

Figure 3-4b, shows the time response of ψ_i and $y_{e,i}$ to a 0.1 Hz sinusoidal steer input $\delta_{ref,i}$. It can be observed that the phase delay for both ψ_i and $y_{e,i}$ is approximately 90 and 180 degrees

Table 3-1: Vehicle parameters for a benchmark vehicle.

	Toyota Prius
a [m]	1.1
b [m]	1.6
C_f [N/rad]	100000
C_r [N/rad]	200000
m [kg]	1650
I_z [N/m ²]	2900
ζ [-]	0.7
ω_n [rad/s]	17.5

which corresponds to the phase delay in the phase plot of Figure 3-4a at 0.1 Hz. The extra 90 degree phase delay of $y_{e,i}$ with respect to ψ_i is because the transfer function from $\delta_{ref,i}$ to $y_{e,i}$ includes a double integrator, compared to a single integrator for the yaw angle ψ_i . In other words, a vehicle first has to rotate before $y_{e,i}$ is affected which causes an additional phase delay and the heading error acts like the derivative of $y_{e,i}$.

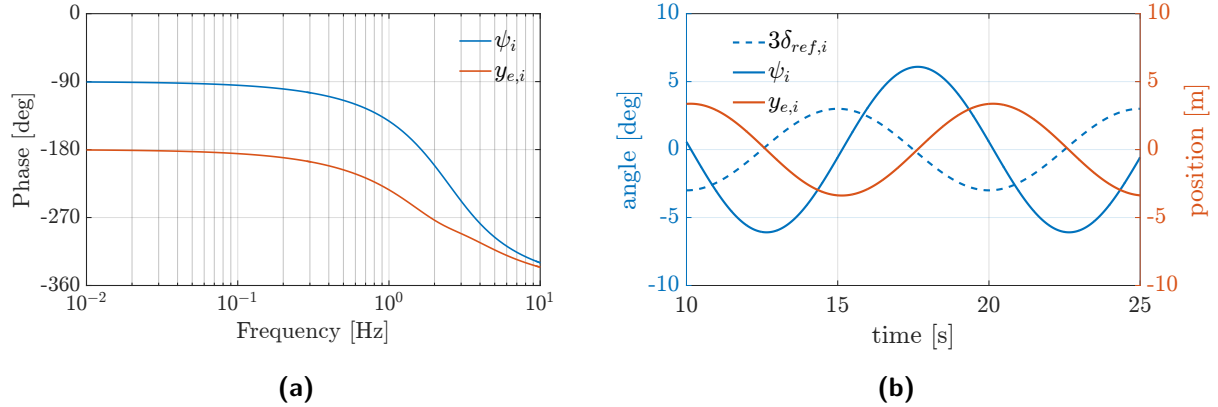


Figure 3-4: Response of $y_{e,i}$ and ψ_i of a single track model with steer input $\delta_{ref,i}$. (a) Phase plot of transfer function from $\delta_{ref,i}$ to $y_{e,i}$ and ψ_i and (b) time response of $y_{e,i}$ and ψ_i for a 0.1 Hz sinusoidal steer input. The steer input $\delta_{ref,i}$ was multiplied by a factor 3 to better visualize the signal with respect to ψ_i and $y_{e,i}$.

Knowing this, it is easy to understand that the system becomes unstable if the heading error $\psi_{e,i}$ is not or hardly penalized. In that case, all the feedback comes from the lateral offset $y_{e,i}$ which means that the feedback signal has a phase lag of at least 180 degrees with respect to the input $\delta_{ref,i}$ resulting in an unstable system.

If the heading error is penalized simultaneously with the lateral offset, part of the feedback signal has a phase delay of 90 degrees with respect to the steer input. This way, the closed-loop system can be stabilized because the phase margin of the input $\delta_{ref,i}$ to the output z_i as defined in (3-2) becomes positive and the unstable poles move to the left-half s -plane.

So the need for sufficient look-ahead distance as often reported in the literature, can be traced back to the phase of the feedback signal. In order to achieve stability and appropriate damping characteristics, the feedback signal should contain enough heading information. One way to achieve this is to incorporate a look-ahead distance, but the heading error could also be penalized directly such that vehicles do not cut corners (which is proposed in this work).

3-2-2 Transient response characteristics

Figure 3-5 shows the time response of the system states for an initial condition perturbation. The initial condition is 0.5 m offset from a straight reference path, i.e. $q(0) = [0 \ 0 \ 0.5 \ 0 \ 0 \ 0]$ and $\dot{\theta}_s = 0$. The vehicle speed $v_{x,i} = 20$ m/s and the vehicle parameters presented in Table 3-1 were used for the simulation.

The time responses in Figure 3-5 show an underdamped response for $y_{e,i}$ and $\psi_{e,i}$ with a low natural frequency for $k_2 = 0.5$. When k_2 is increased to 1, the response of $y_{e,i}$ and $\psi_{e,i}$ is improved, i.e., the damping increases and the states converge to zero faster. If the gain k_2 is increased to 2, the response becomes significantly slower as is clearly seen in the response of $y_{e,i}$ for example. Also, a higher frequency oscillation can be observed in the response of the heading error $\psi_{e,i}$ and in the other vehicle states. This oscillation is caused by two poles that approach the imaginary axis in Figure 3-3 for high values of k_2 .

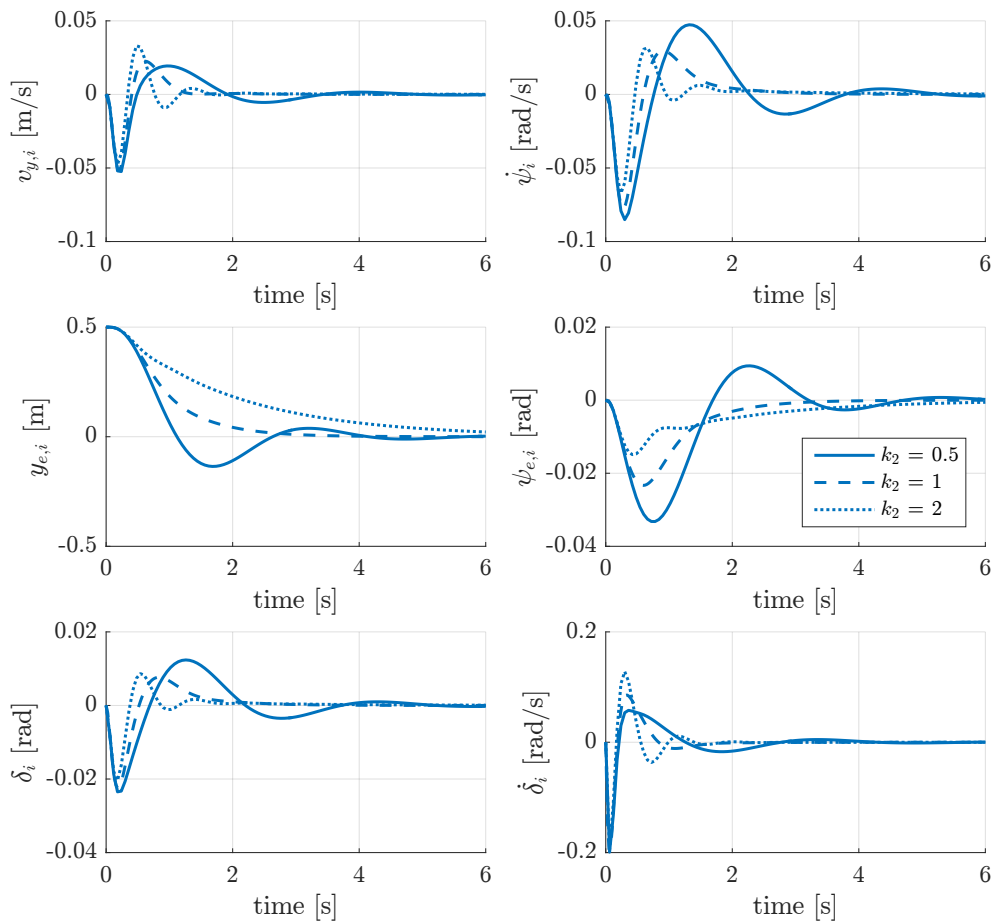


Figure 3-5: Transient response characteristics of the closed-loop system for $k_1 = 0.05$, $k_2 = 0.5$, 1 and 2, using vehicle parameters of Table 3-1 and longitudinal vehicle speed $v_{x,i} = 20$ m/s.

3-2-3 Influence of gain k_1

Now we have a clear understanding of the influence of gain k_2 on the closed-loop system response. Next, the influence of gain k_1 is investigated. Figure 3-6 shows the poles of the matrix in (3-4) for different values of k_1 . Gain k_2 is varied again from 0 to 2 similar to what was done in Figure 3-3 and a longitudinal vehicle speed $v_{x,i} = 20$ m/s is considered.

It can be observed that the gain k_1 mainly affects the most dominant pole pair. The other pole pairs are hardly influenced by k_1 . The overall trend that is observed in Figure 3-6, is that for higher values of k_1 , the dominant pole pair moves towards the imaginary axis. This indicates that the damping of the system is reduced. In addition, it can be observed that k_2 needs to be increased for higher values of k_1 to obtain stability. This corresponds to what was observed earlier in Figure 3-2.

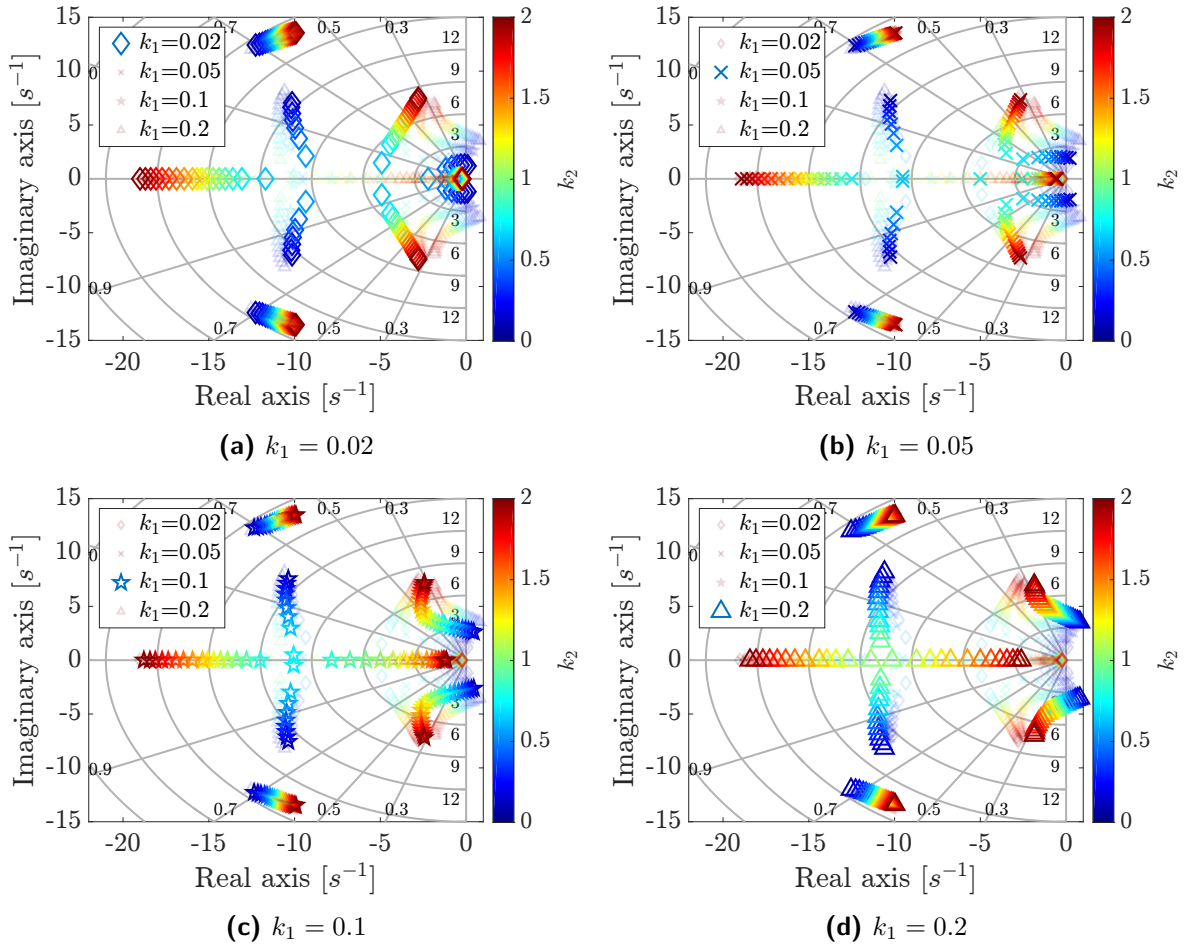


Figure 3-6: Closed-loop poles of the closed-loop system matrix in Equation (3-4), using vehicle parameters of Table 3-1 and $v_{x,i} = 20$ m/s. In all plots, k_2 varies from 0 to 2 and in (a) $k_1 = 0.02$, in (b) $k_1 = 0.05$, in (c) $k_1 = 0.1$ and in (d) $k_1 = 0.2$.

So far, only a longitudinal speed of 20 m/s is considered. However, in Appendix A, the closed-loop poles for longitudinal vehicle speeds of 10, 30 and 40 m/s are presented as well. The main observation is that the dominant pole pair moves towards the imaginary axis for higher

longitudinal speeds. Also, the heading error needs to be penalized more to obtain stability. In conclusion, higher vehicle speeds $v_{x,i}$ appear to have a similar effect on the closed-loop poles as increasing the gain k_1 . In other words, the gain k_1 should be decreased for higher vehicle speeds.

3-2-4 Internal dynamics

It can be observed in Figure 3-5, that for relatively high k_2 gains, the response of $y_{e,i}$ is properly damped, while the response of other states (such as the yaw rate $\dot{\psi}_i$ and steer dynamics δ_i and $\dot{\delta}_i$) can still be oscillatory. In the literature it is reported that if the heading error $\psi_{e,i}$ is penalized too much, the system becomes too sensitive for vehicle yaw motion which induces yaw oscillations [7], [24]. Even though the system is internally asymptotically stable, we do not have full control over all states of the system. That is the reason that we cannot obtain a critically damped response for all states, given the current control architecture.

In order to have more control authority to better control the internal dynamics and the overall system response, the problem should be formulated as a linear output regulation problem as is described in [34]. This provides more control authority to control the dynamic response of the other states of the system as well.

3-3 Feedforward control input

In order to improve the tracking performance of the system, a feedforward controller is introduced. The feedforward controller should cancel out the disturbance $\dot{\theta}_s$ in (2-45), which is the angular rate of change of the reference path. There are multiple ways to design a feedforward controller. The two most obvious approaches are:

- Evaluate the curvature of the reference path and design a feedforward controller based on an inverse vehicle model to obtain the required steer input to track the desired reference curvature.
- Obtain the commanded steer input of the preceding vehicle by wireless communication and apply the same steer input at a later time instance. This, obviously, only holds for homogeneous platoons.

In the next two sections 3-3-1 and 3-3-2, the difference between both feedforward controllers is discussed, after which a feedforward controller is chosen.

3-3-1 Feedforward based on the curvature of the reference path

First, a feedforward controller based on the curvature of the reference path κ_{ref} is considered. In that case, the required steer input needs to be obtained given a reference curvature κ_{ref} . This reference curvature can be translated into a desired angular rate of change of the direction of motion of the vehicle using the vehicle speed. The direction of motion is given by the direction of the vehicle's velocity vector \vec{V}_i . According to Figure 2-3, the angle of the velocity

vector is described by $\psi_i + \beta_i$. Hence, the angular rate of change of the velocity vector is described by its time derivative $\dot{\psi}_i + \dot{\beta}_i$.

Assuming that the lateral velocity component $v_{y,i}$ is small, the magnitude of the velocity $|\vec{V}_i|$ can be approximated by the longitudinal velocity component $v_{x,i}$. Then, the relation between the curvature κ_i of the path of a vehicle and the angular rate of change of the vehicle's velocity vector $\dot{\psi}_i + \dot{\beta}_i$ can be described by

$$\kappa_i = \frac{\dot{\psi}_i + \dot{\beta}_i}{v_{x,i}}. \quad (3-6)$$

The body slip angle β_i is not a state of the system, but by substituting (2-26) in (2-28), the angular rate of change of the velocity vector $\dot{\psi}_i + \dot{\beta}_i$ can be written in terms of vehicle states as

$$\dot{\psi}_i + \dot{\beta}_i = -p_1 v_{y,i} + p_2 \dot{\psi}_i + p_3 \delta_i, \quad (3-7)$$

with constants p_1, p_2 and p_3 which are given in (2-29). The angular rate of change of the vehicle's velocity vector $\dot{\psi}_i + \dot{\beta}_i$ will from here on be denoted by \mathcal{H}_i for its more compact notation, i.e., $\dot{\psi}_i + \dot{\beta}_i =: -p_1 v_{y,i} + p_2 \dot{\psi}_i + p_3 \delta_i =: \mathcal{H}_i$.

In order to obtain a feedforward control input, the open-loop relation between the steer input $\delta_{ref,i}$ and the angular rate of change of the vehicle's velocity vector \mathcal{H}_i has to be obtained. In (2-45), it can be observed that the state space system has two inputs, $\delta_{ref,i}$ and $\dot{\theta}_{s,i}$. So, the output \mathcal{H}_i is obtained by considering both the relation from $\delta_{ref,i-1}$ to \mathcal{H}_i and from $\dot{\theta}_{s,i}$ to \mathcal{H}_i , i.e.,

$$\mathcal{H}_i(s) = G_1(s)\delta_{ref,i}(s) + G_2(s)\dot{\theta}_{s,i}(s). \quad (3-8)$$

However, it can be observed in (2-45) that $\dot{\theta}_{s,i}$ only affects $\psi_{e,i}$ and that $\psi_{e,i}$ only affects $y_{e,i}$ which does not effect any other state. According to (3-7), the angular rate of change of the vehicle's direction of motion depends on the vehicle states $v_{y,i}, \dot{\psi}_i$ and δ_i and is therefore not affected by the disturbance $\dot{\theta}_{s,i}$. Hence, $G_2(s) = 0$ and only the transfer function $G_1(s)$, which will be denoted by the vehicle transfer function from here on, describes the relation between $\delta_{ref,i}$ and \mathcal{H}_i . The vehicle transfer function $G_1(s)$ can be described by

$$G_1(s) = C_2(sI - A)^{-1}B_1 \quad (3-9)$$

where $C_2 = [-p_1 \ p_2 \ 0 \ 0 \ p_3 \ 0]$, $B_1 = [0 \ 0 \ 0 \ 0 \ 0 \ \omega_n^2]^T$, and A is as in (2-45). Hence, the inverse vehicle transfer function $G_1^{-1}(s)$ describes the relation between \mathcal{H}_i and $\delta_{ref,i}$. In order to obtain the required steer input $\delta_{ref,i}$ to follow a reference curvature κ_{ref} , first κ_{ref} has to be multiplied by the longitudinal vehicle speed $v_{x,i}$ to obtain the desired angular rate of change of the vehicle's direction of motion $\mathcal{H}_{ref,i}$, see (3-6). Then, the required steer input $\delta_{ref,i}$ to track $\mathcal{H}_{ref,i}$ is obtained by the inverse vehicle transfer function $G_1^{-1}(s) = \frac{\delta_{ref,i}(s)}{\mathcal{H}_{ref,i}(s)}$. The inverse vehicle transfer function $G_1^{-1}(s)$, which is presented in Figure 3-7, is of the following form

$$G_1^{-1}(s) = \frac{n_4 s^4 + n_3 s^3 + n_2 s^2 + n_1 s + n_0}{d_2 s^2 + d_1 s + d_0}. \quad (3-10)$$

It can be observed that the order of the numerator is larger than the order of the denominator, which means that $G_1^{-1}(s)$ is not proper. However, $G_1^{-1}(s)$ could be approximated (for low frequencies) by a proper transfer function to obtain a feedforward steer input. In order to obtain a proper transfer function, two additional poles need to be added to $G_1^{-1}(s)$. Therefore, $G_1^{-1}(s)$ is multiplied by the following second-order low-pass filter

$$H_2(s) = \frac{1}{\frac{1}{\omega_c^2} s^2 + 2 \frac{\beta}{\omega_c} s + 1} \quad (3-11)$$

where $\omega_c = 1$ Hz and $\beta = 1$, to make the system proper. Now, the required feedforward steer input to track $\mathcal{H}_{ref,i}$ is obtained by $H_2(s)G_1^{-1}(s)$, i.e.

$$H_2(s)G_1^{-1}(s) = \frac{\delta_i}{\mathcal{H}_{ref,i}}. \quad (3-12)$$

In Figure 3-7, it can be observed that $H_2(s)G_1^{-1}(s)$ is a good approximation of $G_1^{-1}(s)$ for low frequencies and that the phase delay is small. This means that for low frequencies $H_2(s)G_1^{-1}(s)$ is a good feedforward controller, but for higher frequencies it will start to perform worse, because for higher frequencies $H_2(s)G_1^{-1}(s)$ does not approximate $G_1^{-1}(s)$ well anymore.

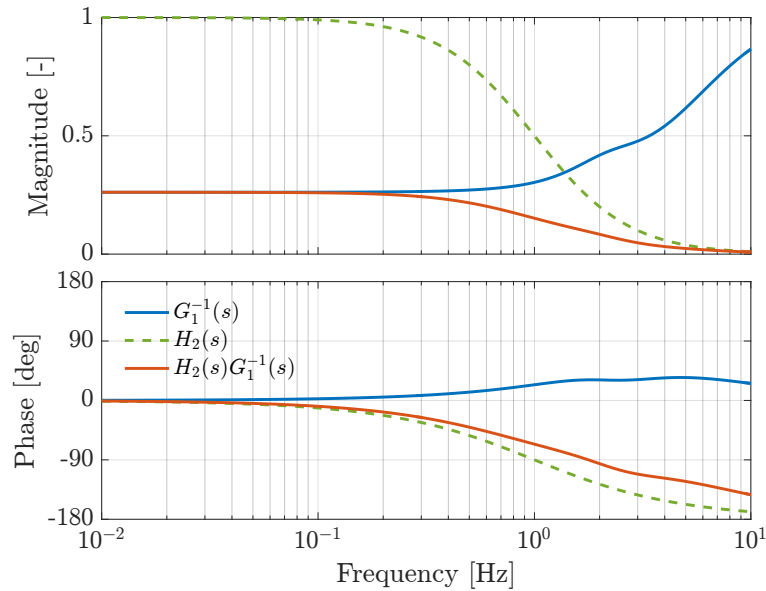


Figure 3-7: Bode plot of the inverse transfer function $G_1^{-1}(s)$ together with the second-order low-pass filter $H_2(s)$ and $H_2(s)G_1^{-1}(s)$.

Despite the fact that the feedforward controller described in (3-12) does not perfectly track the desired reference curvature κ_{ref} , this feedforward controller also has advantages. First, in contrast to the feedforward controller based on the steer input of the preceding vehicle, this

method does not rely on wireless communication. Hence, this feedforward controller is not subjected to communication impairments such as latency and packet loss.

Another difference of using the curvature of the reference path instead of the communicated steer input is that it will not conflict with the feedback controller in case the preceding vehicle experiences an external disturbance such as a wind gust. In that case, the path of the preceding vehicle differs from the path that is expected based on the applied steer input. If the communicated steer input is used as a feedforward input, the feedback and feedforward control input will be conflicting. If the curvature of the reference path is used instead, this conflict does not occur, because both the feedback and feedforward control input are related to the same point on the same reference path. On the other hand, one can argue whether it is actually desired to follow the path of a preceding vehicle which has experienced a lateral disturbance.

3-3-2 Feedforward controller based on steer input of preceding vehicle

A second option to design a feedforward controller is to use the steer input of the preceding vehicle. The steer input that is applied by the preceding vehicle can be obtained through wireless inter-vehicle communication. Due to the inter-vehicle distance, the feedforward steer input should be applied at a later time instance. How and when the received steer input should be applied by the following vehicle, is discussed in more detail later in this section.

First, it should be noted that communicating the commanded steer input only works for homogeneous platoons. For non-homogeneous platoons, a 'commanded reference curvature' could be communicated instead of the commanded steer angle. The commanded reference curvature is the steady-state curvature of the vehicle's path for a constant steer input and longitudinal vehicle speed. Note that for transients, this commanded reference curvature is different from the actual curvature of the path of a vehicle. Using the commanded reference curvature, each vehicle can obtain the required steer input using a vehicle model. In the remainder of this thesis only homogeneous platoons will be considered such that the commanded steer angle can be used.

How to relate the feedforward steer input to position along the path

Let us now explain how the following vehicle determines when it should apply the received steer input of its predecessor. Due to the existing inter-vehicle distance, it is obvious that the steer input of the preceding vehicle should not directly be applied once it is received by the following vehicle. Let us at this point define the time gap Δt between two vehicles as the time it takes vehicle i , given its current vehicle speed, to reach the position of vehicle $i - 1$, if it follows the same path driven by vehicle $i - 1$. Then, the feedforward steer input that is received through wireless communication, should be delayed by a time period Δt to follow the same path of the preceding vehicle. However, delaying the feedforward input by a constant time period will induce small errors, because the time gap Δt will not be constant in practice (even if $v_{x,i}$ and $v_{x,i-1}$ are constant).

This is for example the case when a vehicle experiences a lateral disturbance as is illustrated in Figure 3-8. This figure illustrates the error that is made when the received steer input of

the preceding vehicle (described by the black line) is delayed by a constant time period Δt and the following vehicle (described by the red line) experiences a lateral disturbance.

In Figure 3-8, the time gap between vehicle $i - 1$ and i is Δt . At time t_1 , vehicle $i - 1$ starts cornering. Vehicle i follows vehicle $i - 1$, but experiences a lateral disturbance and therefore does not yet reach the corner entry at time $t_1 + \Delta t$. If the steer input of the preceding vehicle would have been delayed by a time period Δt , vehicle i starts cornering at position s_1 which is not desired.

If the steer input of vehicle $i - 1$ would be related to its path, vehicle i could apply the same steer input as vehicle $i - 1$ when it reaches the same position along the path where the input was applied by vehicle $i - 1$. In that case, the feedforward input is not related to the time gap Δt anymore and vehicle i starts cornering at position s_2 in Figure 3-8.

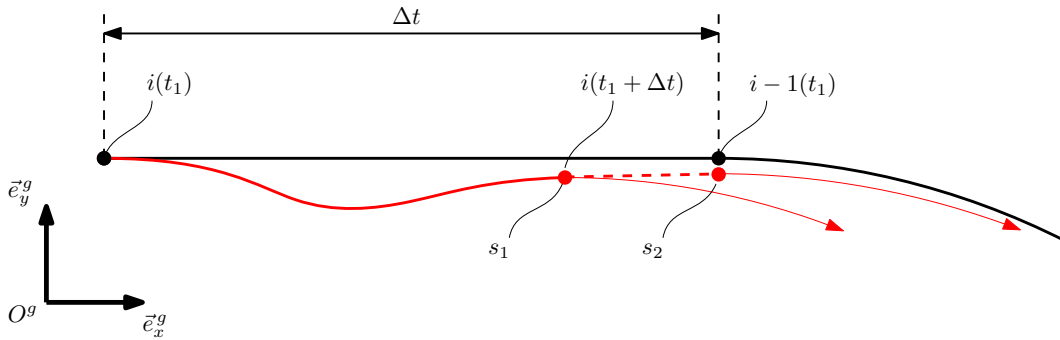


Figure 3-8: Illustration of the effect of a lateral disturbance on the timing of the feedforward input.

Figures 3-9a and 3-9b explain how the steer input of a preceding vehicle can be related to the position along its path. In Figure 3-9a, two vehicles are represented with reference frames $S^i = \{O^i, \vec{e}_x^i, \vec{e}_y^i\}$ and $S^{i-1} = \{O^{i-1}, \vec{e}_x^{i-1}, \vec{e}_y^{i-1}\}$. The path of vehicle $i - 1$ is locally parametrized by the variable s and the position with the shortest distance to O^i is denoted by \bar{s} . Furthermore, the (red) path segment has start point s_0 . Since only recent path information is relevant to the lateral controller, the start point s_0 is updated over time to limit the length of the reference path. The procedure of constructing the path and updating the start point s_0 is explained in more detail in Chapter 5.

In order to relate a new received steer input $\delta_{ref,i-1}$ to the position along the path of vehicle $i - 1$, the position s along the path has to be determined. The position s is obtained by evaluating the length L of the path from s_0 to O^{i-1} . If the path can be described by a polynomial $P(x)$, then according to [35] the length of the path is given by

$$L = \int_{x_1}^{x_2} \sqrt{1 + \left(\frac{dP(x)}{dx}\right)^2} dx, \quad (3-13)$$

where x_1 is the x-position of s_0 and x_2 the x-position of O^{i-1} , with respect to frame S^i . This way, vehicle i keeps track of the applied steer input of its preceding vehicle $\delta_{ref,i-1}$ versus the position s along its driven path. This is visualized in Figure 3-9b where the applied steer input of vehicle $i - 1$ is stored versus the position variable s .

Vehicle i uses this figure as a lookup table to determine its own feedforward input based on \bar{s} . Every time step, vehicle i determines \bar{s} using (3-13) where x_1 is the x-position of s_0 and x_2 the x-position with the shortest distance form O^i to the path. Figure 3-9b is then used as a lookup table to determine the applied steer input of the preceding vehicle at position \bar{s} , as is illustrated by the black dashed line.

As mentioned before, the start point s_0 is updated over time and consequently, all the stored steer inputs have to be assigned to a new s value. This procedure, however, is discussed in more detail in Chapter 5. Also, in practice $\delta_{ref,i-1}$ is not continuously available, because it is received at discrete time instances through wireless communication. Chapter 5 also explains how $\delta_{ref,i-1}$ can be obtained in practice when the steer input $\delta_{ref,i-1}$ is not continuously available.

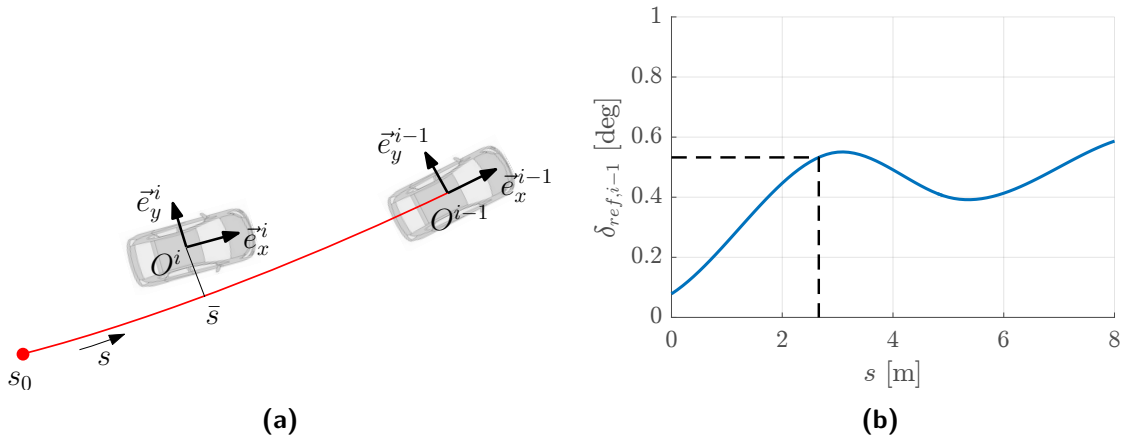


Figure 3-9: Illustration of relating the steer input of a preceding vehicle to the position on its path (a) Projection of the commanded steer input of vehicle $i-1$ on its path and (b) the applied steer input $\delta_{ref,i-1}$ versus the position variable s along its path.

Now that the feedforward input is related to the reference path, the same point \bar{s} on the reference path is used to obtain the control errors $y_{e,i}$ and $\psi_{e,i}$ for the feedback controller, and for the feedforward input. The result is that the controller does not depend on the time gap Δt anymore. So, for the controller it does not matter whether Δt is constant or time varying. This will turn out to be an important insight later on when lateral string stability is analyzed in Chapter 4.

In conclusion, two different feedforward controllers are compared to each other, being 1) a feedforward controller based on the curvature of the reference path and 2) a feedforward controller based on the steer input of the preceding vehicle. Although both feedforward controllers have advantages and disadvantages, the feedforward controller based on the steer input of the preceding vehicle is hereby proposed because it can perfectly track the path of a preceding vehicle.

However, it should be noted, that even if two vehicles command the same steer input at the same location (i.e., $y_{e,i}, \psi_{e,i} = 0$), they do not necessarily follow the same path. This fact is related to the initial condition of the vehicle states as will be discussed in more detail in the next section.

The effect of initial condition

In this section, the influence of the initial conditions on the tracking error is discussed in case the steer input of the preceding vehicle is used as a feedforward input. It should be noted that even if the error states $y_{e,i}$ and $\psi_{e,i}$ are zero and the disturbance $\dot{\theta}_{s,i}$ is perfectly canceled out by a feedforward input, this does not imply that the other states are identical to those of the preceding vehicle at that same point on the path. Consequently, an initial condition response may occur, causing the vehicle to deviate from its desired path.

However, if the closed-loop system is internal asymptotically stable, the system will converge to one unique equilibrium solution determined only by the input. This means that $y_{e,i}$ and $\psi_{e,i}$ asymptotically converge to zero and also the other vehicle states converge to identical values at the same position along the path for $t \rightarrow \infty$, (i.e. $v_{y,i}(t) = v_{y,i-1}(t - \Delta t)$, $\dot{\psi}_i(t) = \dot{\psi}_{i-1}(t - \Delta t)$, $\delta_i(t) = \delta_{i-1}(t - \Delta t)$ and $\dot{\delta}_i(t) = \dot{\delta}_{i-1}(t - \Delta t)$). When this equilibrium point is reached after transients, vehicle i will from that point on stay on the path of vehicle $i - 1$ because the same steer input is applied as a feedforward input and vehicle i has now the same initial condition as vehicle $i - 1$.

3-4 Evaluation of the control requirements

Both feedback and feedforward controllers have been proposed in this section. Now, the requirements that were posed in Section 3-1-1 will be evaluated. In Figure 3-5, the time response for the closed-loop system is presented for a longitudinal vehicle speed of 20 m/s. Based on this figure, the feedback gains k_1 and k_2 that yield a favorable, well-damped response, were determined to be 0.05 and 1, respectively. A similar approach was used to obtain gains k_1 and k_2 for longitudinal vehicle speeds ranging from 10 - 40 m/s. The gains k_1 and k_2 are presented as a function of longitudinal vehicle speed in Figure 3-10. These gains are used in the remainder of this section to evaluate the control requirements that were posed in Section 3-1-1.

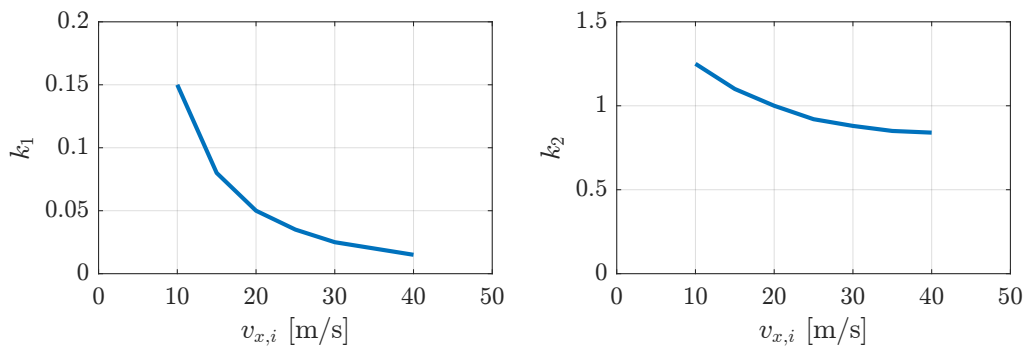


Figure 3-10: Feedback gains k_1 and k_2 versus the longitudinal vehicle speed $v_{x,i}$.

The most important requirement is that the closed-loop system must be asymptotically stable. Figure 3-2 presents sufficient conditions for the control gains k_1 and k_2 to guarantee stability. Using this figure, it can be shown that the gains k_1 and k_2 meet the stability criteria of Figure 3-2 for all longitudinal speeds from 10 - 40 m/s. Hence, the stability requirement is fulfilled.

Secondly, the response of the error states $y_{e,i}$ and $\psi_{e,i}$ must be critically damped. In order to guarantee a critically damped response, sufficient conditions for the gains k_1 and k_2 are iteratively obtained for a range of longitudinal vehicle speeds from 10 - 40 m/s. In Figure 3-11, the maximum longitudinal velocity that provides a critically damped response is presented for a set of k_1 and k_2 gains. The region below the surface, yields a critically damped response. It can be observed that especially for higher speeds, the gain k_1 needs to be small and k_2 needs to be relatively large in order to achieve a critically damped response for $y_{e,i}$ and $\psi_{e,i}$. Also, it can be observed that if the gain k_2 is not large enough, the response of $y_{e,i}$ and $\psi_{e,i}$ is even not critically damped at 10 m/s.

Using Figure 3-11, it can be shown that the gains presented in Figure 3-10 provide a critically damped response for all longitudinal vehicle speeds ranging from 10 - 40 m/s. Hence, also the requirement regarding a critically damped response of the error states $y_{e,i}$ and $\psi_{e,i}$ is fulfilled.

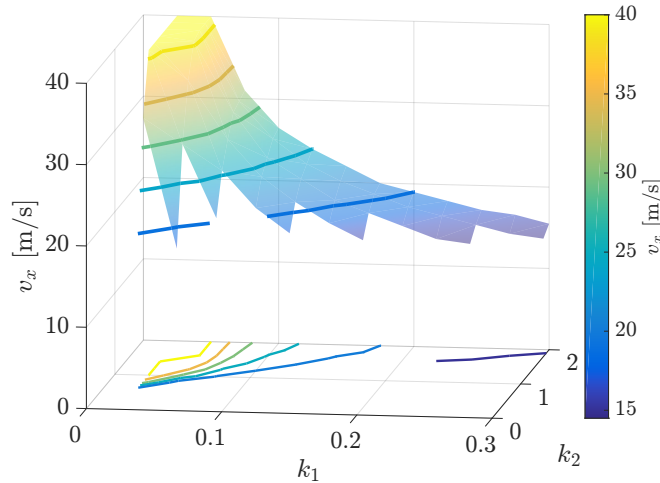


Figure 3-11: Conditions for the gains k_1 and k_2 to obtain a critically damped response for $y_{e,i}$ and $\psi_{e,i}$ for a range of longitudinal vehicle speeds from 10 - 40 m/s. The region below the surface provides a critically damped response.

Third, it was determined that the controller should be able to track curvature changes up to 0.167 Hz. In order to determine the bandwidth of the closed-loop system, the transfer function from the angular rate of change of the reference path $\dot{\theta}_s$ to the angular rate of change of the vehicle \mathcal{H}_i is given by

$$G_{cl}(s) = C_2(sI - A_{cl})^{-1}B_2 \quad (3-14)$$

with $C_2 = [-p_1 \ p_2 \ 0 \ 0 \ p_3 \ 0]$, $B_2 = [0 \ 0 \ 0 \ -1 \ 0 \ 0]^T$ and A_{cl} as given in (3-4). Figure 3-12 shows the bode plot of $G_{cl}(j\omega)$ for longitudinal vehicle speeds from 10 - 40 m/s using the corresponding control gains k_1 and k_2 in Figure 3-10. It can be observed that the minimum bandwidth of 0.167 Hz is met for the whole range of longitudinal vehicle speeds. Therefore, also the minimum bandwidth requirement of the closed-loop system is achieved.

So far, all the requirements that were posed in Section 3-1-1, are met. The only requirement that has not been discussed yet is that the controller must be laterally string-stable. This topic will be discussed in the next chapter.

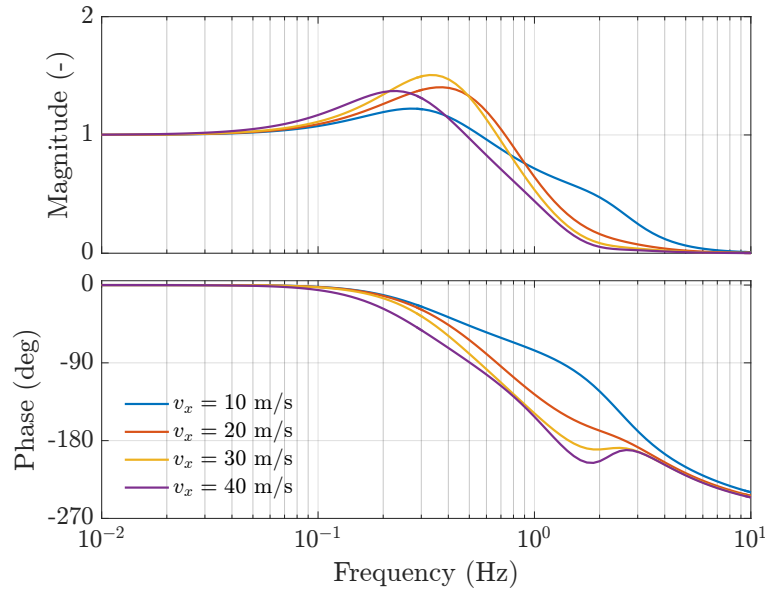


Figure 3-12: Bode plot of the closed-loop system $G_{cl}(j\omega)$ using the feedback gains k_1 and k_2 presented in Figure 3-10 for $v_{x,i}$ ranging from 10 - 40 m/s.

3-4-1 Summary

In this chapter, a static output feedback control law has been designed to regulate the control errors $y_{e,i}$ and $\psi_{e,i}$ (derived in the previous chapter) to zero. In Section 3-1-1, a set of control requirements was posed regarding (string) stability, bandwidth and damping characteristics. Stability conditions were determined for a range of longitudinal speeds from 10 - 40 m/s (see Figure 3-2). It was observed that heading information plays a crucial role in obtaining a stable closed-loop system. One way to include heading information in the feedback signal is to incorporate a look-ahead distance, but in this work it is proposed to penalize the heading error directly because this prevents vehicles to cut corners.

Furthermore, two feedforward controller were compared to each other, being 1) a feedforward controller based on the curvature of the reference path and 2) a feedforward controller based on the steer input of the preceding vehicle. The former controller does not rely on wireless communication and is easier to implement in practice. The disadvantage of this controller is that the required inverse vehicle transfer function $G_1^{-1}(s)$ is not proper and has to be approximated by another (proper) transfer function that does not perfectly track the desired reference path.

On the other hand, the feedforward controller based on the steer input of the preceding vehicle can perfectly track the desired path if the steer input of the preceding vehicle is related to the position on its driven path. Although this controller does rely on wireless communication and is more complex to implement, this feedforward controller is preferred because of its better tracking performance.

In order to satisfy the damping requirement, the closed-loop time response was used to determine conditions for the control gains k_1 and k_2 that provide a critically damped response for the control errors $y_{e,i}$ and $\psi_{e,i}$. Finally, it was verified that the closed-loop system meets

the minimum bandwidth requirement of 0.167 Hz, such that a typical lateral maneuver as a lane change can successfully be tracked.

Lateral string stability

A vehicle platoon can be interpreted as a string of dynamical systems which are virtually connected to each other. The performance of a vehicle platoon can be assessed by the notion of string stability. Where conventional stability notions for dynamical systems consider the evolution of system states over time, string stability, on the other hand, focuses on the propagation of a perturbed system response within a string of interconnected systems on a function of vehicle index.

For a vehicle platoon, a distinction can be made between longitudinal and lateral string stability. Longitudinal string stability focuses on the response of vehicles in the longitudinal direction (e.g., longitudinal velocity), while lateral string stability considers the variation of a system state along the platoon that is related to the lateral dynamics of a vehicle.

In literature, research regarding lateral string stability has been performed for closed-loop systems subject to a control algorithm based on direct vehicle-following, see e.g. [6], [11] and [27]. Although in the literature it is shown that lateral string stability can be achieved for direct vehicle-following, in this work lateral string stability for vehicle path-following is considered as was motivated earlier in this thesis.

In the problem statement given in Section 1-2, it was discussed that ideally, low-frequency curvature changes of the reference path should be tracked while high-frequency changes in the reference curvature should be attenuated for comfort reasons. These high-frequency changes can come from measurement noise or external disturbances such as wind gusts, for example. In Section 3-1, it was determined that the minimum bandwidth of the system has to be 0.167 Hz in order to perform a smooth lane-change within 3 seconds. In the frequency-domain, this means that the transfer function from the disturbance $\dot{\theta}_s$ to the angular rate of change of the velocity vector \mathcal{H}_i given in (3-7) ideally equals 1 for all frequencies up to 0.167 Hz and starts to decrease for higher frequencies. In other words, it is desired to separate low frequencies from high-frequencies in terms of tracking a reference curvature.

In order to analyze lateral string stability, first the platoon dynamics have to be described. It is easier to describe the platoon dynamics for direct vehicle-following than for vehicle path-following, because in the former case the input of the following vehicle depends on the

relative position with respect to its predecessor. Consequently, the motion of one vehicle directly affects the input for the next vehicle and hence the states of two consecutive vehicles can directly be related to each other. With vehicle path-following, however, first the path of the preceding vehicle has to be constructed. The control input for the following vehicle depends on the relative position with respect to the path of its predecessor instead of the current relative vehicle position. This fact makes it more difficult to relate the states of two consecutive vehicles to each other. Therefore, this chapter tries to answer the following two main questions:

- How can the platoon dynamics be described using a vehicle path-following approach?
- Can lateral string stability be achieved with the control architecture presented in Chapter 3?

The remainder of this chapter is organized as follows. First, the platoon dynamics subject to a path-following control approach are derived in Section 4-1. Then, in Section 4-2, sufficient conditions for lateral string stability are posed after which lateral string stability is evaluated for four different control configurations. Section 4-3 presents a simulation setup which is used to simulate the time response of a vehicle platoon for the four different control configurations. Finally, in Section 4-4, the time-domain system responses subject to the four different control configurations are discussed.

4-1 Platoon dynamics

In this section, the lateral dynamics of a vehicle platoon are considered where the lateral control of each individual vehicle is based on vehicle path-following. For vehicle path-following, the path of the preceding vehicle, vehicle $i - 1$, serves as a reference path for the following vehicle i . In order to relate the states of vehicle i to the states of vehicle $i - 1$, the states of vehicle $i - 1$ must be related to the position on its path.

In Chapter 2, the state vector $q_i = [v_{y,i} \ \dot{\psi}_i \ y_{e,i} \ \psi_{e,i} \ \delta_i \ \dot{\delta}_i]$ was used to describe the error dynamics that are related to the path-following control problem. It was explained that in literature, the states $\dot{y}_{e,i}$ and $\dot{\psi}_{e,i}$ are often used instead of the states $v_{y,i}$ and $\dot{\psi}_i$. However, it was observed that the states $\dot{y}_{e,i}$ and $\dot{\psi}_{e,i}$, yield two disturbance terms $\dot{\theta}_{s,i}$ and $\ddot{\theta}_{s,i}$. When the states $v_{y,i}$ and $\dot{\psi}_i$ are used instead, only one disturbance term $\dot{\theta}_{s,i}$ remains. This makes it easier to relate the states of vehicle i to the state of vehicle $i - 1$, because $\dot{\theta}_{s,i}$ is the angular rate of change of the reference path for vehicle i and must be equal to the angular rate of change of vehicle $i - 1$ at that position, i.e. $\dot{\theta}_{s,i} = \mathcal{H}_{i-1}$. Hence, the disturbance for vehicle i can now be related to the states of vehicle $i - 1$.

It was described earlier in (3-7) that the angular rate of change of the velocity vector of a vehicle can be expressed in terms of vehicle states, i.e.

$$\mathcal{H}_{i-1} = -p_1 v_{y,i-1} + p_2 \dot{\psi}_{i-1} + p_3 \delta_{i-1},$$

with constants p_1, p_2 and p_3 which are given in (2-29). Let us define the time gap Δt between vehicle i and vehicle $i - 1$ as the time it requires vehicle i to reach the same position as vehicle $i - 1$. In that case, the angular rate of change of the reference path $\dot{\theta}_{s,i}$ at time t , is related

to the angular rate of change of the velocity vector of vehicle $i - 1$ at time $t - \Delta t$. Hence, $\dot{\theta}_{s,i}$ can be written in terms of the states of vehicle $i - 1$ at time $t - \Delta t$:

$$\begin{aligned}\dot{\theta}_{s,i}(t) &= \mathcal{H}_{i-1}(t - \Delta t) \\ &= -p_1 v_{y,i-1}(t - \Delta t) + p_2 \dot{\psi}_{i-1}(t - \Delta t) + p_3 \delta_{i-1}(t - \Delta t).\end{aligned}\quad (4-1)$$

In (4-1), the disturbance $\dot{\theta}_{s,i}$ for vehicle i has been expressed in terms of the states of vehicle $i - 1$. Therefore, the states of vehicle i and vehicle $i - 1$ can now be related to each other.

Note that the time gap Δt between two vehicles is not always constant. For example, refer to the example illustrated in Figure 3-8. However, assuming a constant Δt is reasonable for normal highway driving scenarios when vehicle speeds are often constant and the time gap with respect to a preceding vehicle is controlled by a longitudinal controller. Only under extreme conditions, when a vehicle performs a severe braking action, for example, the longitudinal controller might not be able to realize a constant time gap. In this work, however, only normal highway driving scenarios are considered. Therefore, it is assumed from here on that Δt is constant.

Although the time gap Δt influences the trajectory of the control response in time, it does not influence the absolute path driven by the following vehicle because both the feedback and feedforward control input are related to the position on the path of the preceding vehicle. Therefore, in order to analyze the lateral platoon dynamics (in terms of string stability), the time gap Δt could also be assumed to be zero. In that case, the disturbance $\dot{\theta}_{s,i}$ for vehicle i can directly be related to the angular rate of change of the direction of motion of the preceding vehicle i.e., $\dot{\theta}_{s,i}(t) = \mathcal{H}_{i-1}(t)$. This observation is used in the next section to describe the lateral platoon dynamics in the frequency-domain.

Describing the lateral platoon dynamics in the frequency-domain

In this section, a controlled vehicle i in a platoon is described in the frequency-domain using the block scheme depicted in Figure 4-1. The plant $\mathcal{P}(s)$ describes the error dynamics of an open-loop vehicle, as presented earlier in (2-45). The plant $\mathcal{P}(s)$ has two inputs and two outputs. The inputs are $\delta_{ref,i}(s)$ and $\mathcal{H}_{i-1}(s) (= \dot{\theta}_{s,i})$, see (2-45). The outputs are $\mathcal{H}_i(s)$ and $Z_i(s)$. The first output, $\mathcal{H}_i(s)$, is the angular rate of change of the direction of motion of the vehicle, as was given in (3-8). It can be observed in Figure 4-1 that $\mathcal{H}_i(s)$ only depends on $\delta_{ref,i}(s)$ and not on $\dot{\theta}_{s,i}$ (i.e., $\mathcal{H}_i(s) = G_1(s)\delta_{ref,i}(s)$), as was explained in Section 3-3-1.

The second output $Z_i(s)$ contains the error states $y_{e,i}(s)$ and $\psi_{e,i}(s)$. In Section (3-1), the control errors $y_{e,i}$ and $\psi_{e,i}$ were defined as the output z_i of the static output feedback controller. Using (2-45), the relation between the output z_i and the inputs $\delta_{ref,i}$ and $\dot{\theta}_{s,i}$ can be described in the frequency-domain as follows:

$$Z_i(s) = G_3(s)\delta_{ref,i}(s) + G_4(s)\dot{\theta}_{s,i}(s), \quad (4-2)$$

where $Z_i(s) = [y_{e,i}(s) \ \psi_{e,i}(s)]^T$ and $\dot{\theta}_{s,i}(s) = \mathcal{H}_{i-1}(s)$ (under the assumption of Δt being zero).

It can be observed in Figure 4-1 that the steer input $\delta_{ref,i}(s)$ is build up from a feedforward steer input $\delta_{ff,i}(s)$ and a feedback steer input $\delta_{fb,i}(s)$, i.e. $\delta_{ref,i}(s) = \delta_{ff,i}(s) + \delta_{fb,i}(s)$. In

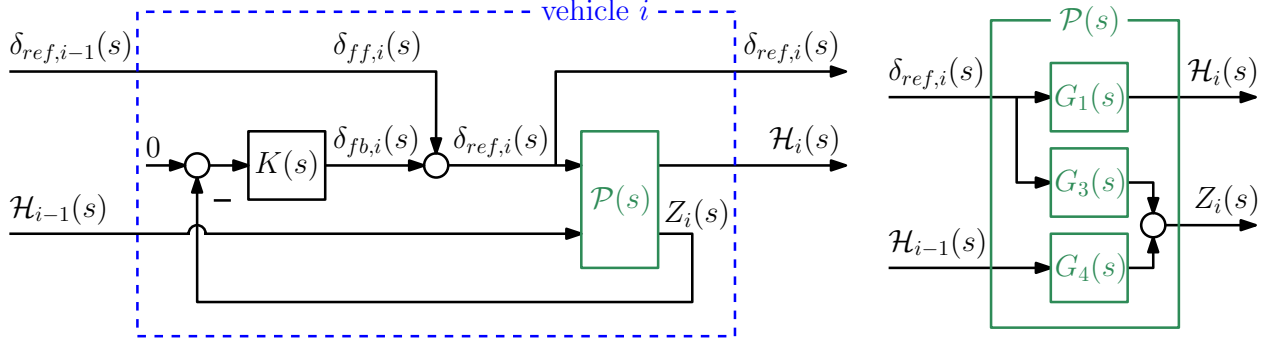


Figure 4-1: block scheme of the lateral control structure for one vehicle in a platoon.

Figure 4-1, it is assumed that the feedforward steer input is the steer input of the preceding vehicle (i.e., $\delta_{ff,i}(s) = \delta_{ref,i-1}(s)$), but $\delta_{ff,i}(s)$ could also be based on the reference curvature κ_{ref} as was explained in Section 3-3-1.

The feedback steer input $\delta_{fb,i}(s)$ is given by the feedback control law presented in (3-3) and can be described in the frequency-domain as

$$\delta_{fb,i}(s) = -K(s)Z_i(s), \quad (4-3)$$

where $K(s) = \begin{bmatrix} k_1 & k_2 \end{bmatrix}$ as was described earlier in (3-1). However, the block scheme in Figure 4-1 can be simplified by taking a closer look at the error dynamics that were presented in (2-45). The dynamics of the error states y_e and ψ_e were earlier described in (2-42). Note from these equations that the expression for $\dot{\psi}_{e,i}$ can also be written as $\dot{\psi}_{e,i} = \mathcal{H}_i - \mathcal{H}_{i-1}$ (assuming $\Delta t = 0$) and that $\dot{y}_{e,i}$ solely depends on $\psi_{e,i}$. Hence, $\psi_{e,i}$ is obtained by integrating $\dot{\psi}_{e,i}$ and $y_{e,i}$ is obtained by integrating $\dot{y}_{e,i}$, which is the product of $v_{x,i}$ and $\psi_{e,i}$, see (2-42).

So, instead of obtaining the control errors $y_{e,i}$ and $\psi_{e,i}$ (denoted by $Z_i(s)$) separately from the vehicle plant $\mathcal{P}(s)$, one could also take this part of the dynamics into a new block $\mathcal{K}(s)$ together with the feedback controller $K(s)$. The block $\mathcal{K}(s)$ is visualized in Figure 4-2. Using (2-42), it can be observed that the control errors $y_{e,i}$ and $\psi_{e,i}$ are derived from the input signal $\dot{\psi}_{e,i}$ in the same manner as in the plant \mathcal{P} . The control errors $y_{e,i}$ and $\psi_{e,i}$ are then multiplied by the feedback gains k_1 and k_2 to obtain the feedback steer input $\delta_{fb,i}$. Hence, the block $\mathcal{K}(s)$ is described by

$$\mathcal{K}(s) = \frac{v_{x,i}}{s^2}k_1 + \frac{1}{s}k_2. \quad (4-4)$$

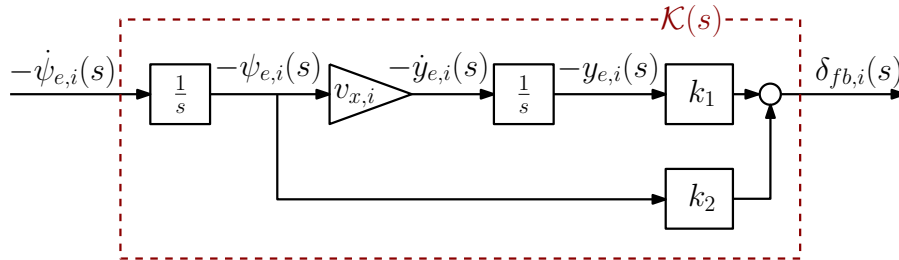


Figure 4-2: Schematic representation of the block $\mathcal{K}(s)$. All the signals in the figure are the Laplace transform of the original time-domain signal, e.g., $\dot{\psi}_{e,i}(s) = \mathcal{L}(\dot{\psi}_{e,i}(t))$.

As mentioned before, the input signal of $\mathcal{K}(s)$ is $\dot{\psi}_{e,i} = \mathcal{H}_i - \mathcal{H}_{i-1}$ where \mathcal{H}_i is the first output of $\mathcal{P}(s)$ and $\mathcal{H}_{i-1} = \dot{\theta}_{s,i}$.

Then, a controlled vehicle i in a vehicle platoon can also be represented by the block scheme depicted in Figure 4-3 which is equivalent to the block scheme that was earlier presented in Figure 4-1. It can be observed in Figure 4-3 that the open-loop vehicle can now be represented by the vehicle transfer function $G_1(s)$, see (3-9).

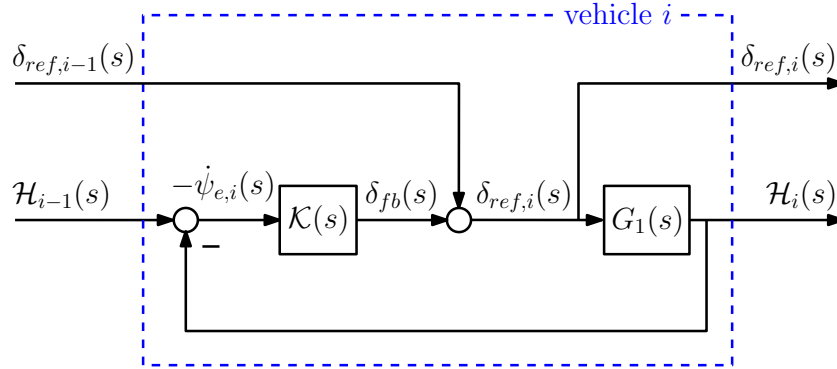


Figure 4-3: Block scheme of the simplified lateral control structure for one vehicle in a platoon. All the signals in the figure are the Laplace transform of the original time-domain signal, e.g., $\dot{\psi}_{e,i}(s) = \mathcal{L}(\dot{\psi}_{e,i}(t))$.

Each vehicle block has two inputs, being the steer input of a preceding vehicle $\delta_{ref,i-1}$ and the angular rate of change of the reference path $\dot{\theta}_{s,i}$ which equals the angular rate of change of the preceding vehicle, $\dot{\theta}_{s,i} = \mathcal{H}_{i-1}$ (for $\Delta t = 0$). Equivalently, each vehicle block also has two outputs, being the applied steer input $\delta_{ref,i}$ and the angular rate of change of its own direction of motion \mathcal{H}_i .

Now, the lateral dynamics of a vehicle platoon can be described by connecting the inputs and outputs of multiple vehicle blocks to each other. This concept is illustrated in Figure 4-4.

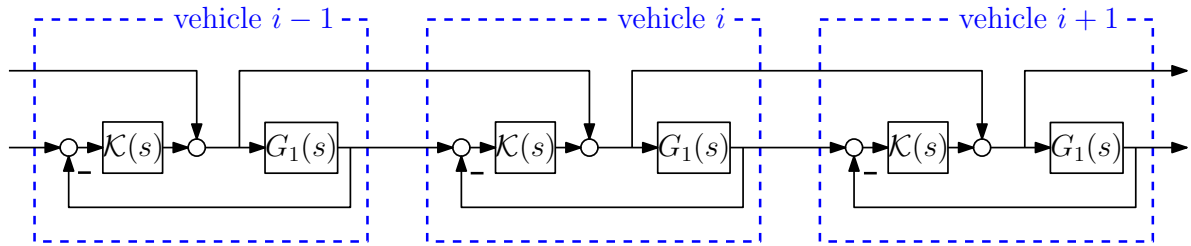


Figure 4-4: Illustration of a model that describes the coupled lateral dynamics of multiple vehicles in a platoon.

To summarize, in order to describe the platoon dynamics, the states of the individual vehicles must be related to each other. For vehicle path-following, the reference path of the following vehicle is generated by its preceding vehicle. Therefore, the angular rate of change of the reference path for vehicle i , $\dot{\theta}_{s,i}$, corresponds to the angular rate of change of vehicle $i-1$ at that point, \mathcal{H}_i .

It was motivated that it is reasonable to assume that the time gap Δt between two vehicles is constant and that the control response does not depend on Δt . Therefore, in order to analyze

the platoon dynamics, Δt could also be assumed to be zero. Consequently, the lateral motion of one vehicle directly influences the lateral dynamics of the next vehicle. Therefore, the disturbance $\dot{\theta}_{s,i}$ for vehicle i can be expressed in terms of the states of vehicle $i-1$ as in (4-1). In this way the states of two consecutive vehicles can be coupled and the lateral platoon dynamics can be described using the simplified block scheme depicted in Figure 4-3.

4-2 String stability analysis

In the previous section, the platoon dynamics for lateral motion were derived. Next, lateral string stability can be assessed for a vehicle platoon using the output feedback control method presented in Chapter 3. However, first conditions for lateral string stability have to be obtained.

As mentioned before, string stability in general is assessed by considering the propagation of a disturbance along a cascade of interconnected systems. According to [6], a vehicle platoon is said to be laterally string-stable in the \mathcal{L}_2 sense if the gain of the transfer function from the lateral error of a vehicle to that of the next vehicle has a magnitude less than, or equal to, 1. Equivalently, the angular rate of change of the velocity vector \mathcal{H}_i can be considered. The transfer function from \mathcal{H}_{i-1} to \mathcal{H}_i is denoted by the complementary sensitivity function Γ_i , i.e.

$$\Gamma_i(j\omega) = \frac{\mathcal{H}_i(j\omega)}{\mathcal{H}_{i-1}(j\omega)}. \quad (4-5)$$

Then, the following condition suffices to guarantee lateral string stability

$$\|\Gamma_i(j\omega)\|_\infty = \left\| \frac{\mathcal{H}_i(j\omega)}{\mathcal{H}_{i-1}(j\omega)} \right\|_\infty \leq 1 \Rightarrow \left\| \frac{\mathcal{H}_i(j\omega)}{\mathcal{H}_{i-1}(j\omega)} \right\| \leq 1, \forall \omega. \quad (4-6)$$

Note that $\mathcal{H}_{i-1} = \dot{\theta}_{s,i}$, so $\Gamma_i(j\omega)$ is the transfer function from $\dot{\theta}_{s,i}$ to \mathcal{H}_i in Figure 4-3. Now, conditions are determined to guarantee lateral string stability for a vehicle platoon where the lateral control of each individual vehicle is based on vehicle path-following. Lateral string stability is evaluated for four different control configurations which are denoted by Case 1 up until Case 4:

- **Case 1:** Static output feedback control without feedforward,
- **Case 2:** Static output feedback and feedforward,
- **Case 3:** Static output feedback and filtered feedforward,
- **Case 4:** Static output feedback with filtered feedforward and filtered path.

4-2-1 Case 1: Static output feedback control without feedforward

In this section, lateral string stability is evaluated for the static output feedback controller presented in Chapter 3. Initially, only feedback control is considered and the feedforward input is excluded. Using the block scheme presented in Figure 4-3, the complementary sensitivity function $\Gamma_{i,1}(s) = \frac{\mathcal{H}_i(s)}{\mathcal{H}_{i-1}(s)}$ (without feedforward input $\delta_{ref,i-1}$) can be shown to be equal to

$$\Gamma_{i,1}(s) = \frac{\mathcal{K}(s)G_1(s)}{1 + \mathcal{K}(s)G_1(s)}, \quad (4-7)$$

where $\mathcal{K}(s)$ is given in (4-4) and $G_1(s)$ in (3-9). Using $v_{x,i} = 20$ m/s, $k_1 = 0.05$ and $k_2 = 1$, Figure 4-5a shows the gain $|\Gamma_{i,1}(j\omega)|$. Clearly, it can be observed that the system is not strictly string-stable, because the criterion of (4-6) is not met. The gain $|\Gamma_{i,1}(j\omega)|$ has been evaluated for a wide range of control gains k_1 and k_2 of which four examples are shown in Figure 4-5b, but it appears that the condition of (4-6) is not met for any combination of k_1 and k_2 .

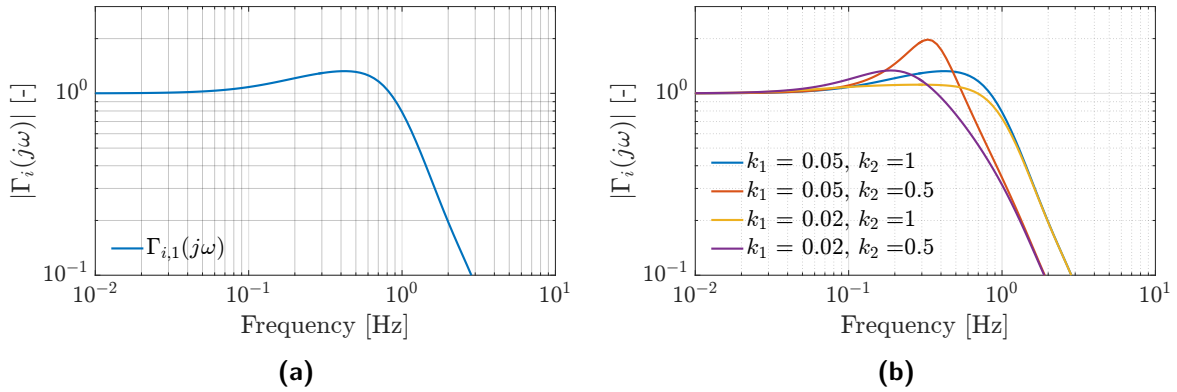


Figure 4-5: Figure (a) shows the complementary sensitivity function $|\Gamma_{i,1}(j\omega)|$ for $v_{x,i} = 20$ m/s, $k_1 = 0.05$ and $k_2 = 1$ and (b) shows the same function for a range of different control gains k_1 and k_2 .

4-2-2 Case 2: Static output feedback and feedforward

With only feedback control, it was observed that the closed-loop platoon dynamics do not show a string-stable behavior in the lateral direction. In order to increase the tracking performance, the steer input of the preceding vehicle $\delta_{ref,i-1}(s)$ is used as an additional feedforward input (as illustrated in Figure 4-3). From Figure 4-3, it can be observed that $\dot{\theta}_{s,i}(s) = G_1(s)\delta_{ref,i-1}(s)$. Then, based on Figure 4-3 it can be shown that the complementary sensitivity function $\Gamma_{i,2}(s) = \frac{\mathcal{H}_i(s)}{\mathcal{H}_{i-1}(s)}$ becomes

$$\Gamma_{i,2}(s) = \frac{1 + \mathcal{K}(s)G_1(s)}{1 + \mathcal{K}(s)G_1(s)}. \quad (4-8)$$

Figure 4-6 shows the gain $|\Gamma_{i,2}(j\omega)|$ in addition to gain $|\Gamma_{i,1}(j\omega)|$. It can be observed that $|\Gamma_{i,2}(j\omega)| = 1, \forall \omega$ which means that the system is marginally string-stable. Consequently, the system perfectly track low-frequency disturbances, but does not attenuate high-frequency disturbances which is desired for comfort reasons.

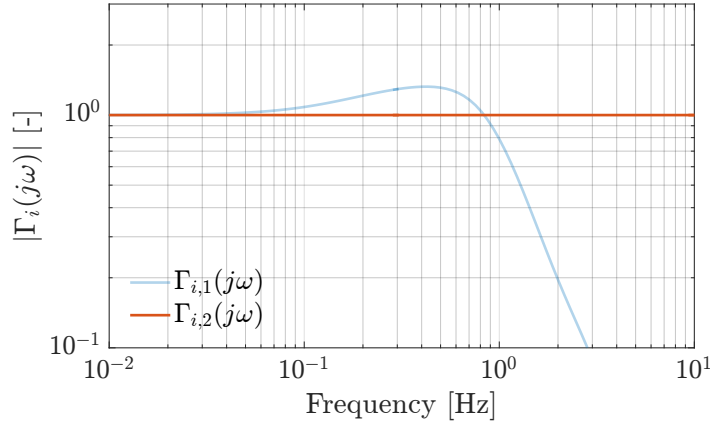


Figure 4-6: Complementary sensitivity function $\Gamma_{i,2}(s)$ for both feedback and feedforward input for $v_x = 20$ m/s, $k_1 = 0.05$ and $k_2 = 1$.

4-2-3 Case 3: Static output feedback and filtered feedforward

In the previous section, it was observed that the feedforward input $\delta_{ref,i-1}(s)$ yields perfect tracking for all frequencies (i.e. $|\Gamma_{i,2}(j\omega)| = 1, \forall \omega$). However, this also means that the system is not robust against high-frequency disturbances. As discussed in the beginning of this chapter, it is desired to attenuate high-frequency disturbances in upstream platoon direction. It was determined in Section 3-1 that the vehicle should be able to track curvature frequencies up to 0.167 Hz to be able to perform a lane-change within 3 seconds. For the complementary sensitivity function this means that the gain should be equal to 1 for all frequencies up to 0.167 Hz and starts to decrease for higher frequencies.

This raised the idea to filter the feedforward input with a first-order low-pass filter such that low-frequency steering inputs are passed through and high-frequency steer inputs are attenuated. This configuration is depicted in Figure 4-7a where the first-order low-pass filter $H(s)$ is described by

$$H(s) = \frac{1}{\frac{1}{\tau}s + 1}. \quad (4-9)$$

Using Figure 4-7a, The complementary sensitivity function $\Gamma_{i,3}(s)$ from $\dot{\theta}_{s,i}(s)$ to $\mathcal{H}_i(s)$ is derived and is described by

$$\Gamma_{i,3}(s) = \frac{H(s) + \mathcal{K}(s)G_1(s)}{1 + \mathcal{K}(s)G_1(s)}. \quad (4-10)$$

Figure 4-7b shows the gain $|\Gamma_{i,3}(j\omega)|$ for three different cutoff frequencies τ of the filter $H(s)$, being 0.167, 1 and 5 Hz, respectively. It is directly observed that non of the filters yields a satisfactory response, because $|\Gamma_{i,3}(j\omega)| \not\leq 1, \forall \omega$. A similar response is observed for a various range of different gains k_1 and k_2 in combination with the different cutoff frequencies for the low-pass filter $H(s)$.

However, it can be observed in Figure 4-7b, that for higher cutoff frequencies for the filter $H(s)$, the gain $|\Gamma_{i,3}(j\omega)|$ is significantly smaller in the frequency range between approximately 0.1 - 1 Hz. On the other hand, increasing the cutoff frequency also compromises the ability

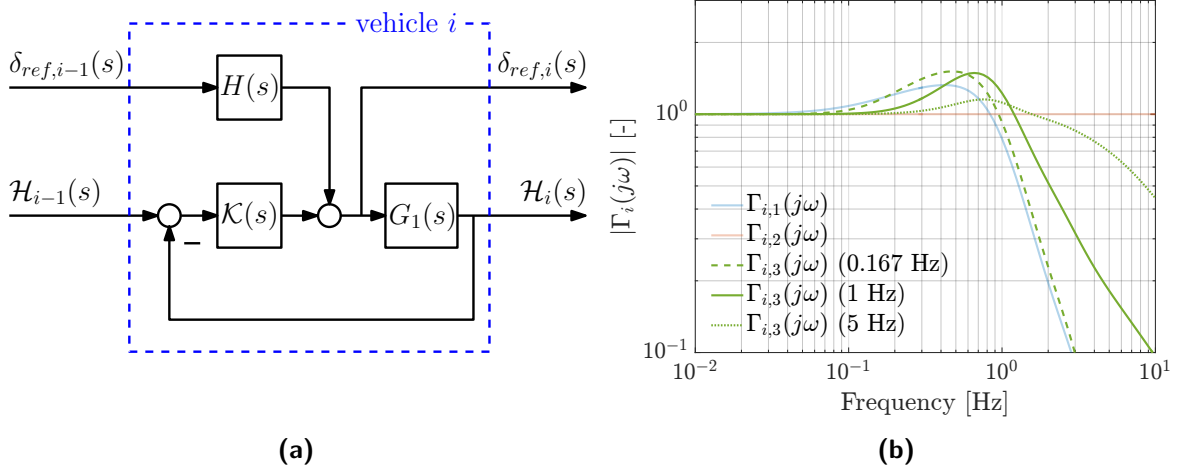


Figure 4-7: Figure (a) provides an illustration of the block scheme of the lateral control structure in case the feedforward input $\delta_{ref,i-1}$ is low-pass filtered and (b) shows the gain $|\Gamma_{i,3}(j\omega)|$ for $v_x = 20$ m/s, $k_1 = 0.05$, $k_2 = 1$ and $\tau = 0.167, 1$ and 5 Hz.

of the system to attenuate high-frequency disturbances. For $\tau \rightarrow \infty$, the gain $|\Gamma_{i,3}(j\omega)|$ will become equal to $|\Gamma_{i,2}(j\omega)|$. Hence, a compromise between a better response for low frequencies and better attenuate high-frequency disturbances has to be made, but lateral string stability is not obtained.

4-2-4 Case 4: Static output feedback with filtered feedforward and filtered path

Since only low-pass filtering the feedforward input does not provide lateral string stability, the effect of filtering both the feedforward input $\delta_{ref,i-1}$ and the reference path (which is expressed in $\dot{\theta}_{s,i}$) is now investigated. This configuration is presented in Figure 4-8a. Based on this block scheme, the complementary sensitivity function from $\dot{\theta}_{s,i}$ to \mathcal{H}_i is given by

$$\Gamma_{i,4}(s) = H(s) \frac{1 + \mathcal{K}(s)G_1(s)}{1 + \mathcal{K}(s)G_1(s)}, \quad (4-11)$$

with the low-pass filter $H(s)$ which is given in (4-9). The response of the gain $|\Gamma_{i,4}|$ is given in Figure 4-8b. It can be observed that the response is exactly the low-pass filter $H(s)$ with the desired cutoff frequency of 0.167 Hz. Hence, it can be concluded that the system is laterally string-stable and that the frequency response approximates the desired behavior because reference curvatures up to 0.167 Hz are tracked while high-frequency curvature changes are attenuated.

So far in this chapter the platoon dynamics have been described in the frequency-domain and conditions for lateral string stability were given. Four different control configurations (Case 1 - Case 4) have been evaluated in the frequency-domain and marginal lateral string stability has been obtained for a static output feedback controller in combination with a feedforward controller that is based on the steer input of the preceding vehicle. Now, the time response of

4-3-1 Model description

The simulation model contains one lead vehicle (Vehicle 0) and allows to add multiple following vehicles to form a vehicle platoon as is illustrated in Figure 4-9. The input for the lead vehicle is a predefined steer input and velocity profile. The single track model presented in Section 2-1 is used to describe the dynamics of each vehicle. The vehicles starts at an initial position and orientation $(x_{i,0}, y_{i,0}, \psi_{i,0})$ and the global position over time is obtained using the equations presented in Section 2-1-1. The following vehicles have the same longitudinal velocity as the lead vehicle and maintain a constant time gap with respect to their predecessor. Furthermore, all vehicles are described by the same dynamical model, i.e. the platoon is assumed to be homogeneous.

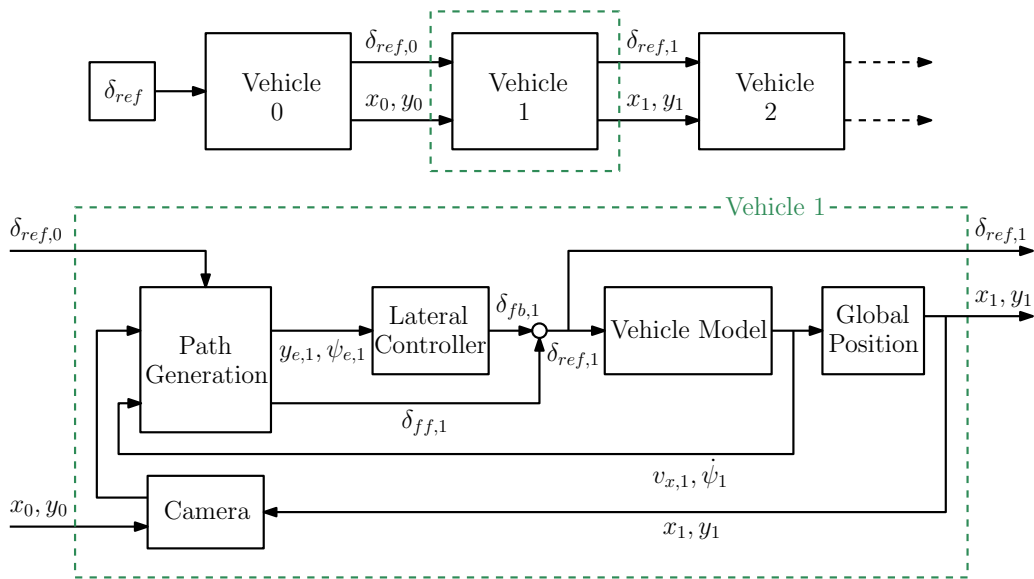


Figure 4-9: Illustration of the simulation model that is used to simulate the time response of a vehicle platoon.

In Figure 4-9, it can be observed that each vehicle receives the global position and the steer input of its predecessor. The global positions of two consecutive vehicles are used to determine the relative vehicle position in the block ‘Camera’. This block actually simulates a camera sensor. These relative vehicle position measurements are used to construct the reference path for the following vehicle in the block ‘Path generation’. The motion parameters $v_{x,1}$ and $\dot{\psi}_1$ of the following vehicle are used to update the relative position measurements that are stored in a history buffer for the vehicle’s motion over time. The following vehicle’s global position is used to determine the the control errors $y_{e,1}$ and $\psi_{e,1}$ with respect to the constructed reference path. In the block ‘Lateral Controller’, the feedback steer input $\delta_{fb,1}$ is determined using the control law in (3-3). The path generation and the derivation of the control errors $y_{e,1}$ and $\psi_{e,1}$ is explained in more detail in Subsection 5-1-1 and Subsection 5-1-3, respectively. The steer input $\delta_{ref,0}$ is also an input of ‘Path Generation’. In this block, it is associated with the position on the path where the steer input is applied. The same steer input is then applied by the following vehicle as a feedforward steer input once it reaches that same position. The construction of the feedforward input is explained in more detail in Section 5-1-4. The input of the block ‘Vehicle Model’ is $\delta_{ref,1}$ which is the sum of $\delta_{fb,1}$ and $\delta_{ff,1}$, see Figure

4-9. The output of ‘Vehicle Model’ is the vehicle’s velocity $v_{x,1}$ and yaw rate $\dot{\psi}_1$. These signals are used in ‘Global Position’ to keep track of the global position of the vehicle using the equations described in Section 2-1-1.

In order to analyze the time response of the vehicle platoon, a lane-change maneuver is performed at 20 m/s by the lead vehicle with two following vehicles. The initial position for the lead vehicle (Vehicle 0) is $[x_{0,0} \ y_{0,0} \ \psi_{0,0}] = [0 \ 0 \ 0]$. The following vehicles start at $[x_{1,0} \ y_{1,0} \ \psi_{1,0}] = [-14 \ 0 \ 0]$ and $[x_{2,0} \ y_{2,0} \ \psi_{2,0}] = [-28 \ 0 \ 0]$, respectively as is illustrated in Figure 4-10. Furthermore, each vehicle has a longitudinal velocity of 20 m/s and the initial condition for all the other states is zero, i.e., $v_{y,i,0} = \dot{\psi}_{i,0} = y_{e,i,0} = \psi_{e,i,0} = \delta_{i,0} = \dot{\delta}_{i,0} = 0$. The red line represents the initial reference path for the following vehicles. The result of the time-domain simulations for the four control configurations that were presented in the previous section are presented next.

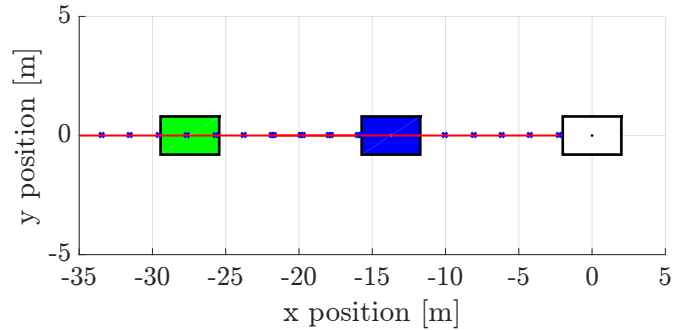


Figure 4-10: Illustration of the initial conditions for a simulation of a three vehicle platoon.

Case 1: Static output feedback control without feedforward

First, a lane-change maneuver is simulated where the following vehicles only apply feedback control and no feedforward input. Figure 4-11 shows the result of the lane-change maneuver. The path driven by each vehicle is plotted in the corresponding color of the vehicle. It can be observed that there is a significant amount of overshoot, but the control errors are successfully regulated to zero and the following vehicles converge to the path of the lead vehicle.

It can also be observed that \mathcal{H}_i increases for each next vehicle in the platoon during the lane-change maneuver. This suggests that the vehicle platoon is not string-stable in the lateral direction which corresponds to what was observed in the frequency-domain for this control configuration in Section 4-2-1.

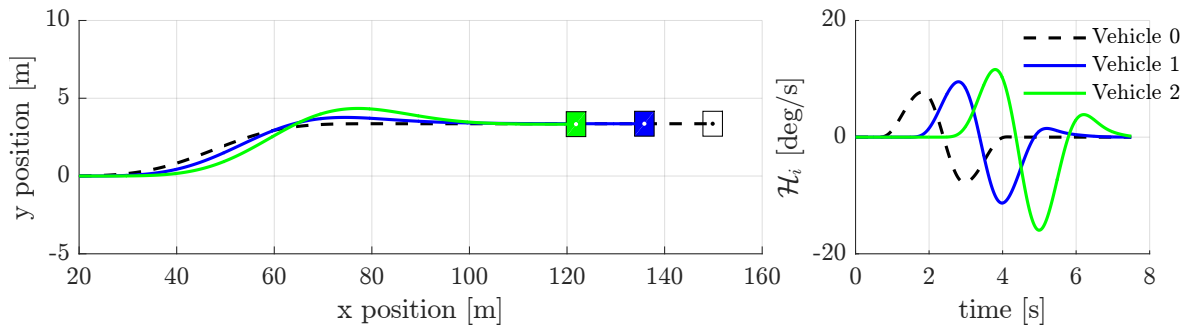


Figure 4-11: Simulation of a lane-change maneuver with only static feedback control performed at 20 m/s with $k_1 = 0.05$ and $k_2 = 1$.

Case 2: Static output feedback and feedforward

Now, the same lane-change maneuver is simulated while the following vehicles apply a feedforward input, which is the steer input of the preceding vehicle as explained in Section 3-3-2. The result is shown in Figure 4-12. It can be observed that in this case, the following vehicles instantly react to the lane-change maneuver of the lead vehicle such that no error is observed at all.

Considering the response of \mathcal{H}_i , it can be observed that the response for all three vehicles is identical. The response of the lead vehicle is neither amplified nor attenuated in upstream platoon direction. This indicates that the system is marginally lateral string-stable which corresponds to what was observed in the frequency-domain in Section 4-2-2.

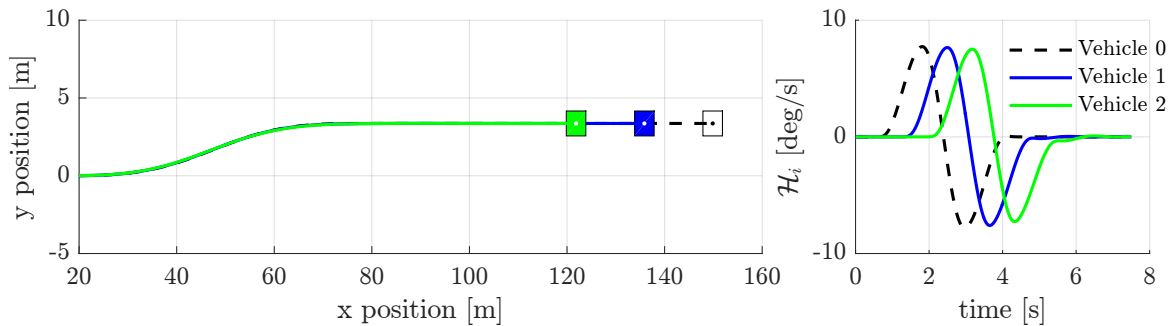


Figure 4-12: Simulation of a lane-change maneuver with feedback and feedforward control performed at 20 m/s with $k_1 = 0.05$ and $k_2 = 1$.

Case 3: Static output feedback and filtered feedforward

This time, the same lane-change maneuver is performed, but now the feedforward input is filtered with a first-order low-pass filter with a cutoff frequency of 1 Hz. In Figure 4-13, it can be observed that the tracking performance looks quite good, but still has some overshoot. This corresponds to what is expected by looking at the frequency response of this control configuration in Section 4-2-3.

The overshoot is also observed in the response of \mathcal{H}_i in Figure 4-13. So although the tracking performance is not bad, it can be concluded that no lateral string-stable behavior is observed

in the time-domain, which corresponds to what has been observed in the frequency-domain in Section 4-2-3.

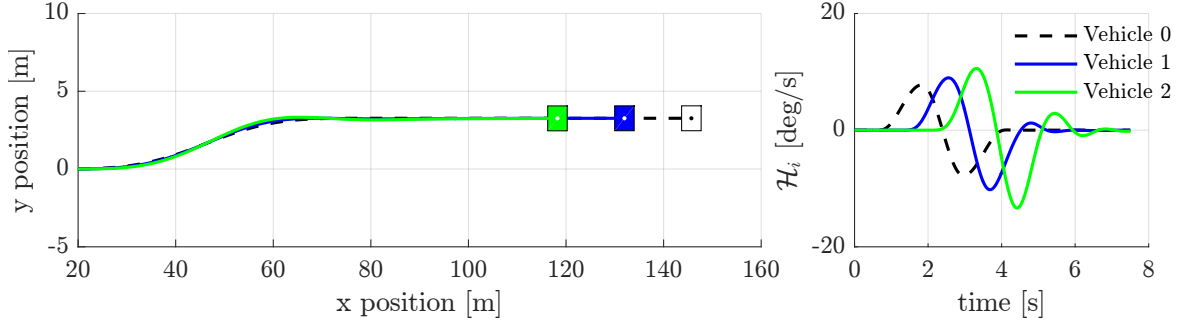


Figure 4-13: Simulation of a lane-change maneuver with feedback and filtered feedforward control performed at 20 m/s with $k_1 = 0.05$, $k_2 = 1$ and $\tau = 1$ Hz.

Case 4: Static output feedback with filtered feedforward and filtered path

Finally, the same lane-change maneuver is performed once more, but now both the feedforward input $\delta_{ref,i-1}$ and the reference path $\hat{\theta}_{s,i}$ are filtered. This method shows promising results regarding lateral string stability in the frequency-domain (in Section 4-3-1) and Figure 4-14 also shows laterally string-stable behavior in the time-domain, because \mathcal{H}_i decreases in upstream platoon direction.

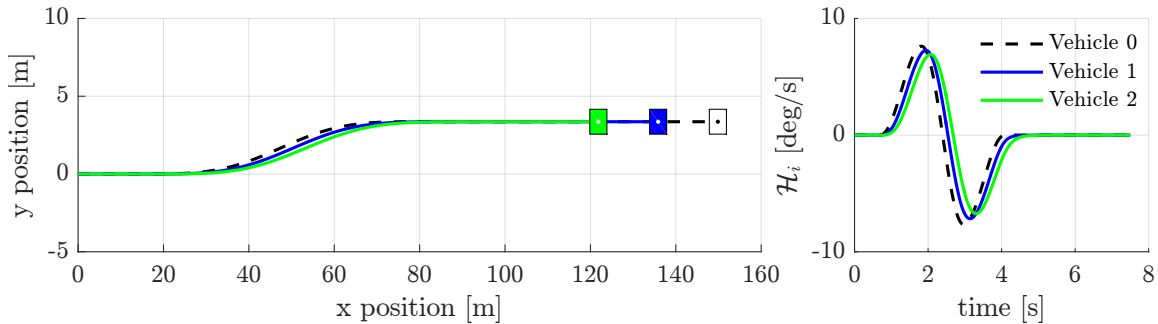


Figure 4-14: Simulation of a lane-change maneuver for a filtered feedforward input and filtered reference path $\hat{\theta}_{s,i}$ performed at 20 m/s with $k_1 = 0.05$ and $k_2 = 1$.

So, lateral string-stable behavior is observed both in the frequency-domain and in time-domain simulations. However, after further investigation of the time-domain simulations, it can be observed that steady-state errors appear in the response. This is explored in more detail in the next section.

Steady-state error

Although the presented control structure in Figure 4-8a shows laterally string-stable behavior, steady-state offset errors with respect to the real path of a preceding vehicle appear in the response. This is not seen in the performed lane-change maneuver in Figure 4-13, but is

clearly seen when a left hand corner maneuver is simulated as is shown in Figure 4-15. In Figure 4-15a the reference path $\dot{\theta}_{s,i}$ is not filtered while in Figure 4-15b the path $\dot{\theta}_{s,i}$ is filtered according to the control configuration presented in Figure 4-8a. It can be observed that if $\dot{\theta}_{s,i}$ is not filtered, the following vehicles converge to the path of their predecessor while a steady-state offset error remains when $\dot{\theta}_{s,i}$ is filtered.

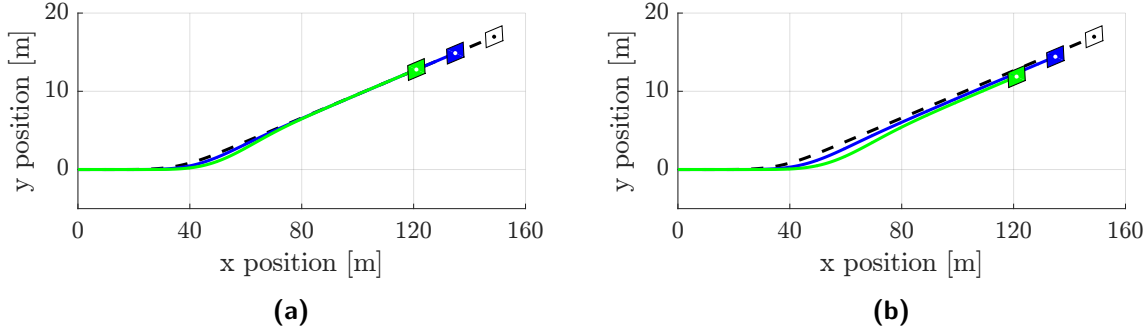


Figure 4-15: Simulation of a left hand corner for a filtered reference path $\dot{\theta}_{s,i}$ performed at 20 m/s. In (a) the angular rate of change of the reference path $\dot{\theta}_{s,i}$ is not filtered and in (b) the angular rate of change of the reference path $\dot{\theta}_{s,i}$ is filtered.

Therefore, let us analyze in more detail what happens if the reference path is filtered. The commanded steer input $\delta_{ref,i}$ for a left hand cornering maneuver is plotted in Figure 4-16a. The path driven by the vehicle expressed in x_i and y_i coordinates is shown in Figure 4-16c. Equivalently, the path could also be expressed in terms of $\theta_{s,i}$ instead of x_i and y_i coordinates, see Figure 4-16b. Finally, the time derivative of $\theta_{s,i}$, i.e the path, is presented in Figure 4-16d.

If $\dot{\theta}_{s,i}$ is filtered (with a first-order low-pass filter with a cutoff frequency of 0.167 Hz) as suggested in Figure 4-8a, the reference path is described by the dashed line in Figure 4-16d. If this filtered signal is converted back into x_i and y_i coordinates, the reference path can be represented by the dashed line in Figure 4-16c. In this figure, it is clearly observed that filtering $\dot{\theta}_{s,i}$ yields a steady-state offset of the reference path with respect to the original path.

So, the steady-state error that is observed in the corner maneuver in Figure 4-15b is the result of filtering $\dot{\theta}_{s,i}$ which actually modifies the reference path for the following vehicle. Even though the feedback controller successfully regulates $y_{e,i}$ and $\psi_{e,i}$ to zero, a steady-state error with respect to the real path of the preceding vehicle remains.

For left hand cornering maneuvers, a positive steady-state error remains while a negative error remains for right hand cornering maneuvers. This explains that no steady-state error is observed in the lane-change maneuver in Figure 4-14. During a lane change, the vehicles steer the same amount to the left as to the right such that the positive and negative steady-state error cancel each other out.

To summarize, in order to assess laterally string-stable behavior, the relation between \mathcal{H}_i and \mathcal{H}_{i-1} is considered. Although the control configuration presented in Figure 4-8a shows laterally string-stable behavior, steady-state errors are observed with respect to the real path of a preceding vehicle. So, the relation between \mathcal{H}_i and \mathcal{H}_{i-1} does not guarantee that a vehicle actually tracks the path of the preceding vehicle. Therefore, another string stability function, that explicitly considers the relation between the position of two consecutive vehicles, should be considered.

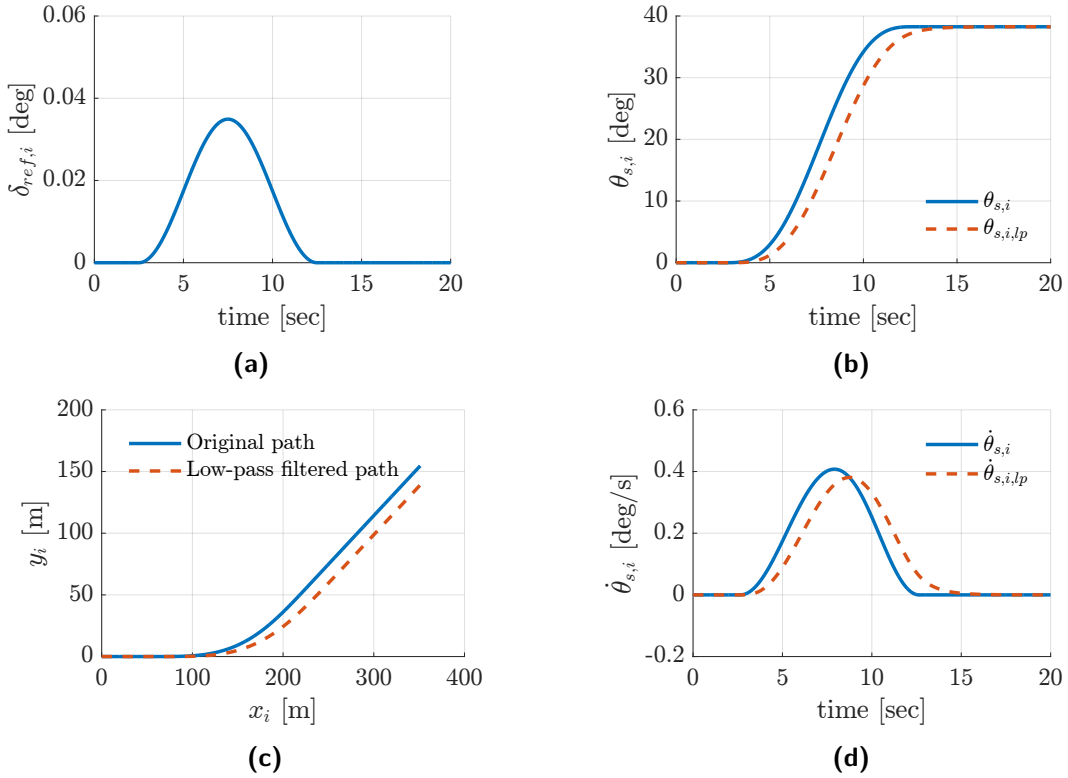


Figure 4-16: Simulation of a cornering maneuver performed at 20 m/s where (a) shows the applied steer input $\delta_{ref,i}$, (b) the path of the vehicle in terms of the angle $\theta_{s,i}$, (c) the x_i, y_i position of the vehicle and (d) the path of the vehicle expressed in $\dot{\theta}_{s,i}$.

4-4 Discussion

In the beginning of this chapter, two main questions were posed. The first question was how to describe the platoon dynamics when the lateral control of each individual vehicle is based on a path-following control approach. In Section 4-1, a method has been used to describe the dynamics of a vehicle platoon. The presented method is only valid under the assumption that the time gap Δt between two consecutive vehicles is constant. This is a reasonable assumption because it is assumed that the lateral controller runs in parallel to a longitudinal controller that controls the time gap with respect to the preceding vehicle. Only in extreme situations (e.g., heavy braking actions), the longitudinal controller cannot properly control the time gap with respect to a preceding vehicle anymore.

The second question was whether laterally string-stable behavior can be obtained using the controller presented in Chapter 3. It turned out that a static feedback controller that penalizes the lateral offset y_e and heading error ψ_e on itself does not yield laterally string-stable behavior.

If an additional feedforward steer input based on the steer input of the preceding vehicle is applied, marginally lateral string-stable behavior can be obtained (i.e. $|\Gamma_{i,ff}(j\omega)| = 1, \forall \omega$). This means that the platoon of vehicles is not robust for high-frequency disturbances (i.e., these will be followed one-on-one).

As mentioned before, it is desired to have accurate tracking performance for low frequencies, but attenuate high-frequency disturbances in upstream platoon direction. Therefore, in ‘Case 3’ in Section 4-2-3, the feedforward input is filtered using a low-pass filter such that low frequencies are passed through while high-frequency steer maneuvers are attenuated. The resulting response, however, was not satisfactory because the conditions for lateral string stability were not met.

Finally, in Section 4-3-1, the angular rate of change of the reference path $\dot{\theta}_s$ was filtered in addition to the feedforward steer input δ_{ref} . Although this approach shows a laterally string-stable behavior in the frequency-domain, in time-domain steady-state errors are observed. This is because the reference path is modified which is the result of filtering $\dot{\theta}_{s,i}$.

Considering the four investigated control configurations, ‘Case 2’ which contains a static output feedback controller in combination with a feedforward controller that is based on the steer input of the preceding vehicle, shows the best performance. Although it does not attenuate high frequency disturbances, it is considered as the best control configuration.

Chapter 5

Experiments

The vehicle-following control algorithm developed in Chapter 3 is implemented such that experiments can be performed using an experimental vehicle. A Toyota Prius III is used as an experimental vehicle to test the lateral control algorithm. In this chapter, first the practical implementation of the control algorithm is discussed in Section 5-1. Then, the experimental setup is discussed in Section 5-2. In Section 5-3, the experimental results are presented and, finally, in Section 5-4 conclusions are summarized.

5-1 Practical implementation

The implementation of the control algorithm to a benchmark vehicle is similar to the simulation setup that was presented in Figure 4-9. The main difference is that in the simulation model the relative position between two vehicles is determined by comparing the global position of both vehicles. In the real vehicles, the relative position is directly measured by the on-board sensors. In the next sections, different aspects regarding the practical implementation of the lateral control algorithm are discussed in more detail.

5-1-1 Path generation

In this thesis work, a path-following control approach is proposed to follow a preceding vehicle. Therefore, first the path of the preceding vehicle has to be constructed. The goal is to construct the path of a preceding vehicle using cost-effective forward-looking sensors as was mentioned before in Section 1-3.

Both a camera and radar are used to perform relative position measurements with respect to a preceding vehicle. The authors in [15] and [16] present a method to construct the path of a preceding vehicle using only relative position measurements. In order to realize this, multiple relative position measurements and the motion parameters of the vehicle (i.e. yaw rate and vehicle speed) have to be stored in a ‘history buffer’. In this way, the path of a preceding

vehicle can be constructed using forward-looking sensors which are the mainstream sensing choice for active safety applications in today's vehicles. Therefore, this method is chosen here to construct the path of the preceding vehicle.

The sampled relative position measurements, which are illustrated by the points $\xi_{1}^{i-1}, \xi_{2}^{i-1}, \dots, \xi_n^{i-1}$ in Figure 5-1, represent the trajectory of vehicle $i - 1$. This figure shows a fixed reference frame $S^g = \{O^g, \bar{e}_x^g, \bar{e}_y^g\}$ and a vehicle i with reference frame $S^i = \{O^i, \bar{e}_x^i, \bar{e}_y^i\}$ at two different time instances t_1 and t_2 . Each point ξ_j^{i-1} is described by x and y coordinates with respect to the following vehicle's reference frame S^i , i.e. $\xi_j^{i-1} = [x_j^{i-1} \ y_j^{i-1}]^T$. Since the reference frame S^i moves along with vehicle i , the points that describe the path of the preceding vehicle $\xi_{1}^{i-1}, \xi_{2}^{i-1}, \dots, \xi_n^{i-1}$, need to move within frame S^i according to the motion of vehicle i .

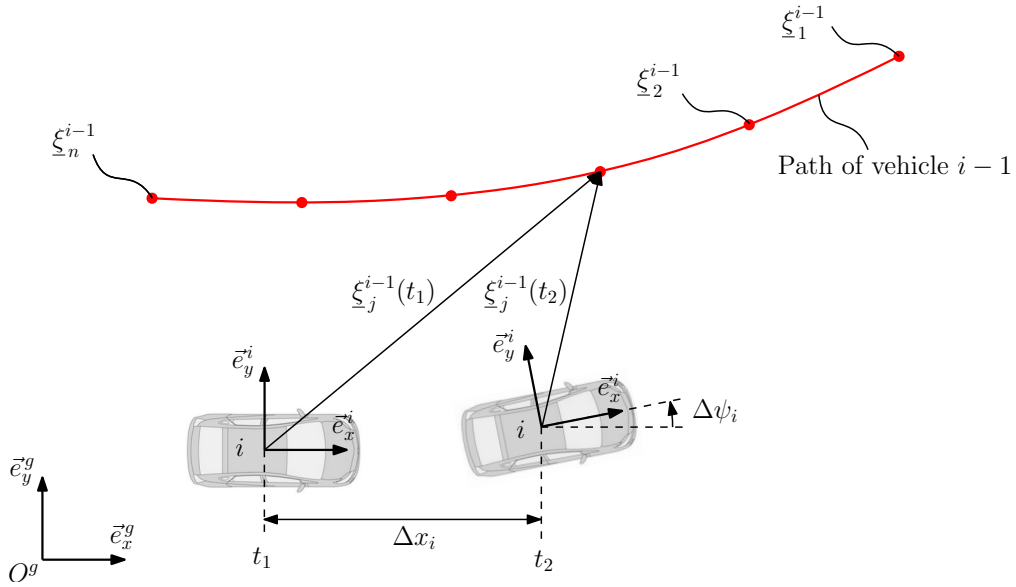


Figure 5-1: Illustration of the relative position measurements $\xi_{1}^{i-1}, \xi_{2}^{i-1}, \dots, \xi_n^{i-1}$ in the history buffer ξ_{i-1} that move within the frame S^i .

The work of [16] presents a method to compensate the relative position measurements for the i^{th} vehicle motion using its yaw rate $\dot{\psi}_i$ and the longitudinal velocity $v_{x,i}$. During a time step $dt = t_2 - t_1$, the vehicle has translated along its longitudinal axis by $\Delta x_i = v_{x,i} dt$ and rotated around its vertical axis by $\Delta \psi_i = \dot{\psi}_i dt$. The lateral velocity $v_{y,i}$ cannot be measured in practice. However, $v_{y,i}$ is typically small for normal highway driving scenarios and can therefore be neglected such that the translation in the lateral direction Δy_i can be assumed to be zero. It can be observed that each point ξ_j^{i-1} has different x and y coordinates with respect to frame S^i . All the points $\xi_{1}^{i-1}, \xi_{2}^{i-1}, \dots, \xi_n^{i-1}$, are stored in a history buffer ξ_{i-1} which at time t_1 looks like

$$\xi_{i-1}(t_1) = \begin{bmatrix} x_1^{i-1}(t_1), & x_2^{i-1}(t_1), & \dots, & x_n^{i-1}(t_1) \\ y_1^{i-1}(t_1), & y_2^{i-1}(t_1), & \dots, & y_n^{i-1}(t_1) \\ 1, & 1, & \dots, & 1 \end{bmatrix}, \quad \text{where } \xi_{i-1} \in \mathbb{R}^{3 \times n}. \quad (5-1)$$

All the elements of the third row of ξ_{i-1} are equal to 1 such that this matrix can be multiplied by a transformation matrix T to transform all relative position measurements to compensate

for the vehicle motion over time. Therefore, at the next time step, t_2 , the history buffer ξ_{i-1} is updated by multiplying ξ_{i-1} with the following transformation matrix T :

$$T = \begin{bmatrix} \cos \Delta\psi_i & \sin \Delta\psi_i & -\Delta x_i \\ -\sin \Delta\psi_i & \cos \Delta\psi_i & -\Delta y_i \\ 0 & 0 & 1 \end{bmatrix}, \quad (5-2)$$

Hence, the history buffer ξ_{i-1} at time t_2 is obtained as follows:

$$\xi_{i-1}(t_2) = T\xi_{i-1}(t_1). \quad (5-3)$$

At each time instance, all the points ξ_j^{i-1} , $j \in \{1, \dots, n\}$, are compensated for the vehicle motion by integrating the yaw rate $\dot{\psi}_i$ and longitudinal vehicle speed $v_{x,i}$ to obtain $\Delta\psi_i$ and Δx_i , respectively. Note that the polynomial will show small ‘jumps’, because the yaw rate $\dot{\psi}_i$ and vehicle speed $v_{x,i}$ which are used to update the relative position measurements in ξ_{i-1} contain measurement noise. Also, due to the integration of these signals, small errors are made because these signals may start to drift. However, the error made as a result of sensor drift will be limited, because after some time when a vehicle has passed a point ξ_j^{i-1} , it is removed from the history buffer ξ_{i-1} because it is not of interest, anymore. This is illustrated in Figure 5-2. Every 0.1 second (which is equal to the sampling time of the camera), a new relative position measurement is added to the history buffer ξ_{i-1} . In Figure 5-2, a new relative position measurement is added to the history buffer ξ_{i-1} between time t_1 and t_2 . Simultaneously, the last point in the history buffer is discarded and from time t_2 , the reference path has a new start point s_0 .

It can also be observed that at time t_1 the path of vehicle $i - 1$ is only described until the last relative position measurement, which is denoted by ξ_1^{i-1} . This is important to realize when the steer input of vehicle $i - 1$ has to be related to its position s on the path as will be discussed in Section 5-1-4.

A new relative position measurement is added to the history buffer ξ_{i-1} depending on the sampling frequency of the camera. In the practical implementation, it was not detected which precise time instance a new camera measurement is obtained. As a result, it can occur that it takes a few time stamps before a new measurement is added to the buffer. Therefore, it would be better to detect when a new camera measurement becomes available such that it can directly added to the history buffer ξ_{i-1} .

In order to describe the actual path of vehicle $i - 1$, a polynomial $P(x)$ is fitted through the points in the history buffer ξ_{i-1} . The order of the polynomial should be high enough to be able to describe the path that is driven by the preceding vehicle during the time gap time Δt . On the other hand, the order should not be too high because than the polynomial will fit the noise of the individual relative position measurements ξ_j^{i-1} . A third-order polynomial seems to be a good compromise between having enough degree of freedom to describe the actual path and filtering out the measurement noise. Therefore $P(x)$ looks like:

$$P(x) = C_0 + C_1x + C_2x^2 + C_3x^3, \quad (5-4)$$

where x is the x -coordinate with respect to frame S^i . The polynomial $P(x)$ describes the reference path for vehicle i , and can be used to obtain the control errors $y_{e,i}$ and $\psi_{e,i}$. Before

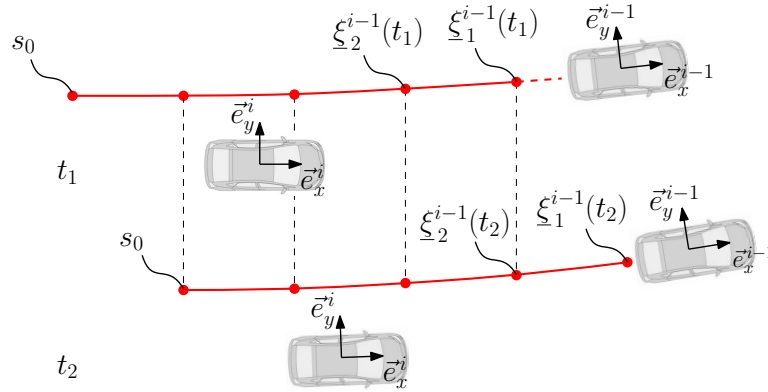


Figure 5-2: Illustration of updating the preceding vehicle's path. When a new relative position measurement is added to the buffer ξ_{i-1} , also the last point is discarded and also the start point s_0 is updated.

the lateral offset and heading error are determined based on the polynomial $P(x)$, first the effect of the delay of the camera on performing a correct relative position measurement is discussed, in the next section.

5-1-2 Effect of sensing delay on path generation

The camera that runs image recognition software suffers from significant delays due to the computationally-intensive image recognition algorithms. This results in delayed relative position measurements as is illustrated in Figure 5-3. In this figure, two vehicles (i and $i - 1$) have a constant inter-vehicle distance d_i . At time t_1 , a new relative position measurement of vehicle i with respect to vehicle $i - 1$ starts. Due to the sensing delay time ϕ , the measurement is obtained at time t_2 . During the sensing delay time $\phi = t_2 - t_1$, both vehicles have moved towards a new position. Consequently, at time t_2 the obtained relative position measurement d_i (which is represented by the blue cross in Figure 5-3) is added to the history buffer ξ_{i-1} . At time t_2 , also a new measurement starts which is then obtained at time t_3 . Again, the new obtained relative position measurement represented by the second blue cross is added to the history buffer ξ_{i-1} . Now, it is clearly observed that at time t_3 , the path that is described by the blue crosses does not represent the actual path of vehicle $i - 1$. This is caused by the delay of the camera, because vehicle i moves a distance of Δx_i during the sensing delay time. If the distance Δx_i is subtracted from the blue crosses, the red circles are obtained which represent the real path of vehicle $i - 1$.

In this example, vehicle i only moves in the longitudinal direction, but in general it can also rotate $\Delta\psi_i$ around its vertical axis during the sensing delay time. If each measurement is corrected for the motion of the vehicle (rotation and translation) during the sensing delay time ϕ , the correct path of the preceding vehicle is obtained. This, of course, only works if the time gap between two consecutive vehicles is larger than the sensing delay time which is typically the case. In the next section, the delay compensation is discussed in more detail.

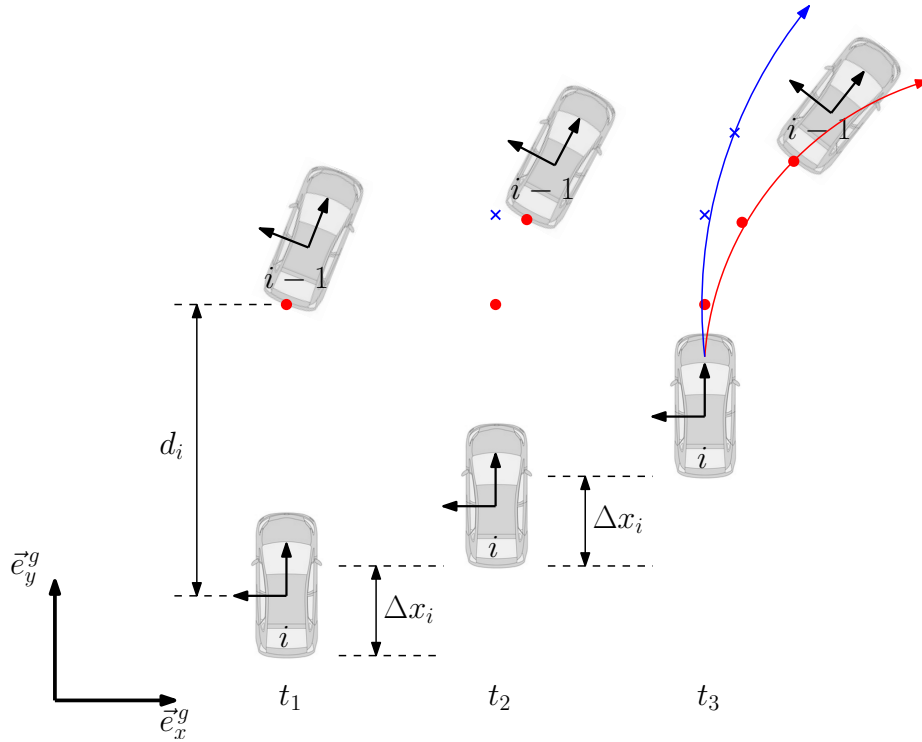


Figure 5-3: Illustration of the influence of sensing delay on the path generation of a preceding vehicle. The real path of the preceding vehicle is represented by the red segment and the path that is obtained as a result of sensing delay is represented by the blue segment.

Compensation of sensing delay

In the previous section it was observed that the delay of the camera yields errors in the construction of the path of the preceding vehicle. It was also motivated that if each relative position measurement conducted by the camera is corrected for the motion of the following vehicle during the sensing delay time, the correct path of the preceding vehicle is obtained. In this section, it is explained how a new relative position measurement ξ_j^{i-1} is corrected for the vehicle motion during the sensing delay time before it is added to the history buffer ξ_{i-1} .

In order to compensate for the error that is made due to the sensing delay time, the delay time should be known and the motion parameters of the vehicle (i.e. yaw rate and longitudinal vehicle speed) have to be stored in another history buffer η_i during the sensing delay time. The history buffer η_i that stores the motion parameters of the vehicle is described by

$$\eta_i = \begin{bmatrix} \psi_1^i & \psi_2^i & \cdots & \psi_{n_i}^i \\ v_{x,1}^i & v_{x,2}^i & \cdots & v_{x,n_i}^i \end{bmatrix}, \quad \text{where } \eta_i \in \mathbb{R}^{2 \times n_i}. \quad (5-5)$$

Each column stores the motion parameters of the vehicle for one time step dt .

The process to correct a relative position measurement ξ_j^{i-1} for the sensing delay time ϕ is similar to correcting the history buffer ξ_{i-1} for the vehicle motion during one time step dt . A new relative position measurement $\xi_{j,m}^{i-1}$ is multiplied by a transformation matrix T_s which is the product of multiple transformation matrices T_j , where $j \in \{1, \dots, n_i\}$, i.e.

$$T_s = T_1 T_2 \dots T_{n_i}. \quad (5-6)$$

Each transformation matrix T_j is described by (5-2), where Δy_j is assumed to be zero and the terms $\Delta \psi_j$ and Δx_j are obtained by multiplying the j^{th} column of the motion parameter buffer $\boldsymbol{\eta}_i$ by the time step dt , (i.e. $\Delta \psi_j = \psi_j dt$ and $\Delta x_j = v_{x,j} dt$). The amount n_i of transformation matrices T_j that are multiplied with each other to obtain T_s is determined by multiplying the sensing delay time ϕ by the sampling frequency f (Hz) of the camera, i.e.

$$n_i = \phi f. \quad (5-7)$$

The transformation matrix T_s is then multiplied by the new relative position measurement $\xi_{j,m}^{i-1}$ to finally obtain the corrected measurement ξ_j^{i-1} which is then added to the buffer ξ_{i-1} :

$$\xi_j^{i-1} = T_s \xi_{j,m}^{i-1}. \quad (5-8)$$

The real delay time of the camera ϕ is unknown. Therefore, the delay time was determined iteratively during the experiments by trying different delay times to see more or less which delay time yielded the best performance. This way, the delay time was determined to be 0.21 seconds. However, it is recommended to identify the camera delay time more accurately to be able to better compensate for it.

5-1-3 Calculation of the control errors

So far, the path generation has been explained and a method to compensate for the sensing delay time of the camera is discussed. Next, the lateral offset $y_{e,i}$ and the heading error $\psi_{e,i}$ are determined using the polynomial $P(x)$ given in (5-4). The polynomial $P(x)$ is expressed in coordinates with respect to frame S^i . The lateral offset y_e is defined as the distance of the origin O^i to the point \bar{s} on the reference path C , see Figure 2-3. The reference path C is now approximated by the polynomial $P(x)$ and the distance d from O^i to a point s on $P(x)$ is given by

$$d = \sqrt{x^2 + y^2}, \quad (5-9)$$

where $y = P(x)$. In order to find $y_{e,i}$, which is the shortest distance from O^i to $P(x)$, the following minimization problem has to be solved

$$\begin{aligned} y_{e,i} &= \min_x(d) \\ &= \min_x \left(\sqrt{x^2 + P(x)^2} \right). \end{aligned} \quad (5-10)$$

This minimization problem is further solved in Appendix B. The x coordinate that corresponds to the minimum distance between O^i and C is denoted by x_{min} and is also derived in

Appendix B.

The heading error $\psi_{e,i}$ is the slope of $P(x)$ evaluated at x_{min} , i.e.

$$\begin{aligned}\psi_{e,i} &= \arctan\left(\frac{\partial P(x_{min})}{\partial x}\right) \\ &= \arctan\left(C_1 + 2C_2x_{min} + 3C_3x_{min}^2\right),\end{aligned}\tag{5-11}$$

where C_1, C_2 and C_3 are the coefficients of the polynomial $P(x)$. Note that the body slip angle β_i is not taken into account in the heading error $\psi_{e,i}$. The body slip angle is neglected because it cannot be measured in practice. This will not cause significant errors because the body slip angle is small when operating in the linear region of the tires [30]. However, it would be better to implement an observer to estimate the body slip angle such that it can be taken into account in obtaining the heading error $\psi_{e,i}$.

5-1-4 Design of feedforward controller

Besides a static output feedback controller, also a feedforward controller is used in the control algorithm. In Section 3-3, two different feedforward controllers are discussed. One is based on the curvature of the reference path and the other is based on the steer input of the preceding vehicle which can be obtained through wireless inter-vehicle communication.

It was motivated in Section 3-3, that the tracking performance of the feedforward input based on inter-vehicle communication is better than the one based on the curvature of the reference path. However, the feedforward controller based on the curvature of the reference path is easier to implement and therefore this feedforward controller is implemented to validate the tracking performance of the lateral control algorithm. Hence, the practical implementation of the feedforward controller based on the curvature of the reference path is discussed next while the practical implementation of the feedforward controller based on the steer input of the preceding vehicle is presented in Appendix C.

Implementation of feedforward control based on the reference curvature

Here, the implementation of a feedforward controller based on the curvature of the reference path κ_{ref} is discussed. As mentioned in Section 3-3-1, the reference curvature κ_{ref} can be translated into a desired angular rate of change of the vehicle's direction of motion \mathcal{H}_{ref} by multiplying κ_{ref} by the longitudinal vehicle speed $v_{x,i}$. Furthermore, in Section 3-3-1, it was explained that the inverse vehicle transfer function $G_1^{-1}(s)$ has to be multiplied by the second-order low-pass filter $H_2(s)$ in order to obtain a proper transfer function. The advantage of using $H_2(s)G_1^{-1}(s)$ over the static gain $|G_1^{-1}(0)|$, is that the dynamics of the system are taken into account in the feedforward controller.

Since the objective is to only track low-frequency curvature changes, $H_2(s)G_1^{-1}(s)$ only needs to approximate $G_1^{-1}(s)$ for low frequencies. Figure 3-7 shows that $H_2(s)G_1^{-1}(s)$ indeed is a good approximation of $G_1^{-1}(s)$ for frequencies up to approximately 0.2 Hz. However, it can

also be observed that for low frequencies, the dynamics of the system can well be described by the static gain $|G_1^{-1}(0)|$. Besides, for practical implementation, it is desired to have roll-off in the feedforward controller in order to attenuate the amplification of high-frequency noise. Therefore, for the practical implementation of the feedforward controller, a different approach is used. Instead of using $H_2(s)G_1^{-1}(s)$ as a feedforward controller, the static gain $|G_1^{-1}(0)|$ is filtered using a first-order low-pass filter $H_1(s)$, i.e. $H_1(s)|G_1^{-1}(0)|$. The implemented first-order low-pass filter in $H_1(s)|G_1^{-1}(0)|$ has a cutoff frequency of 1 Hz.

In Figure 5-4, it can be observed that besides $H_2(s)G_1^{-1}(s)$, also $H_1(s)|G_1^{-1}(0)|$ approximates the original inverse vehicle transfer function $G_1^{-1}(s)$ well for low frequencies. Hence, the required feedforward steer input to track the desired angular rate of change of the vehicle's direction of motion, \mathcal{H}_{ref} , can be obtained using the following feedforward controller

$$\frac{\delta_{ref,i}(s)}{\mathcal{H}_{ref}(s)} = H_1(s) |G_1^{-1}(0)|. \quad (5-12)$$

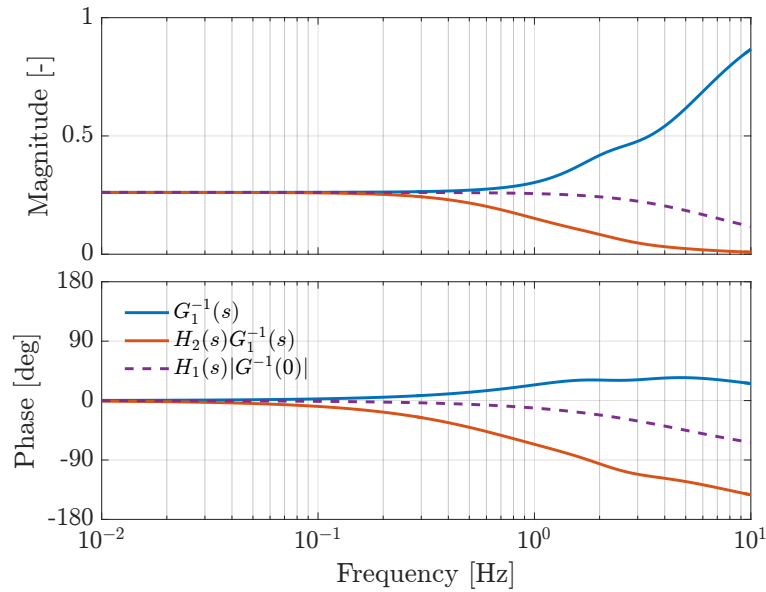


Figure 5-4: Bode plot of the inverse vehicle transfer function $G_1^{-1}(s)$, the inverse vehicle transfer function multiplied by a second-order low-pass filter $H_2(s)G_1^{-1}(s)$ and the steady-state gain of the inverse vehicle's transfer function multiplied by a first-order low-pass filter $H_1(s)|G_1^{-1}(0)|$.

The input of this feedforward controller is \mathcal{H}_{ref} which is obtained by multiplying the curvature of the reference path κ_{ref} with the longitudinal vehicle speed $v_{x,i}$, see (3-6). The reference path is described by the polynomial $P(x)$ as is given in (5-4). According to [35], the curvature of a polynomial is given by

$$\begin{aligned}\kappa_{ref}(x) &= \frac{\frac{d^2 P(x)}{dx^2}}{\left(1 + \left(\frac{dP(x)}{dx}\right)^2\right)^{3/2}} \\ &= \frac{2C_2 + 6C_3x}{\left(1 + C_1^2 + 4C_1C_2x + (6C_1C_3 + 4C_2^2)x^2 + 12C_2C_3x^3 + 9C_3^2x^4\right)^{3/2}},\end{aligned}\quad (5-13)$$

where C_0, C_1, C_2 and C_3 are the coefficient of the third-order polynomial $P(x)$. In order to obtain the correct feedforward input, the curvature of the reference path has to be evaluated at the position \bar{s} along the path which is obtained by substituting x_{min} (derived in Appendix B) for x in Equation (5-13).

Once the reference curvature κ_{ref} is determined, the feedforward controller $H_1(s) \Big| G^{-1}(0) \Big|$, as described in (5-12), is used to determine the feedforward steer input. As mentioned before, this feedforward controller is implemented in a benchmark vehicle to test the lateral control performance in practice. In the next section, the influence of this new feedforward controller on the frequency response of a vehicle platoon is analyzed.

Frequency response of a vehicle platoon with feedforward based on curvature

In Chapter 4, the frequency response of a vehicle platoon was analyzed for four different control configurations which were denoted by Case 1 up until Case 4. In this section, a new control configuration is analyzed where the feedforward controller is based on the curvature of the reference path. This control configuration will be denoted by ‘Case 5’.

In order to analyze Case 5, first the block scheme presented in Figure 4-3 has to be modified, because the new feedforward controller depends on $\dot{\theta}_{s,i}$ and the steer input $\delta_{ref,i-1}$ is not required anymore. In Figure 5-5a, the control configuration with feedforward controller $H_1(s) \Big| G^{-1}(0) \Big|$ is depicted. Using this block scheme, the complementary sensitivity function $\Gamma_{i,5}(s) = \frac{\mathcal{H}_i(s)}{\mathcal{H}_{i-1}(s)}$ can be shown to be equal to

$$\Gamma_{i,5}(s) = \frac{G_1(s)H_1(s) \Big| G_1^{-1}(0) \Big| + \mathcal{K}(s)G_1(s)}{1 + \mathcal{K}(s)G_1(s)}, \quad (5-14)$$

where $\mathcal{K}(s)$ is given in (4-4) and $G(s)$ in (3-9). Using the same parameters as in Chapter 4 (i.e. $v_{x,i} = 20$ m/s, $k_1 = 0.05$ and $k_2 = 1$), Figure 5-5b shows the gain $|\Gamma_{i,5}(j\omega)|$. It can be observed that this feedforward input does not yield laterally string-stable behavior, because the gain $|\Gamma_{i,5}(j\omega)|$ does not meet the criteria for lateral string stability that were posed in (4-6). A similar response has been observed for different control gains k_1 and k_2 , and also for different cutoff frequencies of the first-order low-pass filter $H_1(s)$. In all cases, the criteria for lateral strings stability are not met.

However, for frequencies up to 0.1 Hz, the gain $|\Gamma_{i,5}(j\omega)|$ is approximately 1. This means that if the frequency content of the curvature of the reference path is small as well, this controller should have good tracking performance. Hence, this feedforward controller is used to validate the tracking performance of the lateral control algorithm for low-frequency steer maneuvers.

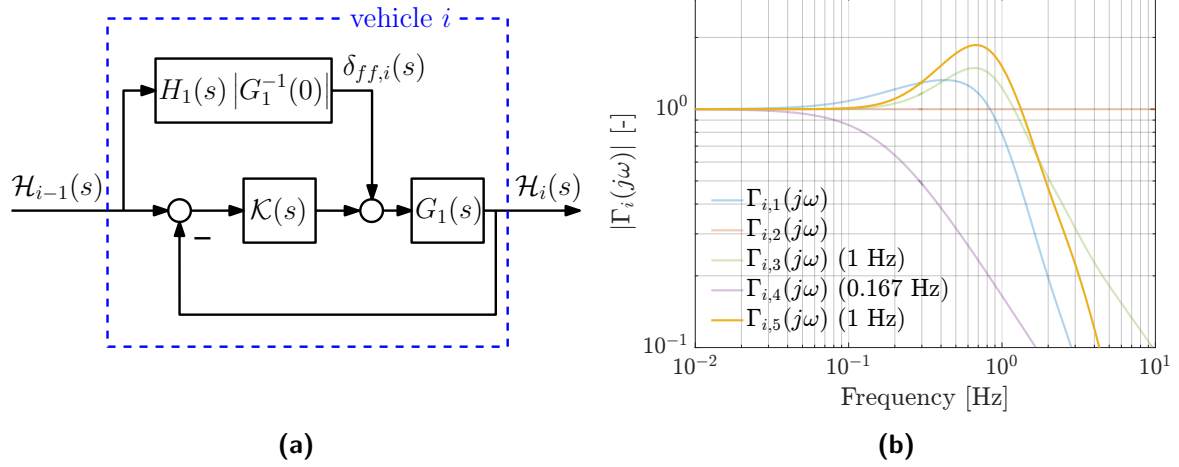


Figure 5-5: Figure (a) provides an illustration of the block scheme of the lateral control structure in case the feedforward input $\delta_{ref,i-1}$ is filtered using a first-order low-pass filter with cutoff frequency of 1 Hz and (b) shows the gain $|\Gamma_{i,5}(j\omega)|$ for $v_x = 20$ m/s, $k_1 = 0.05$ and $k_2 = 1$.

5-2 Experimental setup

In order to test the developed control algorithms in practice, a Toyota Prius III vehicle was used to perform experiments. In order to test the vehicle-following controller, a two vehicle platoon was made as is depicted in Figure 5-6a. The Toyota Prius III is modified with additional sensors and hardware, such as a forward-looking camera with image recognition software, a forward-looking radar, a wireless communication module and a Global Positioning System (GPS) sensor.

Besides the added sensors, some additional hardware components are positioned in the trunk of the vehicle as shown in Figure 5-6b. First, there is a Real-Time Platform which is a computer that runs a real-time operating system. This real-time machine allows one to run control algorithms developed in Matlab/Simulink in the vehicle. The Real-Time Platform is connected to the Controller Area Network (CAN) bus of the vehicle through the Vehicle Gateway. This provides the possibility to communicate with the vehicle's sensors and to control the actuators such as the PAS system. In the trunk, also an ethernet switch is placed which provides the communication between the Real-Time Platform and the Human-Machine Interface (HMI) of the vehicle. The ITS-G5 Gateway is a module that enables the wireless communication with other vehicles. Finally, a GPS sensor keeps track of the global position of the vehicle.

5-2-1 Test description

In order to test the tracking performance of the lateral path-following controller, multiple tests are performed at different velocities. The tests are performed at the test track of the RDW test center in Lelystad in The Netherlands which is depicted in Figure 5-7. As mentioned before, the feedforward controller based on the curvature of the reference path has been implemented for the experimental validation. Since this feedforward controller does

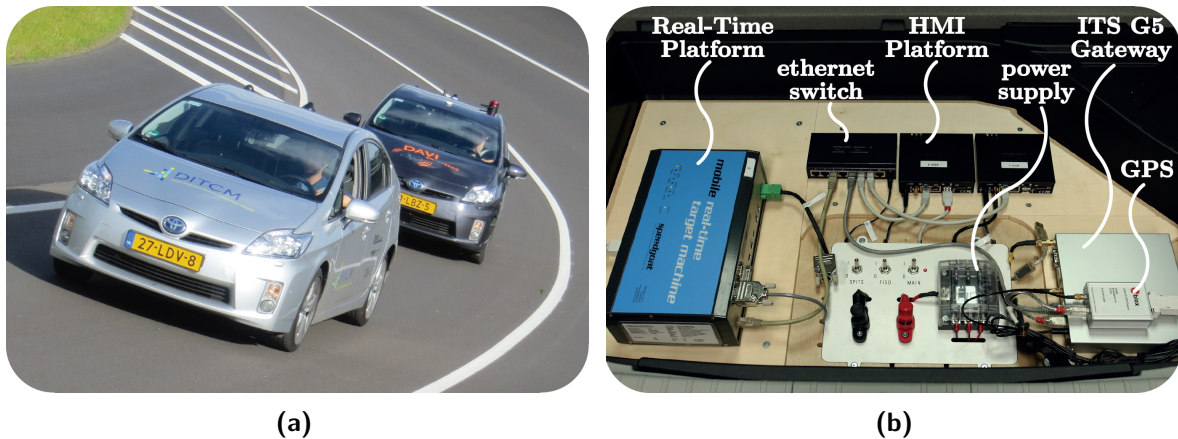


Figure 5-6: Figure (a) shows a two vehicle platoon as used during experiments and (b) shows an overview of the hardware located in the trunk of the following vehicle.

not require real time state information from the preceding vehicle, a regular vehicle without inter-vehicle communication ability is used as a lead vehicle. Consequently, the minimum time gap between the two vehicles that could be realized was 1 second when driving in ACC mode. Although lane marking can easily be detected at this time gap, this still allows us to test the concept of the vehicle-following control algorithm.

The lead vehicle is manually driven and performs different maneuvers such as performing lane-changes, cornering and driving sinusoidal paths at different velocities. The following vehicle drives in ACC mode where the steering is done by the implemented lateral control algorithm. Hence, the following vehicle follows the lead vehicle fully autonomously. In the next section, the experimental results for driving a sinusoidal path are discussed, because this is good test scenario to analyze the lateral control performance.



Figure 5-7: Illustration of the RDW test track in Lelystad, The Netherlands.

5-3 Experiment results

In this section, the experimental results for driving a sinusoidal path are presented. Figure 5-8, shows the experimental data where the lead vehicle drives a sinusoidal path at approximately 70 kph. In order to get a feeling for the tracking performance, the path of both vehicles is

shown in x and y-coordinates at the bottom of this figure. The path of ‘vehicle 1’ is obtained by integrating its yaw rate $\dot{\psi}_1$ and longitudinal velocity $v_{x,1}$. And the path of ‘vehicle 2’ is constructed by adding the lateral offset $y_{e,2}$ to the path of vehicle 1. Hence, this figure does not show the real measured x and y positions of both vehicles, but it provides an approximate illustration of the tracking performance of the lateral controller.

First of all, it can be observed that the following vehicle smoothly tracks the path of its preceding vehicle which corresponds to the smooth and comfortable ride that was experienced during the tests. However, it is also observed that the following vehicle shows a significant amount of overshoot with respect to the path of the lead vehicle. It was observed that the vehicle always steers to the right which is probably caused by a poor suspension alignment, because in open loop the vehicle also tends to steer to the right. This explains that the lateral offset error $y_{e,2}$ is larger in the positive direction than in the negative direction as can be observed in the $y_{e,2}$ plot. The average of the maximum positive and negative $y_{e,2}$ value is approximately 0.32 m.

In order to prevent steady-state errors as a result of external forces such as a suspension misalignment, a small integral action could be added to the lateral error $y_{e,2}$.

The overshoot that is observed in the control response is partly explained by the feedforward input. It was motivated in Section 3-3-1 that the inverse vehicle transfer function $G^{-1}(s)$ has to be filtered by a second-order low-pass filter to make this transfer function proper. In Section 5-1-4, it was explained that for the practical implementation, the feedforward controller $H_1(s) \Big|_{G^{-1}(0)}$ also imitates $G^{-1}(s)$ well for low frequencies. The first-order low-pass filter that is implemented in this feedforward controller introduces phase delay in the feedforward steer input which causes a tracking error with respect to the reference path. The amount of phase delay depends on the cutoff frequency of the implemented low-pass filter and the frequency content of the reference curvature signal κ_{ref} which is discussed next.

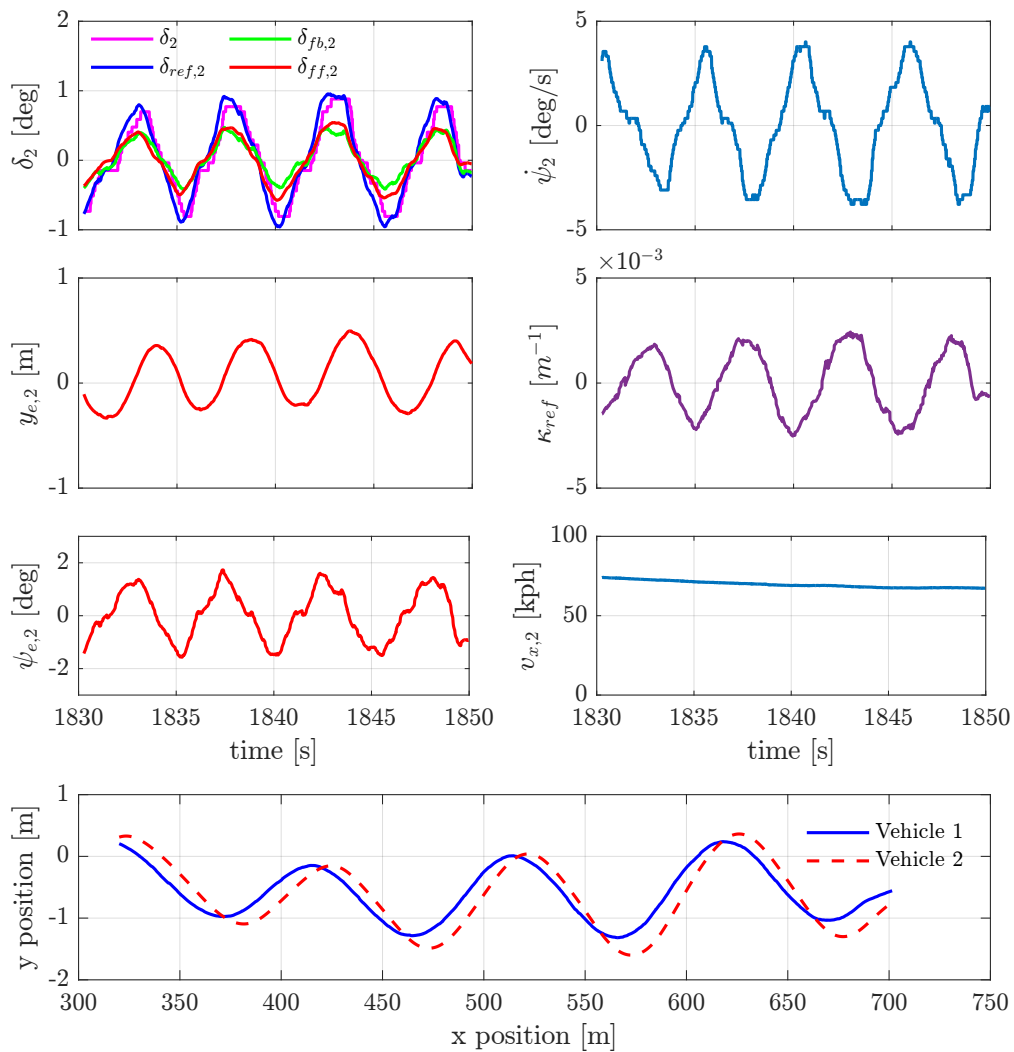


Figure 5-8: Experimental data of a vehicle-following test performed at $v_{x,i} = 70$ kph when the following vehicle drives approximately a 0.6 m amplitude sinusoidal path.

Frequency content of the reference curvature

In Section 5-1-4 the complementary sensitivity function $\Gamma_{i,5}(s)$ was given for the closed-loop system with a feedforward controller based on the reference curvature κ_{ref} . It was motivated that if the frequency content of $\kappa_{ref} < 0.1$ Hz, the following vehicle should have a minimal amount of overshoot with respect to the path of its predecessor because $|\Gamma_{i,5}(j\omega)| \approx 1$ for $\omega < 0.1$ Hz. For larger frequencies, the gain $|\Gamma_{i,5}(j\omega)| > 1$ and the following vehicle will show more overshoot when tracking the reference path.

Therefore, the frequency content of the reference curvature κ_{ref} is analyzed and presented in Figure 5-9a. It can be observed that the signal κ_{ref} has a frequency content up to approximately 0.35 Hz. According to Figure 5-5b, the gain $|\Gamma_{i,5}(j\omega)|$ is larger than 1 in this frequency range which explains the overshoot that is observed in the experimental data in Figure 5-8.

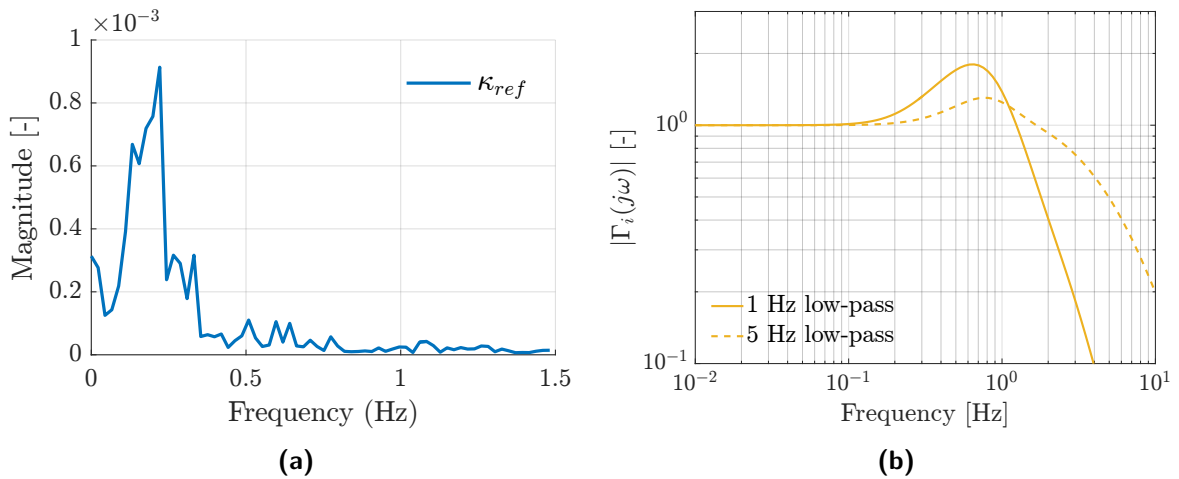


Figure 5-9: Figure (a) shows the frequency content of the measured reference curvature κ_{ref} and (b) shows the complementary sensitivity function for $H_1(s) \left| G_1^{-1}(0) \right|$ with a cutoff frequency of 1 Hz and 5 Hz.

Knowing that the reference curvature contains frequencies up to 0.35 Hz, the feedforward controller could be redesigned to obtain a better tracking performance for this frequency range. Figure 5-9b shows the complementary sensitivity function for the feedforward controller $H_1(s) \left| G_1^{-1}(0) \right|$ with a cutoff frequency of the low-pass filter $H_1(s)$ of 1 Hz and 5 Hz, respectively. It can be observed that gain $|\Gamma_i(j\omega)|$ significantly decreases for a higher cutoff frequency of 5 Hz. This means that the overshoot and hence the tracking error can also significantly be reduced if a 5 Hz low-pass filter is applied instead of a 1 Hz low-pass filter. Obviously, the tracking performance can be increased even more for an infinitely high cutoff frequency, but then the feedforward controller has no roll-off anymore which means that high-frequency disturbances are amplified. Hence a trade-off has to be made between tracking performance and attenuating high-frequency disturbances.

Actuator delay

A second cause for the overshoot in of the following vehicle with respect to the path of the lead vehicle can be explained by the actuator delay of the Park Assist System (PAS). It was mentioned before in Section 2-1-2 that the PAS system has a delay γ of approximately 0.1 seconds. This delay causes overshoot, because it takes 0.1 seconds before the Park Assist System (PAS) reacts to a steer command. In order to reduce the amount of overshoot that is caused by the actuator delay, the reference curvature could also be evaluated at a certain look-ahead distance. The commanded feedforward steer input is then actually applied by the PAS system at the precise moment that the vehicle has reached the position where the curvature of the reference path was determined. Hence, the feedforward steer input is not delayed which should reduce the amount of overshoot. The correct look-ahead distance depends on the longitudinal vehicle speed and the actuator delay and is obtained by

$$l_a = v_{x,i}\gamma, \quad (5-15)$$

where γ is the actuator delay of the PAS system. Note that the feedback input cannot be treated in the same manner, because the feedback input depends on the relative position of the vehicle with respect to the reference path. This means that the desired feedback steer input that should be applied at the look-ahead distance depends on the relative position of the vehicle with respect to the reference path at the look-ahead distance, which is not known in advance.

Comparison of experimental data to simulation results

In order to better quantify to what extent the tracking error can be reduced by taking both the actuator delay into account and applying a 5 Hz low-pass filter instead of a 1 Hz low-pass filter in the feedforward controller, simulations are performed. Using the simulation model presented in Section 4-3-1, the test scenario has been reproduced, i.e., a two vehicle platoon drives at approximately 70 kph and the lead vehicle drives a sinusoidal path with with similar amplitude and frequency as in the experiment. In Figure 5-10, the global path of the lead vehicle is expressed in x and y-coordinates by the dashed black line. In order to quantify the effect of the actuator delay and the cutoff frequency of the low-pass filter in the feedforward controller, three different cases are compared to each other.

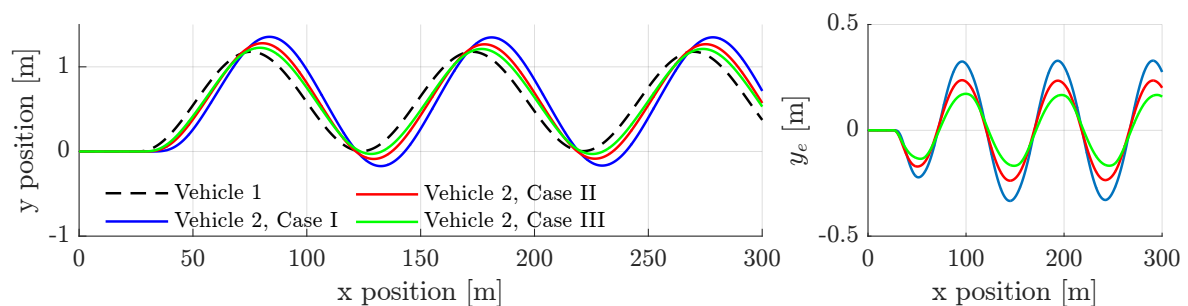


Figure 5-10: Time-domain simulation of a sinusoidal maneuver for a two vehicle platoon with the lead vehicle 'Vehicle 1' and the following vehicle for three different cases (Case I, II and III).

Case I In case I, the following vehicle tracks the path of its predecessor using the same feedforward controller and feedback gains as in the experiment. It can be observed in Figure 5-10 that the response of the following vehicle is very similar to the experimental data presented in Figure 5-8. The maximum lateral error $y_{e,2}$ is approximately 0.33 m. The average maximum lateral error observed in the experimental data is approximately 0.32 m which means that the simulation shows very similar results as observed during the experiment.

Case II In case II, the reference curvature for the feedforward controller is evaluated at the look-ahead distance as described by (5-15). This way the effect of the actuator delay on the feedforward input is eliminated. It can be observed in Figure 5-10 that the tracking performance of case 2 improves significantly with respect to case 1. The maximum lateral error is now 0.24 m which means that the error is reduced by 27%.

Case III Finally, case III is similar to case 2, but now also the cutoff frequency of the first-order low-pass filter in the feedforward controller is increased from 1 Hz to 5 Hz. Considering Figure 5-10, it can be observed that this yields another significant improvement in the tracking performance. The maximum lateral error for case 3 is even further reduced to only 0.17 m which is another reduction of 21% for the lateral error y_e .

All in all, based on these simulation results, it is expected that the maximum lateral error y_e can be reduced by 48 % which would significantly improve the tracking performance.

5-4 Discussion

In this chapter, the implementation of the lateral vehicle path-following control algorithm on an experimental vehicle has been discussed. The lateral path-following controller has been tested on a test track in order to validate the lateral control algorithm. Due to time constraints, the proposed feedforward controller based on the commanded steer input of the preceding vehicle could not be tested in practice. Instead a feedforward controller based on the curvature of the reference path has been used for experimental validation of the control algorithm. In contrast to the feedforward controller based on wireless communication, it has been evaluated that the implemented feedforward controller based on the curvature of the reference path does not yield laterally string-stable behavior.

The experimental data shows that the following vehicle smoothly tracks the path of its predecessor. Hence, the vehicle path-following controller has successfully been implemented and shows to a good alternative for existing direct vehicle following control methods for vehicle platoons. However, more tests are required to further improve the tracking performance. The average maximum lateral offset error that was observed when performing 0.6 m amplitude sinusoidal maneuvers at 70 kph is approximately 0.32 m.

This result can be reproduced in simulation. Using the same simulation model, it seems that if the feedforward controller takes the delay of the PAS system into account and if a 5 Hz instead of a 1 Hz low-pass filter is implemented in the feedforward controller, the tracking performance can significantly be improved. Simulation results show that the proposed modifications in the control algorithm could reduce the maximum lateral error by 48 %. This

means that the maximum error stays within 0.2 m for the sinusoidal maneuvers that were performed during the experiment.

Although this tracking performance is already quite acceptable, it is expected that the tracking performance can be improved even further if the feedforward controller described in Appendix C is implemented. This feedforward controller can, theoretically, perfectly track the path of a preceding vehicle without any tracking error.

Conclusions and recommendations

In this chapter, first the conclusions based on the performed research are presented after which recommendations are given for future work.

6-1 Conclusions

The aim of this master thesis was to design and implement a lateral vehicle path-following controller for automated vehicle platoons. This allows vehicles to drive safely at small inter-vehicle time gaps of well below one second even if lane markings cannot reliably be detected. In this way, the road capacity of existing roads can be increased and the aerodynamic drag of the individual vehicles, and hence their emissions, can be reduced.

The objective of designing and implementing a lateral controller that can follow the path of a preceding vehicle has been accomplished. However, none of the investigated controllers provide laterally string-stable behavior, and attenuate high-frequency disturbances without introducing steady-state errors with respect to the path of a preceding vehicle.

In this work, a method has been derived to describe the lateral dynamics of a vehicle platoon in case the lateral control of each individual vehicle is based on a path-following control method. Multiple lateral control designs were evaluated using this method. The best performance was obtained using a static output feedback controller in combination with a feedforward controller that is based on the steer input of the preceding vehicle. This controller shows marginal laterally string-stable behavior which is evidenced both in frequency-domain and in time-domain simulation. The same feedback controller in combination with a feedforward controller based on the curvature of the reference path only approximates laterally string-stable behavior for low-frequency curvature changes.

However, due to time constraints, only the latter feedforward controller has been implemented in an experimental vehicle to validate the path-following control algorithm. The experimental data shows that the path of the preceding vehicle is smoothly tracked. Hence, the path of a preceding vehicle can successfully be constructed by relative position measurements using only cost-effective forward-looking sensors.

However, still a certain amount of overshoot is observed in the response. This corresponds to the predicted frequency response of the platoon model and the obtained test results can be reproduced in the developed simulation model. This simulation model also shows that the tracking error can be reduced by 48 % if 1) the reference curvature, that is used by the feedforward controller, is filtered with a 5 Hz low-pass filter instead of a 1 Hz low-pass filter and 2) the reference curvature is evaluated at a look-ahead distance to compensate for the delay of the Park Assist System.

Other conclusions that can be made based on this thesis work are presented next as bullet points:

- A static output feedback controller can be used to let a vehicle track a desired reference path. It was found that heading information is required in order to obtain closed-loop stability. One way to do this is to incorporate a look-ahead distance but this yields vehicles to cut corners. If the heading error is penalized directly, stable path-following control is achieved without cutting corners.
- As a result of the vehicle-following control strategy, the lateral dynamics of the individual vehicles are coupled and lateral string stability has to be considered as well. In literature, lateral string stability has been achieved for direct vehicle-following control methods, but not path-following control methods. In this work, a method has been obtained to describe the lateral platoon dynamics in the frequency domain. This method is valid under the assumption that the time gap between two vehicles is constant and is based on the fact that the angular rate of change of the reference path is equal to the angular rate of change of the preceding vehicle at that point. The results of this method correspond to what is observed both in time-domain simulations and in experimental data.
- The presented method to describe the lateral platoon dynamics and to assess lateral string stability considers the evolution of the angular rate of change of the direction of motion of the vehicles in a platoon. Using this method, the effect of a disturbance entering the platoon can be analyzed in the frequency domain, but this method cannot guarantee that the path of a preceding vehicle is tracked without steady-state errors. Therefore, another string stability function, that explicitly considers the relation between the position of two consecutive vehicles, has to be considered.

6-2 Recommendations

The lateral vehicle path-following control approach as presented in this master thesis shows to be a good alternative for the existing direct vehicle-following control approaches for automated vehicle platoons. However, more research is required; for example, for the feedforward controller that is based on the curvature of the reference path.

First, the influence of the applied low-pass filter on the tracking error should be further investigated. And secondly, the influence of evaluating the reference curvature for the feedforward controller at a look-ahead distance to compensate for the delay of the Park Assist System is worthwhile exploring more into depth. Both modifications show significant improvements in tracking performance in simulation, and should also be tested in practice.

Although the tracking performance could significantly be improved, the objective of achieving lateral string stability is not met. Therefore, it is suggested to also implement the feedforward controller that is based on the steer input of the preceding vehicle. This feedforward controller shows marginal laterally string-stable behavior in both frequency-domain and in time-domain simulations. It is therefore expected that using this feedforward controller, the tracking error can be even further reduced.

However, even with this feedforward controller, only marginal laterally string-stable behavior is obtained. As a result, high-frequency disturbances are not attenuated in upstream platoon direction which is the goal as was discussed in the problem statement in the introduction of this thesis. Therefore, more research must be performed to explore different path-following control methods that provide strictly lateral string-stable behavior, at least in the operating frequency range.

Other recommendations that can further improve the lateral path-following controller are:

- Firstly, during the experiments it was observed that the experimental vehicle has a steady-state offset to the right which is probably caused by a poor suspension alignment. In order to be more robust for steady-state errors, it is recommended to add a small integral action to the lateral offset error.
- Secondly, the same vehicle-following experiments should be performed at inter-vehicle time gaps of well below 1 second. In that case, lane marking cannot reliably be detected anymore and that is why a vehicle-following control approach was chosen.
- Thirdly, it is recommended to better identify the delay time of the camera. In that case, the relative position measurements can be compensated more accurately for the delay time before they are added to the history buffer.
- fourthly, it is recommended to design an observer that estimates the vehicle yaw rate such that the level of noise, that is introduced by compensating the relative position measurements for the vehicle motion, can be reduced. If also the lateral velocity is observed, the relative position measurements can also be compensated for the lateral translation of the vehicle.
- Finally, it is recommended to detect when a new camera measurement becomes available, such that a new relative position measurement is directly added to the history buffer. In the current implementation, every 0.1 seconds the last obtained measurement is added to the history buffer, but this does not necessarily happen directly after the measurement was obtained. Consequently, small errors are made in constructing the path of the preceding vehicle.

Appendix A

Closed-loop poles

In this appendix, the closed-loop poles of the closed-loop system matrix A_{cl} presented in (3-4) are presented for longitudinal speeds $v_x = 10, 30$ and 40 m/s. In all presented cases, the closed-loop poles are evaluated for $k_1 = 0.02, 0.05, 0.1, 0.2$ and gain k_2 is varied from 0 to 2, similar to what was done in Chapter 3.

vehicles speed = 10 m/s

In Figure A-1, the closed-loop poles are presented for a longitudinal vehicle speed of 10 m/s. It can be observed that the poles are much better damped compared to the closed-loop poles presented in Figure 3-6. Also, the poles are located close to the origin which is associated with slower dynamics. This corresponds to what is expected for driving at low speed.

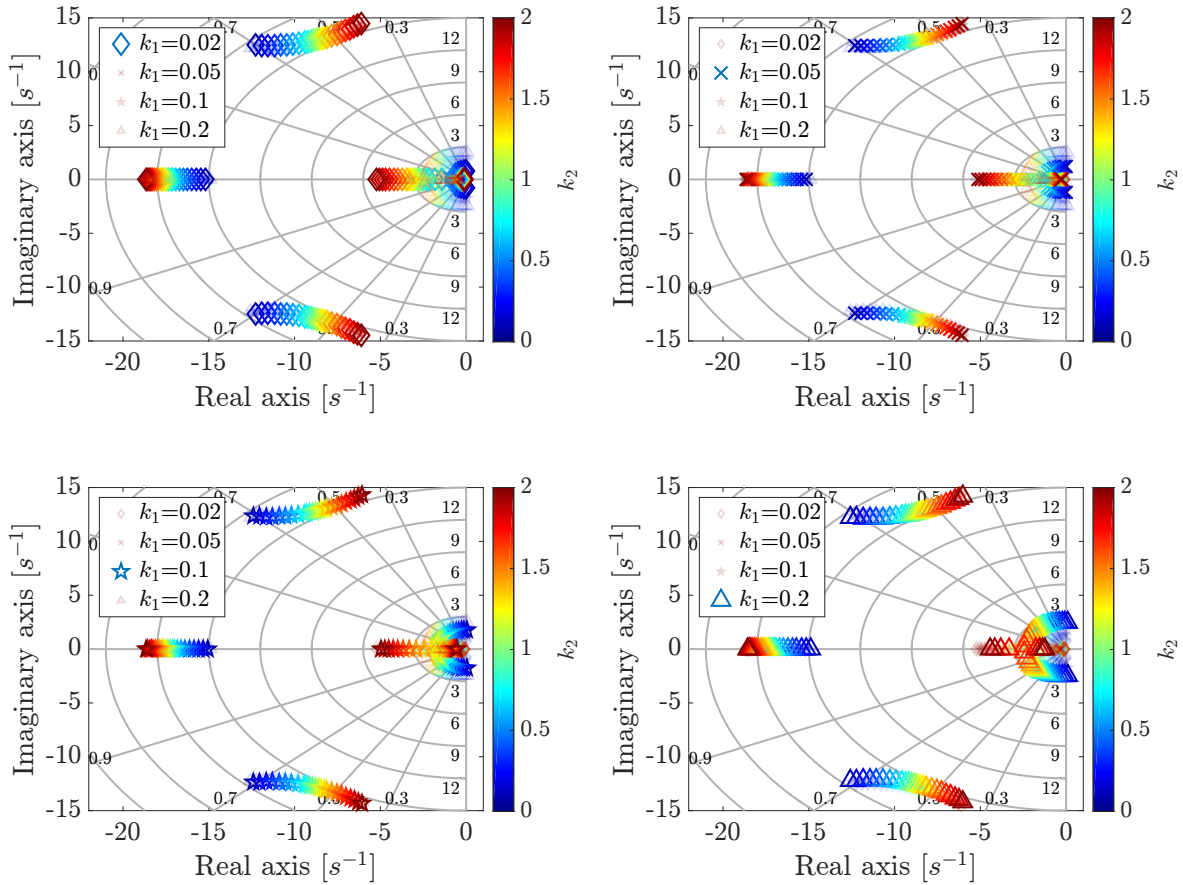


Figure A-1: Closed-loop poles of the closed-loop system matrix in Equation (3-4), using vehicle parameters of Table 3-1 and $v_{x,i} = 10$ m/s. In all plots, k_2 varies from 0 to 2 and in (a) $k_1 = 0.02$, in (b) $k_1 = 0.05$, in (c) $k_1 = 0.1$ and in (d) $k_1 = 0.2$.

vehicles speed = 30 m/s

In Figure A-2, the closed-loop poles are presented for a longitudinal vehicle speed of 30 m/s. A significant difference is observed with respect to the closed-loop poles for $v_{x,i} = 10$ m/s, because the dominant poles are located much closer to the imaginary axis which indicates that the system becomes more oscillatory. Also, it can be observed that the gain k_2 needs to be increased more in order to guarantee that all the poles are in the left-half plane.

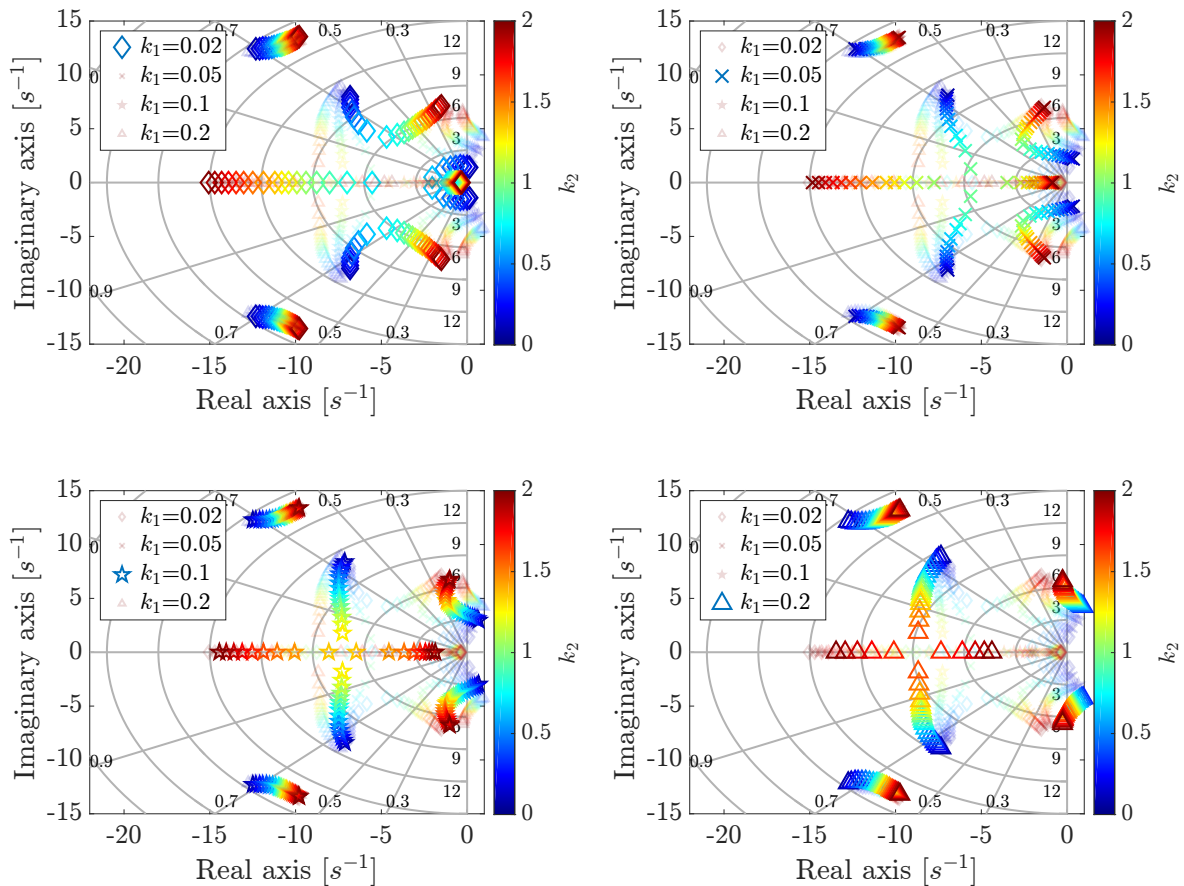


Figure A-2: Closed-loop poles of the closed-loop system matrix in Equation (3-4), using vehicle parameters of Table 3-1 and $v_{x,i} = 30$ m/s. In all plots, k_2 varies from 0 to 2 and in (a) $k_1 = 0.02$, in (b) $k_1 = 0.05$, in (c) $k_1 = 0.1$ and in (d) $k_1 = 0.2$.

vehicles speed = 40 m/s

In Figure A-3, the closed-loop poles are presented for a longitudinal vehicle speed of 40 m/s. It can be observed that the dominant poles are located even more towards the imaginary axis with respect to the closed-loop poles for $v_{x,i} = 30$ m/s. Also, it can be observed that for k_1 , the poles are always located in the right-half plane which means that the system is unstable.

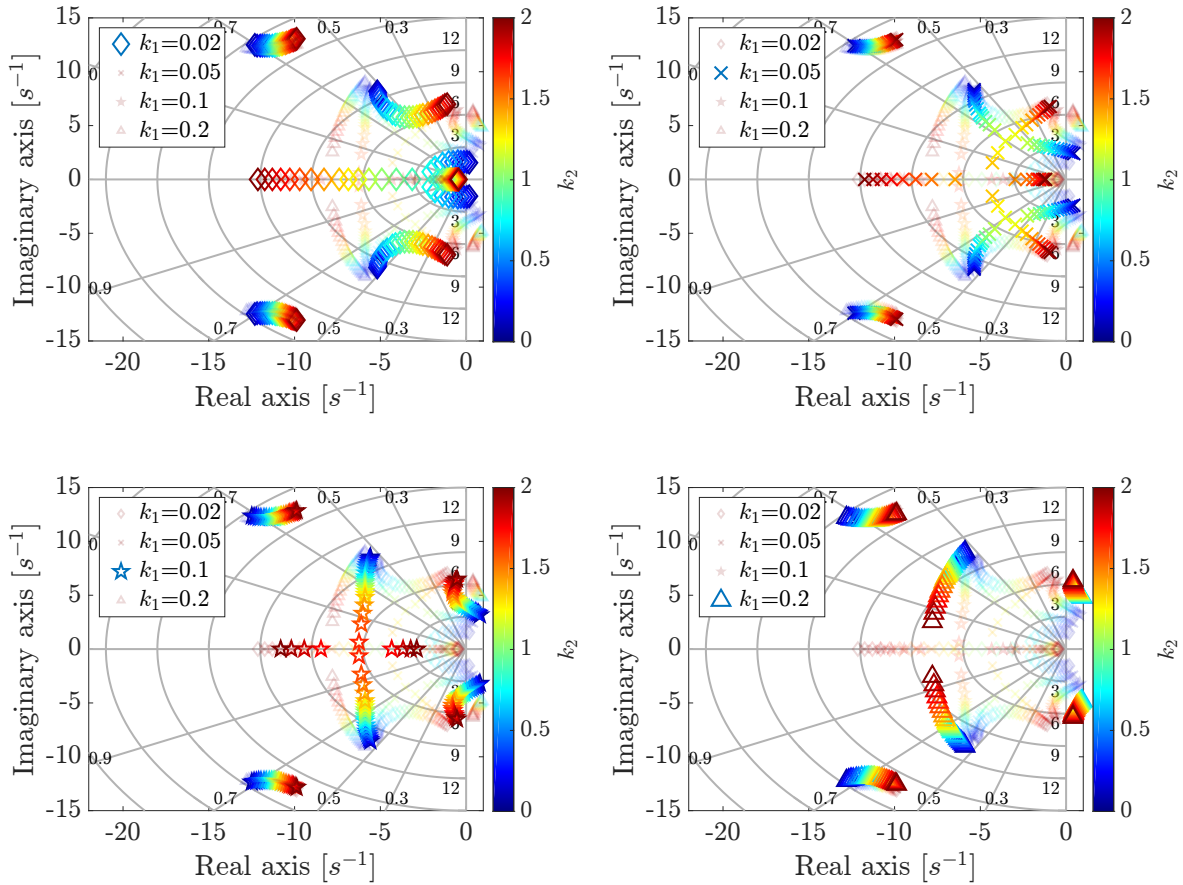


Figure A-3: Closed-loop poles of the closed-loop system matrix in Equation (3-4), using vehicle parameters of Table 3-1 and $v_{x,i} = 40$ m/s. In all plots, k_2 varies from 0 to 2 and in (a) $k_1 = 0.02$, in (b) $k_1 = 0.05$, in (c) $k_1 = 0.1$ and in (d) $k_1 = 0.2$.

Appendix B

Calculation of the control errors

In this appendix, the control errors $y_{e,i}$ and $\psi_{e,i}$ as defined in Figure 2-3, are calculated if the reference path is described by a third-order polynomial $P(x)$ as given in (5-4).

In Section 5-1-3, it was shown that the distance d from O^i to a point s on $P(x)$ is given by

$$d = \sqrt{x^2 + P(x)^2} \quad (\text{B-1})$$

and that the shortest distance $y_{e,i}$ is obtained by minimizing the expression for d , i.e.

$$y_{e,i} = \min_x \left(\sqrt{x^2 + P(x)^2} \right). \quad (\text{B-2})$$

Instead, also d^2 could be minimized. The x coordinate that corresponds to the minimum distance x_{min} is then obtained by

$$\begin{aligned} x_{min} &= d^2 \\ &= \arg \min_x \left(x^2 + P(x)^2 \right). \end{aligned} \quad (\text{B-3})$$

This minimization problem can be solved by taking the derivative of d^2 with respect to x and solve $\frac{\partial d^2}{\partial x} = 0$. If the expression for $P(x)$ is substituted in the expression for d^2 , $\frac{\partial d^2}{\partial x}$ becomes

$$\frac{\partial d^2}{\partial x} = 2C_0C_1 + 2(1 + 2C_0C_2 + C_1^2)x + 6(C_0C_3 + C_1C_2)x^2 + 4(2C_1C_3 + C_2^2)x^3 + 10C_2C_3x^4 + 6C_3^2x^5. \quad (\text{B-4})$$

It can be observed that the equation $\frac{\partial d^2}{\partial x} = 0$ has not 1 unique solution. However, if the heading error is small x_{min} will be close to zero. Therefore, it is assumed that the smallest

absolute value is the solution of the minimization problem in (B-3). In order to check whether the obtained solution actually is a minimum and not a maximum, it is verified whether the second derivative is larger than 0, i.e. $\frac{\partial^2 d^2}{\partial x^2} > 0$.

Then, $y_{e,i}$ (which is the shortest distance from O^i to the polynomial $P(x)$) is obtained by substituting x_{min} in the expression for d in (B-1), i.e.

$$y_{e,i} = \sqrt{x_{min}^2 + \left(C_0 + C_1 x_{min} + C_2 x_{min}^2 + C_3 x_{min}^3\right)^2}. \quad (\text{B-5})$$

The heading error $\psi_{e,i}$ is the slope of $P(x)$ evaluated at x_{min} , i.e.

$$\begin{aligned} \psi_{e,i} &= \arctan\left(\frac{\partial P(x_{min})}{\partial x}\right) \\ &= \arctan\left(C_1 + 2C_2 x_{min} + 3C_3 x_{min}^2\right). \end{aligned} \quad (\text{B-6})$$

Implementaion of feedforward control based on wireless communication

In this appendix, the practical implementation of a feedforward controller based on the steer input of the preceding vehicle is presented. The steer input of the preceding vehicle can be obtained through wireless inter-vehicle communication. It was illustrated in Figure 3-8 that the steer input of a preceding vehicle should be related to the position along its path such that the following vehicle can apply the same steer input once it reaches that same position. In Section 3-3-2, it was explained how the steer input of the preceding vehicle can be related to the position along its path in case the steer input is continuously available. In practice, the steer input of the preceding vehicle is not continuously available, but is received at discrete time instances through wireless communication. Therefore, it is discussed here how a vehicle i determines the feedforward steer input if the steer input of vehicle $i - 1$ is only available at discrete time instances.

In Figure C-1a, the same scenario as in Figure 3-9a is illustrated. Only now the path of vehicle $i - 1$ is approximated by a polynomial $P(x)$ and the red crosses illustrate the time instances when the applied steer input of the preceding vehicle is received. In order to relate a new received steer input to the position along the path of vehicle $i - 1$, the position s along the polynomial $P(x)$ has to be determined. In Section 3-3-2, it was explained that the position s is determined by evaluating the length L of the path from s_0 to O^{i-1} . However, in practice the path is only constructed until the last obtained relative position measurement $\underline{\xi}_1^{i-1}$ from the camera, as is illustrated earlier in Figure 5-2. The length of the last part (illustrated by the dashed line in Figure 5-2), has to be added to the length of the reference path to obtain the length from s_0 to O^{i-1} .

The length from $\underline{\xi}_1^{i-1}$ to the current position O^{i-1} is obtained by integrating the longitudinal vehicle speed of vehicle $i - 1$ during the time interval between the time instant of which the last relative position measurement that was added to the history buffer and the time instant of which a new wireless message is received. Then the s position that is related to a new received steer input $\delta_{ref,i-1}$ is obtained by

$$s = \int_{x_1}^{x_2} \sqrt{1 + \left(\frac{dP(x)}{dx} \right)^2} dx + \int_{t_1}^{t_2} v_{x,i-1}(\sigma) d\sigma, \quad (\text{C-1})$$

where x_1 is the x-position of s_0 , x_2 the x-position of the last relative position measurement ξ_1^{i-1} (see Figure 5-2), t_1 the time instance the last camera measurement is obtained and t_2 the time instance the new wireless message is received.

Once a new received steer input $\delta_{ref,i-1}$ can be related to the correct s position along the path, a similar lookup table as in Figure 3-9b can be constructed that stores the applied steer input of vehicle $i-1$ versus the position variable s . The received steer inputs of vehicle $i-1$ are denoted by red crosses in Figure C-1b. Note that the actual applied steer input of vehicle $i-1$ (which is represented by the blue line) is only known for a limited number of discrete points. In order to obtain the feedforward steer input for an arbitrary value of \bar{s} , the discrete points in Figure C-1b are interpolated to approximate the applied steer input of vehicle $i-1$.

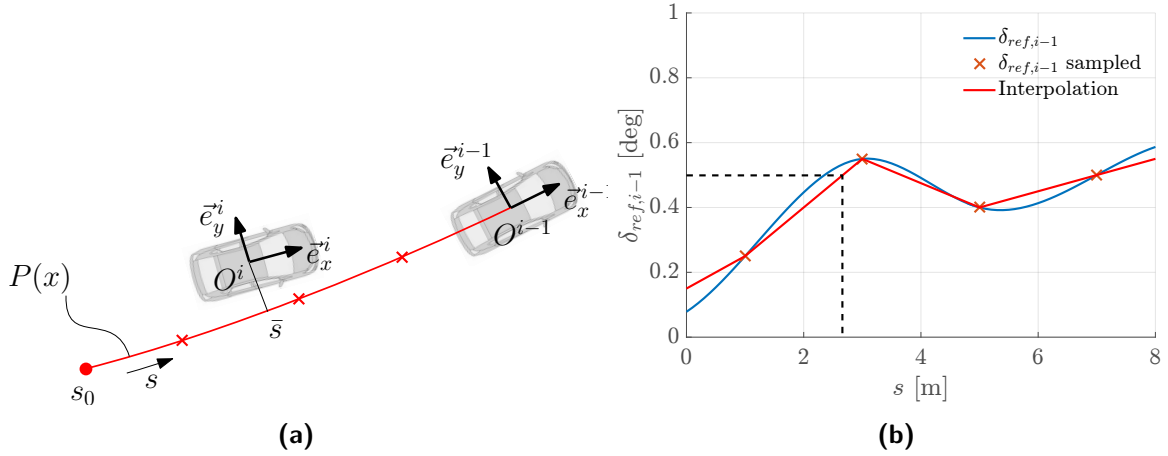


Figure C-1: Figure (a) Shows the projection of the received steer input (red crosses) of vehicle $i-1$ on its path and (b) shows the steer inputs $\delta_{ref,i-1}$ versus position variable s along its path.

Note that due to the interpolation of the sampled steer inputs, the feedforward input in Figure C-1b does not exactly correspond to the input $\delta_{ref,i-1}$ that was actually applied by the preceding vehicle. However, the update frequency of the received steer input is 10 Hz. This is an order of magnitude higher than the bandwidth of the closed-loop system as can be observed in Figure 3-12. Therefore, the effect of discretizing the steer input $\delta_{ref,i-1}$ on the response of the following vehicle is expected to be negligible.

Bibliography

- [1] J. Ploeg, B. Scheepers, E. van Nunen, N. van de Wouw, and H. Nijmeijer. (2011). “Design and experimental evaluation of cooperative adaptive cruise control”, *International IEEE Conference on Intelligent Transportation Systems (ITSC)*.
- [2] S. Shladover, D. Su, and X.-Y. Lu. (2012). “Impacts of cooperative adaptive cruise control on freeway traffic flow”, *Transportation Research Record: Journal of the Transportation Research Board*, no. 2324, pp. 63–70.
- [3] K. Henning, S. Gies, D. Abel, H. Max, et al. (2009). “Electronically coupled truck platoons on german highways”, *IEEE International Conference on Systems, Man and Cybernetics*, pp. 2409–2414.
- [4] D. Swaroop. (1997). “String stability of interconnected systems: An application to platooning in automated highway systems”, *California Partners for Advanced Transit and Highways (PATH)*.
- [5] X. Ma and I. Andréasson. (2006). “Driver reaction time estimation from real car following data and application in gm-type model evaluation”, in *Proceedings of the 85th TRB annual meeting*, pp. 1–19.
- [6] S. Solyom, A. Idelchi, and B. Bin Salamah. (2013). “Lateral control of vehicle platoons”, in *IEEE International Conference on Systems, Man, and Cybernetics (SMC)*, pp. 4561–4565.
- [7] E. J. Rossetter. (2003). “A potential field framework for active vehicle lanekeeping assistance”, *PhD thesis, Stanford University*.
- [8] J. Kosecka, R. Blasi, C. J. Taylor, and J. Malik. (1999). “A comparative study of vision-based lateral control strategies for autonomous highway driving”, in *International Journal of Robotics Research*.
- [9] M. E. Khatir and E. Davidson. (2005). “Decentralized control of a large platoon of vehicles operating on a plane with steering dynamics”, in *American Control Conference*, pp. 2159–2165.

- [10] J. J. Ploeg. (2014). “Analysis and design of controllers for cooperative and automated driving”, *PhD thesis, Eindhoven University of Technology*.
- [11] J. Alleleijn. (2015). “Lateral string stability of automated vehicle platoons”, *Master’s thesis, Eindhoven University of Technology*, DC 2015.075.
- [12] S. Öncü and M. Alirezaei. (2015). “Lateral vehicle control”, *tech. rep., TNO*.
- [13] G. Lu and M. Tomizuka. (2003). “A laser scanning radar based autonomous lateral vehicle following control scheme for automated highways”, in *IEEE American Control Conference*, vol. 1, pp. 30–35.
- [14] H. K. Goi, T. D. Barfoot, B. A. Francis, and J. L. Giesbrecht. (2010). “Vision-based vehicle trajectory following with constant time delay”, in *Field and Service Robotics*, pp. 137–147.
- [15] S. K. Gehrig and F. J. Stein. (1998). “A trajectory-based approach for the lateral control of vehicle following system”, in *IEEE International Conference on Systems, Man, and Cybernetics*, vol. 4, pp. 3596–3601.
- [16] A. Thorvaldsson and V. Bandi. (2015). “Reference path estimation for lateral vehicle control”, *Master’s thesis, Chalmers University of Technology*.
- [17] E. J. Rossetter, J. P. Switkes, and J. C. Gerde. (2014). “Experimental validation of the potential field lanekeeping system”, *International Journal of Automotive Technology*, vol. 5, no. 2, pp. 95–108.
- [18] J.-C. Hsu and M. Tomizuka. (1998). “Analyses of vision-based lateral control for automated highway system”, *Vehicle system dynamics*, vol. 30, no. 5, pp. 345–373.
- [19] J. Kosecka. (1996). “Vision-based lateral control of vehicles: Look-ahead and delay issues” *Internal Memo, Department of EECS, University of California Berkeley*.
- [20] A. S. Abdullah, L. K. Hai, N. A. A. Osman, and M. Z. Zainon. (2006). “Vision based automatic steering control using a pid controller”, *Journal Technology (A)*, vol. 44, no. A, pp. 97–114.
- [21] P. Hingwe and M. Tomizuka. (1998). “A variable look-ahead controller for lateral guidance of four wheeled vehicles”, in *American Control Conference*, vol. 1, pp. 31–35.
- [22] C. J. Taylor, J. Košecká, R. Blasi, and J. Malik. (1999). “A comparative study of vision-based lateral control strategies for autonomous highway driving”, *The International Journal of Robotics Research*, vol. 18, no. 5, pp. 442–453.
- [23] H. Tseng, J. Asgari, D. Hrovat, P. van der Jagt, A. Cherry, and S. Neads. (2005). “Evasive manoeuvres with a steering robot”, *Vehicle system dynamics*, vol. 43, no. 3, pp. 199–216.
- [24] K. Kritayakirana and J. C. Gerdes. (2012). “Autonomous vehicle control at the limits of handling”, *International Journal of Vehicle Autonomous Systems*, vol. 10, no. 4, pp. 271–296.
- [25] D. Swaroop and J. Hedrick. (1996). “String stability of interconnected systems”, *IEEE Transactions on Automatic Control*, vol. 41, no. 3, pp. 349–357.

-
- [26] J. Ploeg, N. van de Wouw, and H. Nijmeijer. (2014). “Lp string stability of cascaded systems: Application to vehicle platooning”, *IEEE Transactions on Control Systems Technology*, vol. 22, no. 2, pp. 786–793.
- [27] I. Papadimitriou and M. Tomizuka. (2004). “Lateral control of platoons of vehicles on highways: the autonomous following based approach”, *International Journal of Vehicle Design*, vol. 36, no. 1, pp. 24–37.
- [28] W. F. Milliken and D. L. Milliken. (1995). “Race car vehicle dynamics”, *Society of Automotive Engineers Warrendale*, vol. 400.
- [29] E. G. Ström. (2011). “On medium access and physical layer standards for cooperative intelligent transport systems in europe”, in *Proceedings of the IEEE*, vol. 99, no. 7, pp. 1183–1188.
- [30] M. Abe. (2015). “Vehicle handling dynamics: theory and application”. *Butterworth-Heinemann*.
- [31] J. Craens and N. Das. (2014). “Taking over the steering of a toyota prius using the electric steering motor”, *tech. rep., Fontys*.
- [32] G. F. Franklin, J. D. Powell, and M. L. Workman. (1998). “Digital control of dynamic systems”, *Addison-wesley Menlo Park*, vol. 3.
- [33] J. Kosecka. (1996). “Vision-based lateral control of vehicles: Look-ahead and delay issues”.
- [34] A. V. Pavlov. (2004). “The output regulation problem: a convergent dynamics approach”, *PhD thesis, Eindhoven University of Technology*.
- [35] J. Stewart. (2006). “Calculus early transcendentals, 6e”, *Belmont, CA: Thompson Brooks/Cole*.

